E.O. Paton Electric Welding Institute of the National Academy of Sciences of Ukraine

International Scientific-Technical and Production Journal

The Paton WELDING JOURNAL

Issue 06 2020

Published Monthly Since 2000

English Translation of the Monthly «Avtomatychne Zvaryuvannya»
(Avtomaticheskaya Svarka/Automatic Welding) Journal Published in Ukrainian and Russian Since 1948

Founders
E.O. Paton Electric Welding Institute
International Association «Welding»

Publisher
International Association «Welding»

Translators
A.O. Fomin, I.M. Kutianova
Editor
N.G. Khomenko
Electron galley
D.I. Sereda, T.Yu. Snegiryova

Address
E.O. Paton Electric Welding Institute,
International Association «Welding»
11 Kazymyr Malevych Str. (former Bozhenko),
03150, Kyiv, Ukraine
Tel.:/Fax: (38044) 200 82 77
E-mail: journal@paton.kiev.ua
www://patonpublishinghouse.com/eng/journals/tpwj

State Registration Certificate
KV 4790 of 09.01.2001
ISSN 0957-798X
DOI: http://dx.doi.org/10.37434/tpwj

Subscriptions
12 issues per year, back issues available.
$384, subscriptions for the printed (hard copy) version, air postage and packaging included.
$312, subscriptions for the electronic version (sending issues of Journal in pdf format or providing access to IP addresses).
Institutions with current subscriptions on printed version can purchase online access to the electronic versions of any back issues that they have not subscribed to.
Issues of the Journal (more than two years old) are available at a substantially reduced price.

CONTENTS

https://doi.org/10.37434/tpwj2020.06.01

THE INFLUENCE OF INTRODUCING REFRACTORY COMPOUNDS INTO THE WELD POOL ON THE WELD METAL DENDRITIC STRUCTURE

V.V. Holovko, D.Yu. Yermolenko and **S.M. Stepanyuk**
E.O. Paton Electric Welding Institute of the NAS of Ukraine
11 Kazymyr Malevych Str., 03150, Kyiv, Ukraine. E-mail: office@paton.kiev.ua

A study was conducted in order to expand the knowledge base on the mechanisms of the influence of refractory compounds in the weld pool on modification of weld metal structure. Results of experiments on inoculation of TiN, SiC, NbC, VC, TiC, TiO_2, Al_2O_3, MgO, ZrO_2 dispersed particles to the liquid metal of the weld pool are given. Possibility of the influence of refractory inoculants as the melt «microcoolants», centers for epitaxial initiation of a new phase in the liquid metal and surface-active compounds on modification of the dendritic structure of the welds was analyzed. It is shown that under the conditions of welding low-alloyed steels by flux-cored wire of «metal core» type in shielding gas atmosphere, the refractory compounds, inoculated to the weld pool, the most actively influence modifying of the primary structure, as surface-active compounds. It is established that the change of dendrite morphology in the weld metal influences the temperature range of the recrystallization process, formation of secondary microstructure and mechanical properties of the welds. 10 Ref., 5 Tables, 8 Figures.

Keywords: low-alloyed steel, weld, refractory inclusions, dispersed particles, dendritic structure, modification, austenite grains

At present, structural steels make up the main base of welded metal structures. The range of low-alloyed rolled stock is characterized by a wide variety, and development of new grades is going on, which are capable of providing further improvement of service properties of welded metal structures. Improvement of the characteristics of higher and high strength low-alloyed steels is achieved due to complication of their production technology, comprehensive alloying by such elements as nickel, molybdenum, niobium and vanadium. The high cost of these elements in Ukraine makes urgent the investigations, aimed at finding alternative possibilities of metallurgical influence on metal structure formation. Such work is performed both for low-alloyed rolled stock, and metal of welds produced during its welding. It should be noted that investigations in the welding field are characterized by additional difficulties, compared to traditional metallurgy, which are associated with a high speed of the processes, presence of gas-plasma phase, increased gradient of contacting phase composition, and a number of other factors.

The current concepts of formation of the primary weld metal structure are based predominantly on investigations of the processes of solidification of large metal volumes in steel ingot production. The identity of metallurgical processes, which are in place in these two cases, allows using the investigation results in the field of ferrous metallurgy, but a significant difference in the parameters of flow kinetics, temperature and concentration gradients, necessitates performance of special investigations as regards the features of formation of primary structure of weld metal.

In welding low-alloyed steels with carbon content above 0.18 %, in keeping with the state diagram of Fe–C system, melt solidification begins at temperatures below 1500 °C. It should be noted, however, that the changes in alloying element content in the liquid metal on the solidification front, which are caused by concentrational overcooling, influence the lowering of this temperature. From practical experience it is known that such a lowering of temperature is equal to approximately 10 °C.

A feature of formation of weld metal primary structure is predominantly epitaxial crystal nucleation on partially melted grains of the base metal. Base metal grains are of a nonuniform orientation, so the crystals, nucleating in the weld pool, will also have different orientation, and those of them, the axes of which coincide with the direction of the largest heat flow, will grow, the most intensively absorbing smaller neighbours. Such crystals, divided by high-energy boundaries, form the structure of primary dendrites. The curvature of the solidification front, i.e. the cur-

V.V. Holovko — https:/orcid.org/0000-0002-2117-0864, D.Yu. Yermolenko — https:/orcid.org/0000-0002-1215-1522,
S.M. Stepanyuk — https:/orcid.org/0000-0001-8876-9153

vature of the solid/liquid surface in the weld pool that changes, depending on the energy source movement, leads to instability of the front and formation of the structure in the form of columnar dendrites. During cooling, δ-, γ-transformation occurs with formation of low-angle boundaries, inside the primary dendrites. Presence of a liquation interlayer of liquid metal, and of surface-active elements, segregation of refractory inclusions in the zone between the growing dendrites, determine the morphology of primary austenite grains, that further on will affect the formation of final microstructure of the metal of welds and their mechanical properties.

One of the promising directions of improvement of the weld mechanical properties is refinement of its structure grains. The methods of metal modification are widely used with this purpose. At present, there is no single description of the mechanism of iron alloy modification. However, the wide application practice is indicative of the effectiveness of such processes. It is known that addition of refractory particles to the metal melt facilitates nucleation of equiaxed crystals in the concentrational overcooling zone, and increase of the number of nucleation centers influences the lowering of the dendrite growth rate. This is also promoted by presence of surface-active compounds, which lower the dendrite surface energy that leads to reduction of primary structure dimensions. To increase the effectiveness, it rational to combine the impact of refractory particles and surface-active compounds [1]. In addition, in is any case, the features of weld pool solidification should be taken into account at selection of modifiers.

This work is devoted to investigation of the features of modifying impact of refractory compound particles, which differed by their physico-chemical indices, with the purpose of substantiation of selection of metal structure modifiers for welds of low-alloyed high-strength steels.

1. Influence of inoculants on the dendritic structure. Formation of the metal alloy structure begins from appearance and growth of dendrites. At weld pool solidification, these processes occur much faster, than in the case of large metal ingots, but, nonetheless, formation of weld metal microstructure, determining the entire complex of its mechanical properties, begins exactly at this stage. Unfortunately, investigations of the features of formation of the dentritic structure of weld metal are not given too much attention in scientific-technical publications. This section gives the results of investigation of the influence of refractory compound particles inoculation into the weld pool on the morphology of dendrites in the weld metal.

1.1 Experimental procedure. By the nature of their action, the modifying additives can be conditionally divided into three types: «microcoolants», epitaxial centers of new phase nucleation, and surface-active compounds. Refractory compounds were selected for investigations. These compounds allow making a conclusion about the effectiveness of each of these directions at formation of the structure of metal of welds of low-alloyed steels with the yield limit of up to 600 MPa. The list of joints selected for experiments and their physico-chemical parameters are given in Table 1.

In order to reveal the nature of the refractory compound action, it is rational to store it in the form of a crystalline phase in the temperature range of metal melt existence. Performed calculations showed that at addition of the selected compounds to the weld pool, the size of the refractory particles should be not less than 200 μm. At addition of particles of 200–500 μm size, they can participate in the process of melt solidification as crystalline inclusions of exogenic type of 50–100 nm size.

Investigations of the influence of refractory particles on modifying the metal structural components were performed on samples of deposited metal, which

Table 1. Physico-chemical characteristics of compounds used in experiments

Compound	T_m, °C	Crystalline lattice type	Lattice parameter, nm	Mismatch to δFe size, %	Interphase energy, mJ/m^2
ZrO_2	2715	Tetragonal	a-3.640c-5.152	1	2863
VC	2810	FCC	a-4.159	13	1559
MgO	2825	FCC	a-4.213	14	2226
TiN	2930	FCC	a-4.260	16	393
TiC	3160	FCC	a-4.336	18	884
NbC	3608	FCC	a-4.469	21	548
TiO_2	1843	Tetragonal	a-4.593c-2.959	25	2444
Al_2O_3	2044	Rhombohedral	a-5.120α-55.25°	39	972

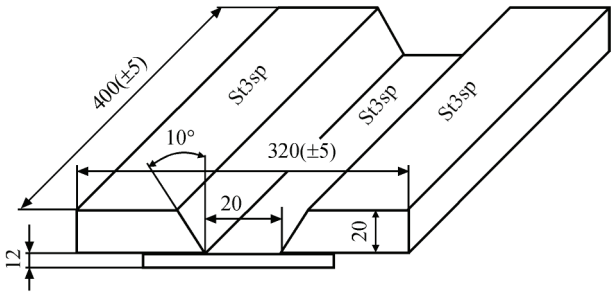

Figure 1. Butt joint preparation for cutting out weld metal samples in keeping with ISO 14171 requirements

were cut out of the last metal layer of a butt weld that was produced using experimental flux-cored wire of «metal core» type of 1.6 (±0.1) mm in M21 shielding gas atmosphere to ISO 14175 standard [2]. Butt joints of 1.4 type to ISO 9692-1 standard [3] (Figure 1) were welded at reverse polarity direct current of 230 (±10) A at arc voltage of 28 (±2) V and welding speed of 18 ((±0.5) cm/min. After each pass the butt joint was cooled in air up to the temperature not higher than 120 °C. The process heat input was equal to 26–28 J/cm.

Particles of refractory compounds of 200–500 μm size were added (inoculated) to the molten metal through the core of flux-cored wire, which was fed to the weld pool in the form of «cold» filler. Schemes of preparation of the butt, welded joint and areas of cutting out the samples for investigations are given in Figures 1–3. The inoculated filler content was equal to 0.1 % of the weld pool mass. The composition of the studied samples and mechanical properties of weld metal are given in Tables 2 and 3, respectively. Figure 2 gives the scheme of the butt joint filling, according to which the passes from the first to the nineth were made by flux-cored wire of the base alloying system, and passes from the tenth to the eighteenth were made using «cold» filler, to the core of which refractory compound particles were added.

The welds had a conditional designation that corresponded to a refractory compound, which was inoculated into the weld pool. Samples of weld metal, with base alloying system (conditional designation BA), were also used in the investigations. In order

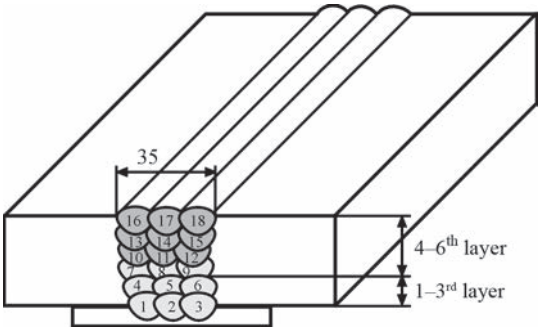

Figure 2. Scheme of bead layout at filling of the butt joint

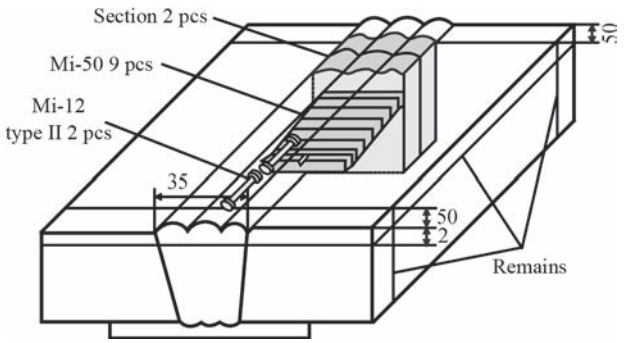

Figure 3. Scheme of sample cutting out to determine the chemical composition, mechanical properties and structure of weld metal

to separate the impact of titanium-containing compounds from increase of titanium content, weld metal samples, additionally alloyed by titanium (conditional designation FeTi), compared to the base system, were also included into investigation.

Transverse samples were cut out of the welded joints in order to study the structure and phase composition of the weld metal, as well as mechanical properties of the welded joints by the scheme, given in Figure 3.

At metallographic investigations the fraction of structural components in the metal and distribution of nonmetallic inclusions were determined. The microstructure was studied by the methods of optical metallography, using light microscope «Neophot-30»with image displaying in the computer screen.

Metallographic investigations of the last pass were conducted in optical microscope «Neophot-30» on transverse microsections of the weld metal, polished and etched in 2 % nital solution. The same sections were used for investigations in the scanning electron microscope. Microstructural analysis was conducted in keeping with the requirements of ISO 17639 standard [4] and IIW recommendations [5].

The primary weld metal structure was studied on polished samples, etched in a boiling saturated solution of sodium picrate ($C_6H_2(NO_2)_3ONa$) in water. Samples were cut out in the direction normal to the longitudinal axis of the weld, so that dendrites were visible on the section surface. They grew towards the largest thermal gradient in the weld pool. When studying the primary structure by the images, obtained by optical microscopy, the dimensions of columnar dendrites (dimensions λ_1 in Figure 4) were determined.

The nature of distribution of nonmetallic inclusions in the weld metal structure was analyzed, using the images of the surface of polished unetched sections, obtained in optical microscope «Neophot-30». The processed images were identified by special software. Each inclusion in the approximation was regarded as a certain polyhedron, the area of which is measured and recorded in the Table for further math-

ematical processing. Thus, each inclusion visible in the micrograph and taking up more than 3 pixels, was analyzed. This way a statistical sample was formed by the dimensions of nonmetallic inclusions in the weld metal. Further processing was performed using proprietary software, which ensures a complete cycle of processing the obtained data and deriving the results in the form of a spreadsheet. Then, the obtained sample was used to plot a histogram of frequencies with preset size ranges. Such a histogram of frequencies represents the size distribution of inclusions in the metal matrix.

Mechanical properties of metal of the studied welds were determined by the procedures, given in ISO 15792 standard [6].

1.2. Investigation results. The results given in Table 2 show that by its chemical composition the metal of the studied welds corresponds to low-alloyed steels. Addition of certain inoculants to the weld pool affected only the content of aluminium and titanium in the weld metal that is attributable to the features of

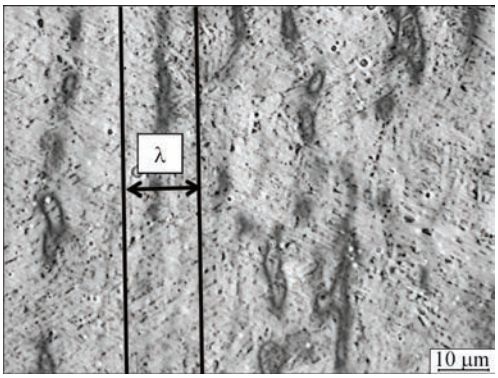

Figure 4. Example of dendrite structure (×1000) of the studied samples (λ is the distance between primary dendrite axes)

Table 2. Chemical composition of the studied weld metal, %

Weld	C	Si	Mn	S	P	Cr	Ni	Mo	Al	Ti	Zr
BA	0.034	0.340	1.21	0.021	0.020	0.12	2.13	0.28	0.028	0.013	N/D
FeTi	0.036	0.335	1.22	0.022	0.021	0.14	2.14	0.26	0.038	0.029	»
TiN	0.035	0.317	1.24	0.019	0.009	0.14	2.15	0.26	0.036	0.021	»
VC	0.052	0.227	1.21	0.022	0.021	0.14	2.13	0.25	0.027	0.004	»
NbC	0.049	0.253	1.19	0.021	0.020	0.13	2.15	0.27	0.029	0.003	»
SiC	0.053	0.351	1.20	0.020	0.025	0.12	2.12	0.26	0.025	0.004	»
TiC	0.046	0.340	1.25	0.021	0.019	0.13	2.15	0.24	0.023	0.021	»
TiO_2	0.035	0.405	1.24	0.018	0.021	0.11	2.17	0.27	0.031	0.027	»
Al_2O_3	0.034	0.424	1.26	0.019	0.023	0.11	2.15	0.29	0.042	0.015	»
MgO	0.031	0.227	1.21	0.025	0.024	0.14	2.15	0.29	0.023	0.013	»
ZrO_2	0.033	0.223	1.25	0.024	0.024	0.12	2.14	0.30	0.024	0.013	0.06

Table 3. Mechanical properties of the studied weld metal

Weld	σ_t, MPa	$\sigma_{0.2}$, MPa	δ, %	ψ, %	*KCV*, J/cm² at *T*, °C			
					+20	0	–20	–40
BA	685	610	15	54	97	87	75	53
FeTi	747	690	19	60	74	69	63	61
TiC	716	644	19	63	110	97	85	73
TiN	712	580	5.3	14.7	55	47	40	–
SiC	726	650	21	62	85	72	65	61
VC	780	706	14	56	57	55	52	–
NbC	820	757	18	57	45	39	31	–
TiO_2	709	636	19	57	85	72	60	50
Al_2O_3	728	621	17	54	82	58	50	36
MgO	644	586	19	60	103	85	69	60
ZrO_2	649	592	21	64	97	91	84	76

Table 4. Results of analysis of nonmetallic inclusion content in the weld metal

Weld	Inclusion fraction (%) in weld metal	Inclusion fraction (%) in the size range			
		<0.31 μm	0.37–0.61 μm	0.67–0.97 μm	1.03–1.57 μm
BA	0.47	29.63	46.67	17.65	6.05
FeTi	0.58	27.36	52.01	14.77	4.99
TiC	0.62	24.51	45.80	22.69	7.00
TiN	0.77	31.11	47.97	16.32	4.60
VC	0.61	26.56	46.48	19.24	7.72
NbC	0.58	29.77	45.74	18.97	5.52
SiC	0.68	27.16	44.89	21.59	6.36
TiO_2	0.81	30.89	40.96	20.37	7.78
Al_2O_3	0.74	30.48	43.95	18.50	7.07
MgO	0.62	33.09	44.69	14.73	6.40
ZrO_2	0.55	35.53	45.43	14.21	4.82

the processes of deoxidation under the impact of the added compounds.

Results given in Table 3 are indicative of the fact that addition of refractory compound particles to the weld pool, makes a noticeable impact on the mechanical properties of the weld metal. Such an impact is associated with the changes in the metal structure, the consideration of which is the subject of this study.

1.3. Size distribution of nonmetallic inclusions. One cubic millimeter of the weld metal can contain up to 10^{10} nonmetallic inclusions of 30 nm to 3 μm size. However, only about 30% of them can have an active impact on new phase nucleation. Nonmetallic inclusions in the studied weld metal differed by their morphology. Very fine inclusions of up to 0.3 μm size had single-phase structure in the form of refractory oxides, carbides or nitrides. Coarser inclusions of up to 1.0 mm size consisted of two or three phases — refractory inclusion and oxide phase based on manganese, silicon or titanium compounds. Inclusions of more than 1.0 μm size had multilayer morphology with presence of low-melting sulphides on the outer surface. It is believed that such inclusions form in the solid-phase metal solution and cannot affect formation of the primary structure [7]. Inclusions of the second type make the most noticeable impact on new phase appearance at formation of the secondary microstructure [8], but their participation in the processes of primary structure nucleation and growth still has not been widely covered. Without doubt the finest refractory inclusions were present in the liquid metal, contacted the growing dendrites and could affect their development. Proceeding from the above considerations, Table 4 gives the results of determination of both the total content of inclusions in the weld metal, and their distribution according to the three specified dimensional ranges.

1.4. Morphology of primary structure grains. Used methods of etching weld metal samples allowed forming data bases on the dimensions of both the dendrites and primary austenite grains. Obtained results are given in Table 5.

Figure 5 gives the images of weld metal samples after etching to reveal the primary structure.

1.5. Discussion of the obtained results. Influence of inoculants on primary structure morphology. Dendrites, which form in the weld metal, initiate on base metal grains, and grow mainly along the maximum thermal gradient to the weld center that leads to columnar dendrite shape. The width of columnar dendrites is associated with the size of base metal grains on the fusion line. However, as growing of some unfavourable oriented dendrites was suppressed by those

Table 5. Dendrite interaxial spaces λ and primary austenite grain size *d*

Size, μm	BA	FeTi	TiC	TiN	VC	NbC	SiC	TiO_2	Al_2O_3	MgO	ZrO_2
Dendrites	80±17	57±13	100±20	55±12	70±15	50±12	100±21	100±19	57±13	152±23	158±22
Austenite	70±15	45±10	80±16	40±9	65±13	35±8	80±18	80±17	45±10	70±13	75±15

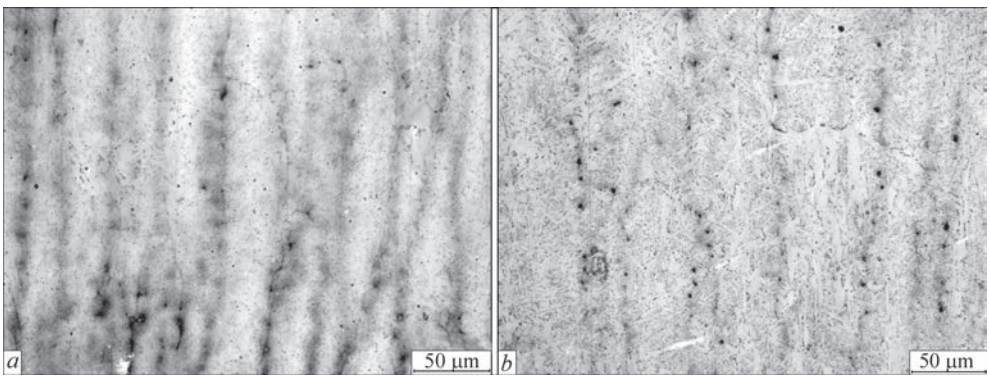

Figure 5. Primary structure of weld metal BA (*a*) and ZrO_2 (*b*)

that grew faster, than certain dendrites increased in size, and, as was expected, were wider than the initial base metal grains.

As is seen from the results, given in Table 5, inoculation of refractory compound particles to the weld pool affects the morphology of dendrites and primary austenite grains. The composition of the refractory compounds for the experiments was selected with the purpose of revealing one of the possible mechanisms of their impact on the primary structure. According to the mechanism of inclusion action as «microcoolants», their effectiveness is determined by the level of latent solidification energy. The process of inclusion melting is accompanied by consumption of this energy and respective lowering of the temperature of the metal melt, in which they are located [8]. The higher the melting temperature of the compound, the larger the value of latent energy of melting and the greater the impact, which such inclusions will have on melt overcooling. Increase of overcooling level should affect the solidification rate, i.e. the dendrite size. Figure 6 shows the histograms, which were plotted by the results, given in Tables 1 and 5.

As one can see from the given results, there is no unambiguous dependence between the melting temperature of particles inoculated into the weld pool and the width of dendrites in the weld metal. The largest width of the dendrites is characteristic for the metal of welds, into the composition of which inclusions with melting temperature of 2715 and 2825 °C were inoculated, whereas dendrites in the metal of welds, inoculated by inclusions with a higher temperature, have much smaller dimensions.

Another mechanism of modification of the metal structure is associated with the possibility of epitaxial nucleation of the new phase in metal melts on the surface of nonmetallic inclusions, having crystalline lattice parameters, close to the dimensions of the lattice of δ- or γ-iron. The smaller the difference in the lattice dimensions, the higher should be the intensity of nucleation of the hard phase in the melt, and the smaller should be the dimensions of this phase (i.e. of dendrites) [9]. Figure 7 shows the histograms, plotted by the results, given in Tables 1 and 5.

Mismatch parameter D was calculated by the following formula

$$D = \frac{\gamma_\delta - \gamma_i}{\gamma_\delta},$$

where γ_δ and γ_i are the parameters of δFe crystalline lattice and inclusion, respectively.

Results of metallographic analysis showed that the greatest width is found in dendrites of the metal of welds, into the composition of which particles of zirconium and magnesium oxide were inoculated, which have the lowest parameters of mismatch to δFe lattice. Here, the weld metal dendrites, to the composition of which vanadium carbide particles with the same mismatch parameter as that of magnesium oxide were added, have noticeably smaller size. It can be assumed that the mechanism of dendrite nucleation on nonmetallic inclusions with crystalline lattice parameters, close to δFe dimensions in the metal of the studied welds, did not have a leading role.

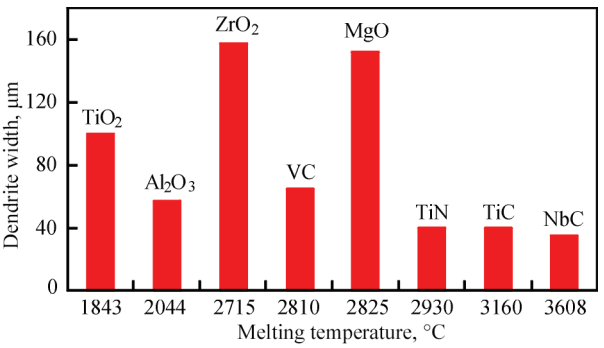

Figure 6. Dependence between the melting temperature of particles inoculated into the weld pool and width of dendrites in the weld metal

It is one of the possible mechanisms of modifying the metal structure, which is related to the impact of surface-active nonmetallic inclusions on interphase energy on the melt solidification front. The value of adsorption of the surface-active compound (Γ) is determined by its concentration in the surface layer, and the connection between adsorption and change of surface-tension value (σ) is described by Gibbs equation

$$\Gamma = -\frac{Q}{kT}\frac{d}{dQ}$$

where Q is the volume activity of the compound.

Compounds that lower the surface tension $\left(\frac{d\sigma}{dQ} \le 0\right)$, should accumulate on the interface, and

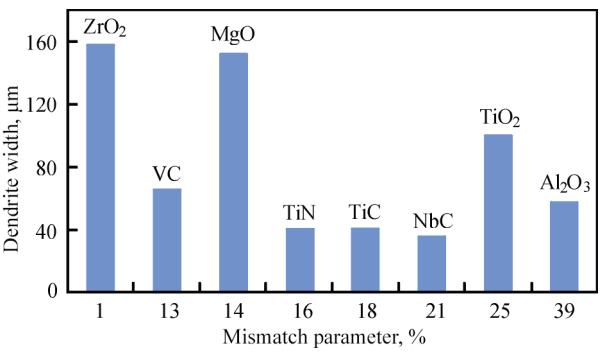

Figure 7. Dependence of the lattice parameter of mismatch of particles inoculated into the weld pool to δFe lattice and width of dendrites in the weld metal

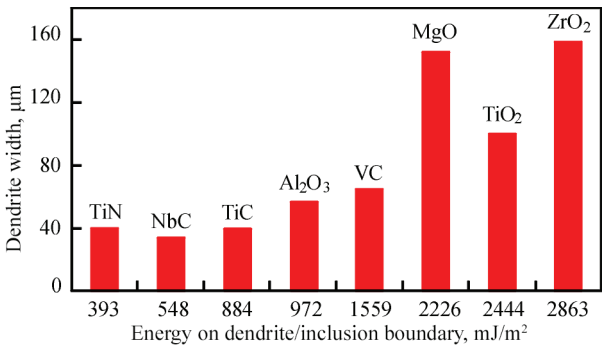

Figure 8. Dependence between the energy on dendrite boundary and particles inoculated to the weld pool and width of dendrites in the weld metal

compounds increasing surface tension $\left(\frac{d\sigma}{dQ} \geq 0\right)$ must move away from it [10].

Reduction of such energy in the zones of inclusion contact with the growing dendrite is accompanied by lowering of the required degree of overcooling and intensification of dendrite growth. Figure 8 shows a histogram, plotted by the results given in Tables 1 and 5.

Results given in Figure 8, are indicative of the fact that the change of surface energy on dendrite boundaries due to inoculation of refractory compound particles into the weld pool, affects the size of the dendrites. The case of adding TiO_2 particles somewhat falls out of this series that may be related to formation of more stable titanium compounds at high temperatures. Obtained results correspond to the dependence, which is described by the above Gibb's formula. Presence of inoculants in the metal melt, which lower the energy of the dendrite boundaries, promotes intensification of their growth in the direction of maximum temperature gradient. Dendrites with a large length-to-width ratio form in the metal of these welds, while inoculation of compounds that increase the dendrite grain boundary, leads to formation of wider dendrites with low length-to-width ratio.

As was already noted, the processes of formation of the weld structure occur at much higher rates than at solidification of large metal ingots. This can serve as an explanation of the fact that the activity of refractory particles in the weld pool melt as «microcoolants» or centers of epitaxial nucleation of the new phase is not as high as the manifestation of their surface-active impact.

During cooling a substructure appears in the columnar dendrite body, which is divided into grains with low-angle boundaries. This substructure can develop in different ways, depending on solidification parameters G/R, where G is the thermal gradient, and R is the solidification front speed. For a dendritic structure with a wider dimension of the dendrites, the solidification front speed is lower, so that they form primary austenite structures with coarser grains (Table 5). Thus, the weld metal forms a primary structure, in which the austenite grains are divided by both the high-energy and low-energy boundaries. The topography of these boundaries affects the nature of further development of weld metal structure during cooling.

Conclusions

Investigations of the impact of dispersed particles of refractory compounds inoculated into the weld pool on the features of formation of weld metal dendrite structure were studied. The connection between physico-chemical properties of the inoculants and morphology of the dendrites was analyzed. It is found that the inoculated compounds the most effectively exert their influence as surface-active substances at solidification of weld pool metal. It is noted that the refractory inoculants do not have any systematic approach on the solidification process as «microcoolants» or centers of epitaxial nucleation of the new phase. It is established that the most massive grains of primary austenite form in the body of the widest dendrites.

1. Yermolenko, D.Yu., Holovko, V.V., Stepanyuk, S.M. (2018) Cellular automata for simulation of dendritic growth with surface active refractory inoculants. *J. of Achievements in Materials and Manufacturing Eng.*, Issue 2 (**88**), June, 49–54.
2. (2008) *International standard ISO 14175:2008*: Welding consumables — Gases and gas mixtures for fusion welding and allied processes.
3. (2008) *International standard ISO 9692-1:2008*: Welding and allied processes — Recommendations for joint preparation. Pt 1: Manual metal-arc welding, gas-shielded metal-arc welding, gas welding, TIG welding and beam welding of steels.
4. (2003) *International standard ISO 17639:2003*: Destructive tests on welds in metallic materials — Macroscopic and microscopic examination of welds.
5. (1990) IIW Doc. No.IX-1533−88: Guide to the light microscope examination of ferritic steel weld metals. *Revue de la Soudure*, **4**, 29–41.
6. (2009) *International standard ISO 15792-1:2009*: Welding consumables –Test methods. Pt 1: Test methods for all-weld metal test specimens in steel, nickel and nickel alloys.
7. Gubenko, S.I., Parusov, V.V., Derevyanchenko, I.V. (2005) *Nonmetallic inclusions in steel*. Dnepropetrovsk, ART-Press [in Russian].
8. Zatulovsky, S.S. (1981) *Suspension pouring*. Kiev, Naukova Dumka [in Russian].
9. Gubenko, S.I., Oshkaderov, S.P. (2013) *Nonmetallic inclusions in steel*. Kiev, Naukova Dumka [in Russian].
10. Babaskin, Yu.Z. (1980) *Structure and properties of cast steel*. Kiev, Naukova Dumka [in Russian].

Received 26.10.2020

https://doi.org/10.37434/tpwj2020.06.02

FEATURES OF STRUCTURE FORMATION AND PROPERTIES OF JOINTS OF S460M STEEL MADE BY PULSED-ARC WELDING

A.V. Zavdoveev[1], **V.D. Poznyakov**[1], **M. Rogante**[2], **S.L. Zhdanov**[1], **V.A. Kostin**[1] and **T.G. Soloveichuk**[1]
[1]E.O. Paton Electric Welding Institute of the NAS of Ukraine
11 Kazymyr Malevych Str., 03150, Kyiv, Ukraine. E-mail: office@paton.kiev.ua
[2]Rogante Engineering Office
62012 Civitanova Marche, Italy

The work is a study of the impact of pulsed-arc welding process on structure formation and properties of the metal of the weld and HAZ, compared to welding by a stationary arc. In the case of high-strength steel S450M, it is shown that pulsed-arc welding allows effective regulation of structure formation. Owing to a change of TWC, the weld and HAZ form a mixed structure that allows achieving high values of strength and brittle fracture resistance. 14 Ref., 1 Table, 6 Figures.

Keywords: pulsed-arc welding, high-strength steel, weld and HAZ metal, thermodeformational cycle, structure, welded joint properties

Pulsed arc welding (PAW) is characterized by periodically changed arc power [1−4], and due to its features, it allows solving complex technological problems in fabrication of unique structures, increasing the productivity of the welding processes, surfacing steels by corrosion-resistant alloys. In industrialized countries PAW is ever wider applied in fabrication of welded structures from structural steels of up to 500 MPa strength. This is attributable to the fact that at PAW the possibilities for controlling the processes of electrode metal melting and transfer in different positions are expanded, weld formation is improved, electrode metal mixing with base metal and HAZ dimensions are reduced [5−12]. This is exactly why the known welding equipment manufacturers in their activity give a lot of attention to development and manufacture of equipment for realization and widening of the possibilities of gas-shielded PAW. The publications provide much more limited coverage of the questions of the influence of PAW parameters on thermal processes, occurring in the metal of welded joint HAZ, as they affect the structure and mechanical properties of this metal, its cold cracking and brittle fracture resistance, etc. For successful application of PAW, during development of modern welding technologies, it became necessary to study the impact of the modes of this welding process on formation of the structure and properties of weld and HAZ metal, compared to welding by a stationary arc.

Investigation procedure. Thermomechanically strengthened S460M steel (C440 strength class), made to DSTU EN 10025-4:2007, was used in the work. Chemical composition of S460M steel is as follows, wt.%: 0.15 C; 0.23 Si; 1.3 Mn; 0.09 Cr; 0.019 Ni; 0.01 V; 0.05 Nb; 0.025 Al; 0.013 S and 0.017 P.

Used as the power source was inverter-type rectifier of ewm Phoenix Pulse 401 model (MULTIMATRIX Company), which ensures different pulse frequency in pulsed-arc welding. Digital oscillograph UTD2000CEX-II was used for determination of welding-technological characteristics of the power source, which allows conducting fixation of volt-ampere characteristic of the power source in a broad range. 75ShSM shunt with 150 μOhm resistance was used for recording the oscillograms. It allowed recording up to 500 A welding current. Here, the voltage drop on the shunt was equal to 75 mV.

Mechanized welding in shielding gases (Ar + 18 % CO_2) of joints of S460M steel 16 mm thick with V-shaped groove was performed by 1.2 mm G3Si1 solid wire. Root passes in welding this steel were made on a copper backing. Welding using a traditional process (stationary arc) was conducted in the following mode: I_w = 180–200 A, U_a = 26 V, v_w = 15–

A.V. Zavdoveev — https://orcid.org/0000-0003-2811-0765, V.D. Poznyakov — https://orcid.org/ 0000-0001-8581-3526,
M. Rogante — https://orcid.org/ 0000-0002-6846-0826, V.A. Kostin — https://orcid.org/0000-0002-2677-4667

18 m/h. The automated PAW mode was as follows: I_{av} = 220–240 A, U_a = 26–28 V, v_w = 14–21 m/h.

In this case

$$I_{av} = \frac{I_i t_i + I_p t_p}{t_i + t_p},$$

where I_i is the pulse current (450 A), I_p is the pause current (160 A), t_i and t_p is the duration of the pulse and pause, respectively.

Note that in addition to average PAW current, also effective PAW current is used, $I_{ef} = \sqrt{(1-\delta)I_p^2 + \delta I_i^2}$, where δ is the pulse duty cycle. So, taking the above PAW parameters into account, $I_{ef} \approx 300$ A that is almost by 25 % higher than I_{av}.

Metallographic investigations were performed using Neophot-32 light microscope, microhardness of individual structural components and integral hardness of the metal were measured in M-400 hardness meter of LECO Company at 100 g load (*HV*). Samples for metallographic studies were prepared by standard procedures with application of diamond pastes of different dispersity. Microstructures were revealed by chemical etching in 4 % alcohol solution of nitric acid.

Standard samples were prepared to conduct mechanical testing and determine the cold resistance of welded joints. Samples for testing for static (short-time) tension corresponded to type II to GOST 6996–96. Impact bend testing was performed to GOST 6996–66 (type IX) at the temperature of 20 and –40 °C. The conducted test results were used to assess the impact of the welding process on the change of the following HAZ metal characteristics: strength (σ_y and σ_t, MPa); ductility (δ_5 and ψ, %) and impact toughness (*KCV*, J/cm^2).

Metal ability to resist brittle fracture was determined using fracture mechanics approaches. In keeping with fracture mechanics procedure, the critical coefficient of stress intensity K_{1C} is used for evaluation of metal sensitivity to stress concentration under the conditions of plane deformation at static loading (more often by bending). At increase of K_{1C}, metal sensitivity to stress concentration decreases. The second criterion of fracture mechanics — critical crack opening δ_c is a deformation criterion, and it is used for evaluation of metal resistance to crack initiation. It is applied for assessment of brittle fracture resistance of the metal under the conditions of high plastic deformation, when the crack reaches critical dimensions, δ_c value in its tip and starts propagating quickly, using the energy released at its further growth.

Values of K_{1C} and δ_c criteria were determined by standard procedures.

The values of critical stress intensity factor K_{1C} were determined by the following formula:

$$K_{1C} = \frac{PLY}{t\sqrt{b^3}}, \quad (1.1)$$

where P is the critical load, at which the sample breaks; L is the distance between the supports; t is the sample thickness; b is the sample width; Y is the sample form factor.

Critical crack opening δ_c was determined by the following formula:

$$\delta_c = \frac{4K_{1C}^2}{\pi\sigma_y E}, \quad (1.2)$$

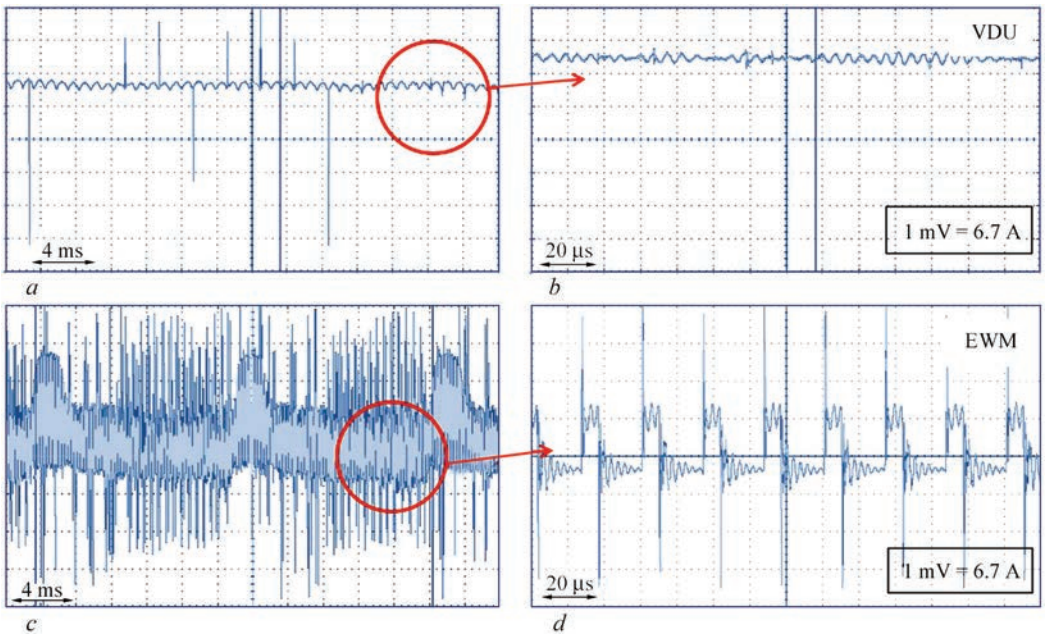

Figure 1. Oscillograms of welding current for power sources of diode and inverter types (for description see the text)

where E is the Young's modulus, which is equal to 200 GPa for steel.

The values of critical stress intensity factor K_{1C} and critical crack opening δ_c were determined on samples of a rectangular cross-section of 10×20×90 mm size with 7 mm long notch and 3 mm long fatigue crack. These samples were tested by three-point bending in the temperature range from 20 to −40 °C.

Research results and their discussion. *Welding-technological characteristics.* Power source ewm Phoenix Pulse 401 is of inverter type. In this connection, comparison of volt-ampere characteristics with VDU500 power source fitted with a rectifier was conducted. Results given in Figure 1 show that the above current sources differ essentially by the characteristics of welding current change. It is established that the stationary welding mode, using VDU power source is characterized by direct current with small oscillations. Current value in the oscillogram corresponds to 120 A. For ewm Phoenix Pulse 401 power source fitted with inverter rectifier, the dependence of the change of welding current is fundamentally different. At small scan waveform ($\tau \sim$ ms) a wide band of dense pulses of rather large amplitude is observed (Figure 1, *c*). In order to reveal the features of ampere characteristic, the scan waveform scale was increased to microseconds (Figure 1, *d*). Under such conditions, the peculiarities of welding current change are manifested, which are of a pulsed nature. Average welding current at pulsed-arc process was selected for comparison with the current of stationary arc welding.

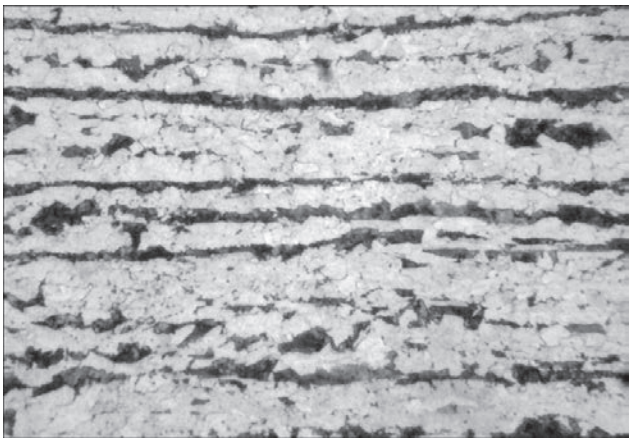

Figure 2. Microstructure (×500) of S460M steel

Base metal structure and properties. Owing to performance of thermomechanical rolling in the temperature range of 900–700 °C with controlled cooling, a ferrite-pearlite banded structure with hardness *HV*195 forms in S460M steel (Figure 2). Grain size number corresponds to No.10 to GOST 5639−82, and band point — to number 5 by scale 3 to GOST 5640−68.

Such a microstructure of S460M steel of the above-given composition ensures the following level of mechanical properties: yield limit $\sigma_{0.2}$ = 452 MPa, ultimate strength σ_t = 581 MPa, relative elongation δ_5 = 26 %; reduction in area ψ = 58 %.

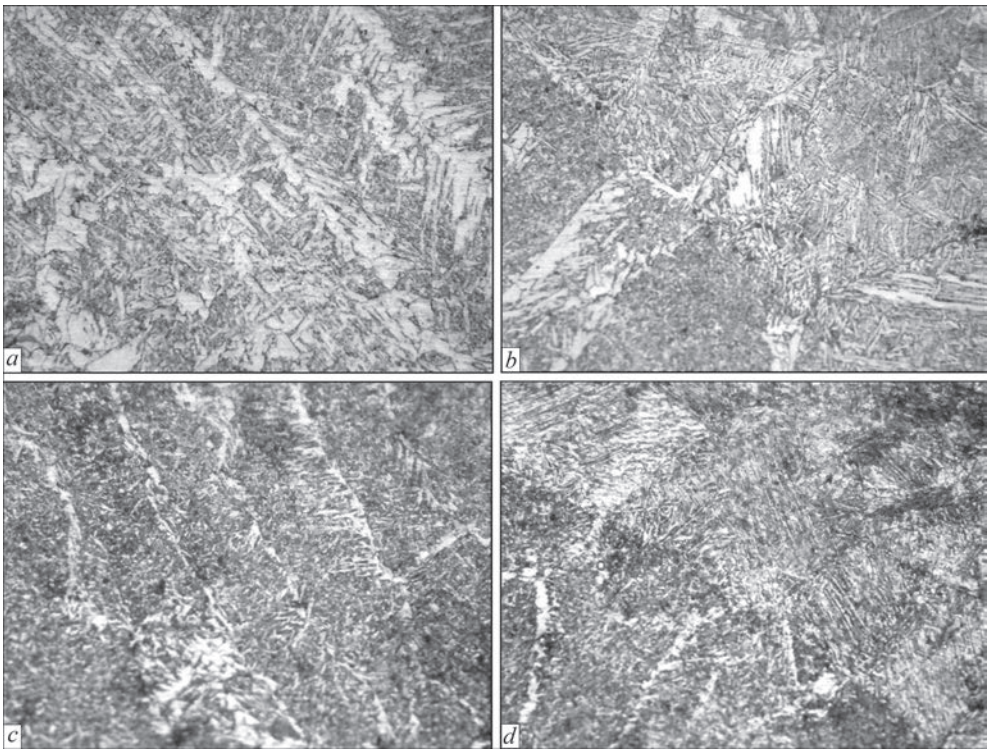

Figure 3. Microstructure (×500) of the metal of weld (*a*, *c*) and HAZ (*b*, *d*) of S460M steel, made by the traditional arc (*a*, *b*) and pulsed-arc welding

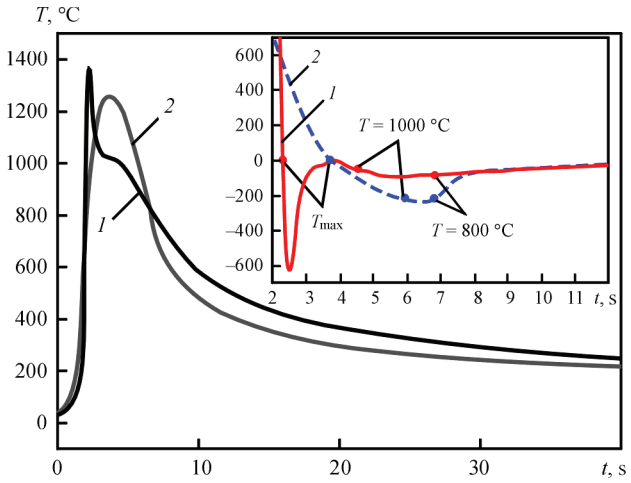

Figure 4. Thermal welding cycles for PAW (*1*) and AW (*2*)

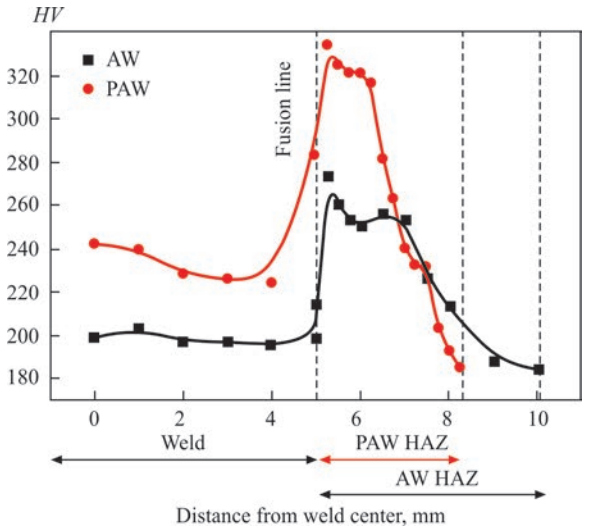

Figure 5. Hardness of welded joints of S460M steel

Metallographic studies of the structure (Figure 3) of welded joints of S460M steel showed that in welding by a stationary arc, the weld forms a predominantly ferrite structure of different modifications (polygonal, polyhedral, coarse acicular). Vickers hardness of such a structure is within 1950 to 2030 MPa. The microstructure of a coarse-grain zone of the HAZ consists of a mixture of upper and lower bainite. Vickers hardness of this HAZ zone reaches 2730 MPa. In the fine-grain zone of HAZ metal predominantly the structure of upper bainite is observed. The hardness of this HAZ zone decreases to 2600 MPa. In incomplete recrystallization zone of the HAZ, ferrite and pearlite form near the bainite zone that essentially lowers the hardness to 2130–2260 MPa.

At PAW the weld metal microstructure differs essentially from that of the metal of a weld, made by arc welding, namely: acicular ferrite needles are refined significantly (to 1–3 μm) and the amount of polyhedral ferrite decreases (to 5–10 %); polygonal ferrite precipitates, located on the boundaries of primary austenite grains, are narrowed considerably (to 3–10 μm). Such microstructural changes lead to increase of weld hardness to 2420 MPa. In the coarse grain zone of the HAZ metal a predominantly bainite structure with a small fraction of martensite (up to 3–5 %) is observed. The hardness of this HAZ region rises to 3250–3340 MPa, respectively. The structure of fine grain zone of the HAZ metal consists of a mixture of upper and lower bainite (2650–2810 MPa). Pearlite and ferrite are found in incomplete recrystallization zone of the HAZ that essentially lower the Vickers hardness of the metal to 2320–2400 MPa.

Such microstructural differences are due to the features of running of thermal welding cycles (TWC) at PAW (Figure 4), namely, metal cooling rate in the HAZ zones, which are heated to temperatures of 1000 °C and more, is lower than that during welding by a stationary arc. Due to that martensite components appear in the structure. In the HAZ, where the metal is heated up to temperatures below 1000 °C, the metal cooling rate is lower than in welding by a stationary arc. This promotes running of the diffusion processes during structural transformations, and, consequently, formation of a mixed bainite-martensite structure.

As noted by the authors of work [13], TWC has a key role at weld metal hardening, as it influences the refinement of the structural components. At PAW arc interruption occurs, which causes thermal «shock» (metal deposition is interrupted) that leads to increase of solidification centers. As a result, the structure is refined and strength characteristics are increased.

Hardness studies (Figure 5) of welded joints revealed that at PAW its level in the weld metal is 20 % higher than metal hardness in a weld made by the arc process. This is due to formation of a fine structure. In

Mechanical properties of 3460M steel welded joints at different welding methods

Weld length	Welding process	σ_y, MPa	σ_t, MPa	δ, %	ψ, %	KCV_{+20}, J/cm²	KCV_{-40}, J/cm²
Weld	AW	477	586	28	73	215	100
	PAW	570	667	24	68	212	111
HAZ	AW	632*	763*	–	–	149	150
	PAW	778*	940*	–	–	137	122
BM		452	581	26	60	111	95

*Calculated values [14]: σ_t — $HV0.31$, σ_y — $HV0.25$.

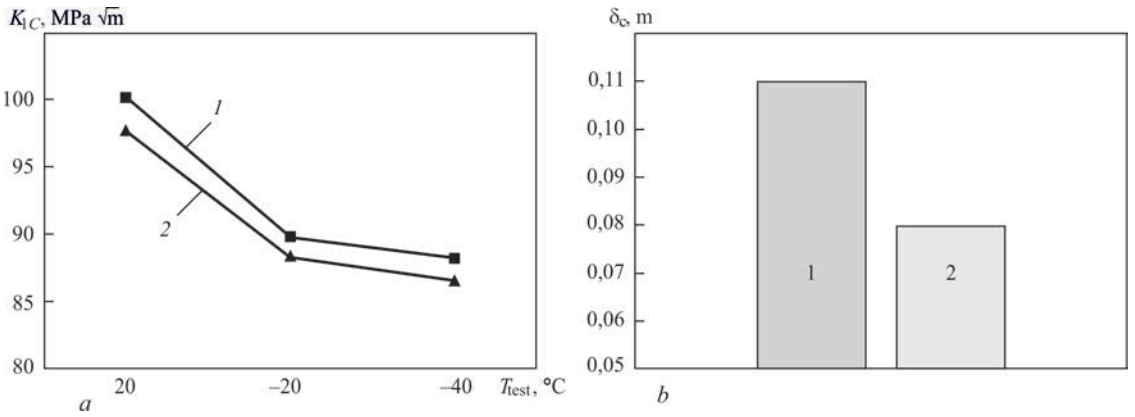

Figure 6. K_{1C} (*a*) and δ_c (*b*) for PAW: *1* — weld; *2* — HAZ

the HAZ the hardness values at PAW are also higher than at AW, but, despite that, they do not exceed the values of *HV*350, i.e. in such metal cold cracking will be improbable. It should be noted that at PAW, HAZ metal hardness decreases to initial metal level faster.

Mechanical properties of welded joints are given in the Table. One can see from the given data that under PAW conditions, higher strength values are achieved at preservation of impact toughness values on the level of the requirements of EN 10025-2 (SBC V2.6.-198:2014), $KCV_{-40} \geq 25$ J/cm^2. The values of brittle fracture resistance of welded joints made by PAW, despite the high hardness values, are at a rather high level (Figure 6) that is due to formation of a fine structure.

Thus, PAW allows effective regulation of structure formation in welded joints of high-strength steels. Under the conditions of approximately the same input energies, the effective welding current at PAW is by 25 % higher than in stationary arc welding. This allows increasing the penetration depth. The features of a pulsed change of welding current essentially change the TWC nature, and, consequently, the HAZ structure. Formation of a mixed structure in the HAZ allows achieving high values of strength and brittle fracture resistance.

Conclusions

Analysis of experimental data showed that at PAW, owing to a change of TWC (increase of the cooling rate in the temperature range > 1000 °C), a refined structure forms in the weld, compared to AW, and quenching structures form in the HAZ. Here, the HAZ metal cooling rate in the temperature range of 600–500 °C decreases practically 1. 5 times, that allows reducing the HAZ width by 40 %. As a result of testing, it was established that the metal of the welds and HAZ of welded joints of S460M steel, made by PAW, has sufficiently high brittle fracture resistance in the studied temperature range, and 20 % higher strength values.

1. Palani, P.K., Murugan, N. (2006) Selection of parameters of pulsed current gas metal arc welding. *J. Materials Proc. Technology*, **172**, 1–10.
2. Tong, H., Ueyama, T. et al. (2001) Quality and productivity improvement in aluminium alloy thin sheet welding using alternating current pulsed metal inert gas welding system. *Sci. Technol. Weld. Join*., 6(**4**), 203–208.
3. Needham, J.C., Carter, A.W. (1965) Material transfer characteristics with pulsed current. *Brit. Weld. J.*, **5**, 229–241.
4. Poznyakov, V.D., Zavdoveev, A.V., Gajvoronsky, A.A. et al. (2018) Effect of pulsed-arc welding modes on the change of weld metal and HAZ parameters of welded joints produced with Sv-08Kh20N9G7T wire. *The Paton Welding J*., **9**, 7−12.
5. Rajasekaran, S. (1999) Weld bead characteristics in pulsed GMA welding of Al–Mg alloys. *Weld. J.*, 78(**12**), 397–407.
6. Murray, P.E. (2002) Selecting parameters for GMAW using dimensional analysis. *Ibid.*, 81(**7**), 125–131.
7. Amin, M., Ahmed, N. (1987) Synergic control in MIG welding 2–power current controllers for steady dc open arc operation. *Met. Construct*., June, 331–340.
8. Amin, M. (1983) Pulse current parameters for arc stability and controlled metal transfer in arc welding. *Ibid.*, May, 272–377.
9. Lambert, J.A. (1989) Assessment of the pulsed GMA technique for tube attachment welding. *Weld. J.* 68 (2), 35–43.
10. Essers, W.G. Van Gompal (1984) Arc control with pulsed GMA welding. *Ibid.*, 6(**6**), 26–32.
11. Amin, M. (1981) Synergetic pulse MIG welding. *Metal Construction*, **6**, 349–353.
12. Dorn, L., Devakumaran, K., Hofmann, F. (2009) Pulsed current gas metal arc welding under different shielding and pulse parameters. Pt 2: Behaviour of metal transfer. *ISIJ Intern*., 49(**2**), 261–269.
13. Devakumaran, K., Ghosh, P.K. (2010) Thermal characteristics of weld and HAZ during pulse current gas metal arc weld bead deposition on HSLA steel plate. *Materials and Manufacturing Processes*, 25(**7**), 616–630, DOI:10.1080/10426910903229347.
14. Chukin, M.V., Poletskov, P.P., Gushchina, M.S., Berezhnaya, G.A. (2016) Determination of mechanical properties of high-strength steels by hardness. *Obrabotka Sploshnykh i Sloistykh Materialov*, 44(**1**), 28–35 [in Russian].

Received 06.02.2020

https://doi.org/10.37434/tpwj2020.06.03

STRUCTURAL CONDITION AND FATIGUE DAMAGEABILITY OF WELDED JOINTS OF STEAM PIPELINES

V.V. Dmytryk, A.K. Tsariuk, O.S. Garashchenko and **T.O. Syrenko**
National Technical University «Kharkiv Polytechnic Institute»
2 Kirpichova Str., 61002, Kharkiv, Ukraine E-mail: garashchenko.helena@gmail.com

At present time, a number of TPP power units having operated about 250000 h. in a relatively stationary operating condition, changed to a maneuver mode. This transition caused a need in studying damageability of their equipment according to the mechanism of fatigue and, in the first turn, welded joints of steam pipelines made of heat-resistant steels, operating under the conditions of creep. A further increase in fatigue damageability causes an improvement in the requirements to the initial structure of both the welded joints being produced as well as the parts to be repaired using welding. 14 Ref., 12 Figures.

Keywords: metal damageability; welded joints; fatigue cracks; structural condition; conditions of creep, dislocations

The operating time of a number of equipment of TPP power units, which are operated in the conditions of maneuver mode, exceeded 270000 h. As the operating time of the equipment increases, its damageability grows, respectively, which is realized both according to the mechanism of creep and the mechanism of fatigue [1, 2]. In our opinion, each of the mentioned mechanisms as well as their joint manifestation requires a separate consideration.

The intensity of the formation of fatigue cracks in welded joints of steam pipelines made of 15Kh1M1F and 12Kh1MF steels is predetermined by the presence of a certain structural, chemical and mechanical heterogeneity. This heterogeneity has a tendency to grow in the process of increasing the operating time of welded joints, which leads to an increase in the intensity of their damageability according to the mechanism of fatigue [3]. The formation of fatigue cracks in TPP equipment, as well as in welded joints of steam pipelines in relation to their operating time of up to 250000 h was considered in [4–6].

It was established that the joint manifestation of deformation processes and structural-phase changes in the metal of welded joints contributes to the reduction of their service life [6–8]. In the process of long-term operation, the initial structure of welded joints metal is transformed into a ferrite-carbide mixture [9], and its residual deformation increases [8]. Accordingly, the fatigue damageability of welded joints increases, which has its own characteristics. Taking into account that the propagation of fatigue cracks occurs mainly according to a brittle mechanism [5–8, 10], it is necessary to study the structural condition of welded joints as a controlling effect of crack propagation.

A tendency of accelerated formation of fatigue cracks is observed, which is associated, respectively, with the structural transformations in the metal of welded joints, which for a long time (over 270000 h) are operated in the conditions of creep and low-cycle fatigue. Therefore, to reduce fatigue damageability, it is advisable to increase the level of stability of the structure of welded joints.

The aim of the work is to specify the relationship between the structural condition of long-term operated (270000–300000 h) welded joints of steam pipelines made of steel 15Kh1M1F and 12Kh1MF and their fatigue damageability.

Procedure of studying microstructural condition. The microstructural condition of metal in the welded joints was studied using the methods and procedures of light and electron microscopy. Also the known procedures of transition from data in the cross-section plane to volumetric data were used. Accordingly, statistical methods were applied. The X-ray diffraction investigation of carbide phases was performed in the powder diffractometer «Siemens D-500» at a monochromatized copper radiation with a graphite monochromator on a reflected beam. The calculation was performed according to the Rietveld method.

A number of carbide phases and their sizes were determined in an experimental way. Metallographic analysis was performed in accordance with the requirements of standard documentation. By studying the crystal structure, determination of the chemical

V.V. Dmytryk — https://orcid.org/0000-0002-1085-3811, O.S. Garashchenko — https://orcid.org/0000-0002-9572-6095,
T.O. Syrenko — https://orcid.org/0000-0001-7333-7753

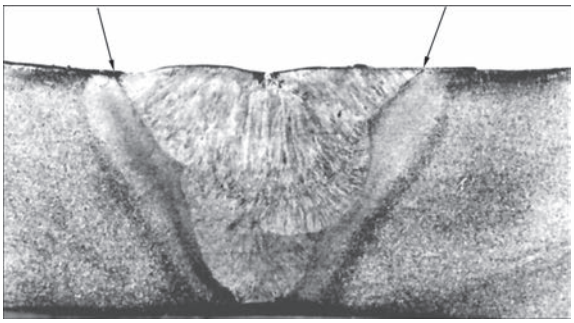

Figure 1. Macrostructure (×1.0) of welded joint of steel 15Kh1M1F (places of the largest stress concentrators are indicated by arrows)

composition and measuring of the average size of carbides in two mutually perpendicular directions, carbide phases were classified.

Metallographic examinations were carried out on 12 specimens of the same type, cut out from the existing steam pipelines made of steels 12Kh1MF and 15Kh1M1F. The operating time of the specimens was 270000–300000 h.

Studying the mechanism of fatigue crack initiation. The initiation and propagation of fatigue cracks in the elements of steam line systems occurs mainly in the areas of elevated stress concentration, which is predetermined by designing, technological and operational factors, as for example, in the upper zone of fillet welds, where the formation of undercuts is possible or in the area of fusion of the heat-affected-zone (HAZ) of welded joints (Figure 1).

Fatigue cracks have a wedged shape (Figures 2, 3) [4–6].

It was established that the influence of corrosive environment contributes to the accelerated propagation of fatigue cracks [4, 5] in the studied welded joints, which requires a separate consideration.

It is important to specify the peculiarities of initiation (incubation stage of formation) of fatigue cracks in welded joints, which significantly depends on their structural condition and plastic deformation.

The initial structure of the HAZ areas, as well as the base metal and the weld metal of welded joints

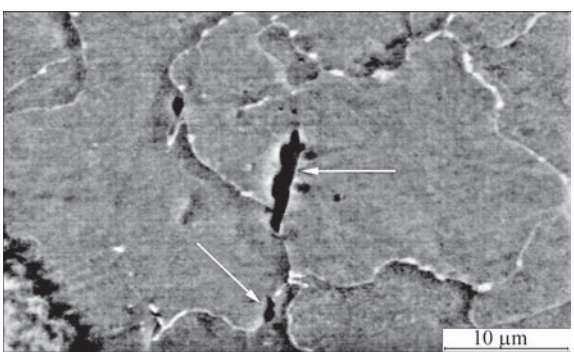

Figure 2. Fatigue cracks at the stage of initiation (arrows). Welded joint of steel 15Kh1M1F

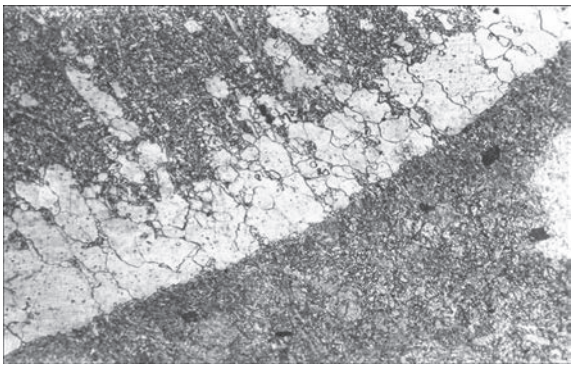

Figure 3. Fatigue crack at the stage of propagation. Welded joint of steel 15Kh1M1F (×2000)

with a different intensity is transformed into a ferrite-carbide mixture. The variable structural condition of long-operated welded joints largely depends on the level of their initial structural heterogeneity. The existence of such heterogeneity, which increases more with the longer operation period of welded joints, contributes to the formation of fatigue cracks. And first of all, the formation of cracks is predetermined by a probable existence of local rejection structures, which so far are not considered by standard documentation, but they are revealed in the existing welded joints of steam pipelines. In most cases, rejection structures have a local nature and their full detection by nondestructive testing methods is not possible. For example, in the area of HAZ fusion, which is subjected to welding heating to the temperature range T_L–T_S and has the sizes of 0.10–0.15 mm, in the initial structure enlarged ferrite grains can be formed, which are grouped in chains (Figure 4).

Ferrite grains can shift towards the area of HAZ overheating (size is 1.5–2.1 mm), which is subjected to welding heating to the temperature range T_S – 1150 °C (approximately). In the areas of fusion, overheating and normalization, the formation of large austenitic grains is possible (grain size number is 3–4, GOST 5639–82), which can be attributed to rejection structures. In the areas of overheating and normalization during welding of thick-walled pipes Widman-

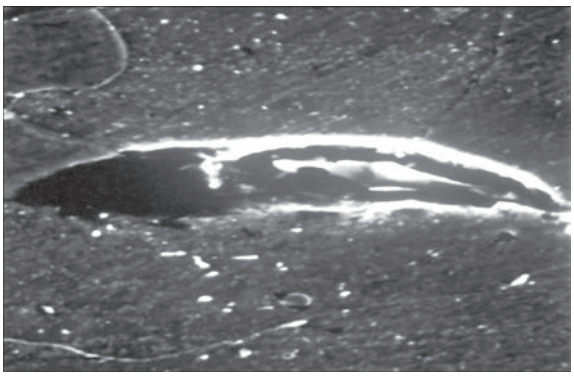

Figure 4. Rejection structure of the area of fusion of heat-affected-zone of welded joint of steel 15Kh1M1F

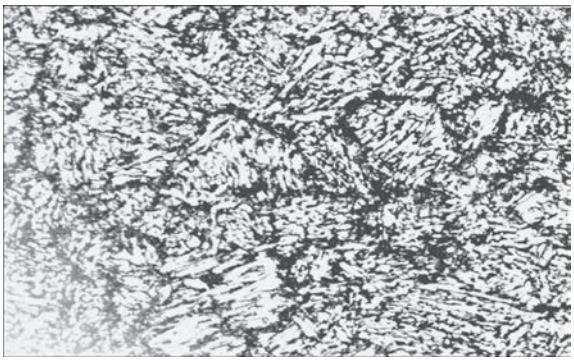

Figure 5. Microstructure (×300) of the area of partial recrystallization of HAZ of welded joint of steel 15Kh1M1F

stätten structure can be formed, which should also be considered as rejection one.

In the structure of the area of partial recrystallization of HAZ (welding heating to the temperature range A_{C1}–A_{C3}) globularized perlite (Figure 5) can be formed. The mentioned structure should also be classified as a rejection one.

Existence of local rejection structures, as well as structures that can be conditionally attributed to rejection ones, promotes the accelerated transformation of the initial structure of long-term operated welded joints into a ferrite-carbide mixture, i.e. degradation of the structure. The main features controlling the structural condition of welded joints (operating time is 270000–300000 h) [6–8, 11–13] are the following: transition of alloying elements from the α-phase to carbides; presence of segregation in the boundary zones of α-phase grains; coagulation of carbides. At the presence of

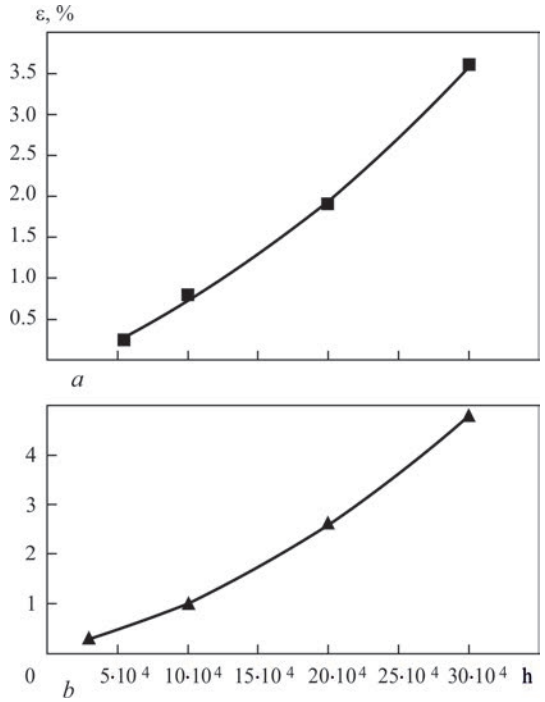

Figure 6. Dependence of deformation of HAZ areas of welded joints of steel 12Kh1MF on their operating time: *a* — metal of overheating area; *b* — areas of partial recrystallization

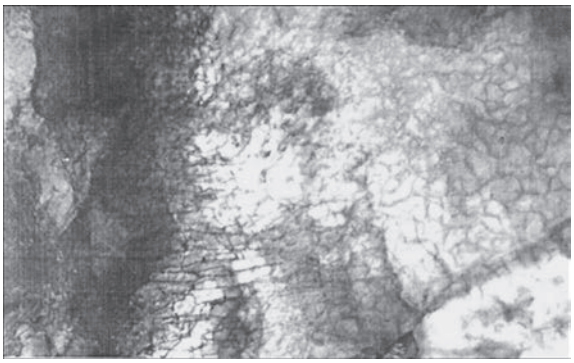

Figure 7. Dislocation structure of outer (near-surface) part of the area of partial recrystallization of HAZ of welded joint of steel 12Kh1MF. Service life is 280000 h, ε = 4 %

initial rejection structures, the structural condition is formed, characterized by the accelerated formation of fatigue damageability, which is approximately by 20–25 % larger as compared to the presence of the initial structure, in which these rejection structures are absent. We should note that damageability increases with an increase in the operating time of welded joints (after 300000 h), which requires an additional study.

It was found that in the abovementioned structures, which are considered to be rejection ones, the transition of chromium, molybdenum and vanadium from the α-phase to carbides is more intensive, it is approximately by 10–20 % higher than in the similar structures, which meet the standard requirements. The transition of chromium, molybdenum and vanadium promotes an increase in the deformation ability of α-phase grains and reduction in heat resistance [8]. At the presence of the considered structures, the resistance to deformation during long-term operation of welded joints decreases, and the damageability by fatigue cracks increases by approximately 15–25 %.

It was grounded that the initial rejection structures are formed in the conditions of an increased welding heating, whose application may be allowed both in producing new welded joints, as well as during welding repair of damaged elements of steam pipelines. We should note that to produce the initial structure of welded joints (especially, thick-walled ones) with the improved quality characteristics its is rational to determine welding heating by its modeling.

Discussion of investigations results. In the standard documentation it is envisaged that the deformation of steam pipelines should not exceed 1.0–1.5 % [11, 14]. However, the deformation of separate areas of HAZ at the duration of operation of welded joints being more than 250000 h is about 3–7 % [4–7]. The initiation of fatigue cracks occurs in the process of microdeformation of the metal of welded joints. The metal of the area of a partial recrystallization of HAZ of welded joints (Figure 5) at their operating time

Figure 8. Dislocation structure of the area of partial recrystallization of HAZ (middle part) of welded joint (see Figure 7)

of 270000–300000 h is deformed by approximately 4–7 %, and the base metal — by 0.5–0.7 %.

Figure 6 shows the dependence of the deformation of the HAZ areas of welded joints of steel 12Kh1MF (ε, %) on their operating time.

It was established that in the surface (outer) zone of the metal of the area of a partial recrystallization of HAZ the relatively highest local density of dislocations in the grains of matrix ferrite is observed (Figure 7). The density of dislocations in the middle and surface (inner surface of the steam pipeline) zones of the welded joint of the steam pipeline is much lower (Figure 8). In the structure of long-term operated welded joints, a change in the dislocation structure is observed. The largest change is typical to the areas of fusion, overheating and partial recrystallization of HAZ, the smaller is typical to the weld metal and the base metal. In the process of plastic deformation at the grain boundaries of the α-phase (matrix ferrite and tempering bainite), new dislocations are generated and dislocation annihilation occurs, which is confirmed by a decrease in the values of microhardness to 10–20 % as compared to the initial microhardness. The rate of weakening exceeds the strengthening.

The increase in local dislocation density is facilitated by $M_{23}C_6$ and M_7C_3 carbides coagulating in length, located at the grain boundaries of the α-phase. The formation of dislocations is associated with the diffusion movement of chromium and molybdenum from

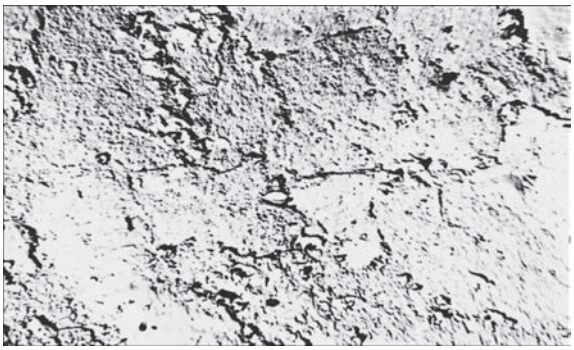

Figure 10. Polygonal structure (×4000) of the area of partial recrystallization of HAZ of welded joint of steel 12Kh1MF. Life is 186000 h

the central zones of α-phase grains to their boundary zones and the formation of segregation [11]. To a lesser extent, dislocations are formed in the grains of the α-phase (matrix ferrite), which is facilitated by the diffusion movement of vanadium and the formation of new, especially fine-dispersed VC carbides.

Microyield as an effect of microplastic deformation in the volume of α-phase grains is provided by running the processes of return and the initial stage of recrystallization [12]. The composition of the dislocation structure changes, which leads to the elimination of fragments of separate grain boundaries, and then to a complete elimination of such boundaries (Figure 9).

In the α-phase grains a polygonal structure is formed (Figure 10). Also blurring of separate initial subboundaries is observed. Near precipitations of the second phases, a developed network of dislocations with a curved shape is formed (see Figure 8). A local density of dislocations in the area of partial recrystallization of HAZ is much higher than in other areas, as well as in the base metal and in the weld metal.

Regarding butt welds (straight areas of steam pipelines), cyclic deformation of the metal has its own peculiarities. Respectively, in the HAZ areas, in the weld metal and in the base metal, the dislocation structure is developed in a differently way. The plastic yield, originating from the grain boundaries of the α-phase grains is also different. At a deformation of 5–7 %, which is

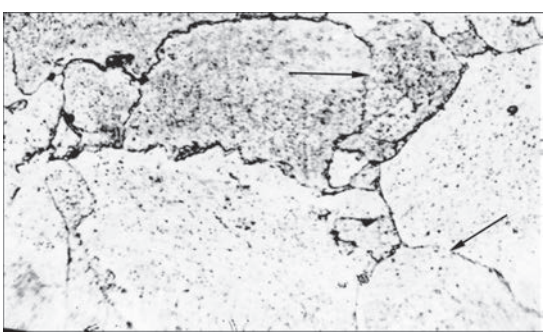

Figure 9. Microstructure (×360) of overheating area of HAZ of welded joint of steel 12Kh1MF (removal of fragments of grain boundaries is marked by arrows). Life is 280000 h

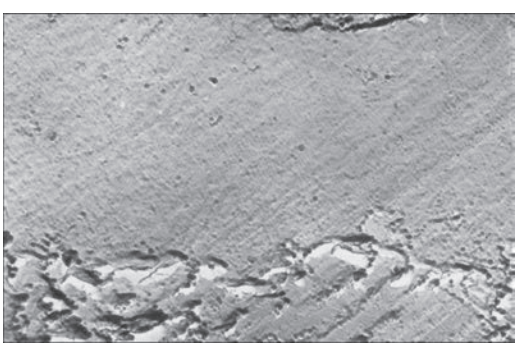

Figure 11. Sliding bands in the matrix ferrite of the area of partial recrystallization of HAZ of welded joint of steel 12Kh1MF. Life is 290000 h (×1100)

typical to the area of partial recrystallization of HAZ of welded joints from steel 15Kh1MF (operating time is 290000 h), in the grains of matrix ferrite, slip bands are revealed (Figure 11). At a lower level of deformation, the manifestation of slip bands is not observed.

It should be assumed that in the process of crack initiation (cyclic damageability) the study of the peculiarities of the formation of stable slip bands as a volume factor has a fundamental importance. The presence of slip bands in the structures of HAZ areas has different features (shape, length, quantity) from similar bands in the weld metal and in the base metal.

It was established that accumulations in the conditions of creep and low-cycle fatigue in the metal of welded joints of plastic deformation, is provided by the simultaneous movement of dislocations by the mechanism of sliding and the mechanism of climb. The presence of the climb mechanism is confirmed by the formation of creep pores near the coagulating carbides along the grain boundaries of the α-phase [7]. The movement of dislocations occurs to a greater extent according to the system {II2} <III> and to a lesser extent according to the systems{II2} <III> and{I23} <III>. When the dislocations intersect with the contact vector, which is normal to their sliding planes, steps are formed. Steps in the structure of welded joints can be single or sparse (deformation is ≤ 1 %). Their number increases at a deformation of 2–8 %. The formation of the configuration of steps is provided by the peculiarities of movement and intersection of dislocations, including the mobile dislocations with sedentary dislocations located along the grain boundaries. In the presence of precipitations of the second phases contacting with the steps, embryonic fatigue microcracks are formed (see Figures 2, 3). Their direction coincides with the greatest tangential stresses within the slip bands. Thus, embryonic fatigue microcracks have a crystallographic nature. The dislocation structure largely depends on the amplitude of the operating stress as well as on the energy of defects in the packing of the α-phase, which causes a local accumulation of dislocations in the grains of the α-phase, which is close to plane one (see Figure 7). The level of formation of sliding bands in the matrix ferrite is higher than in the tempering bainite (initial structure of welded joints bainite is 75–90 %, ferrite is the rest).

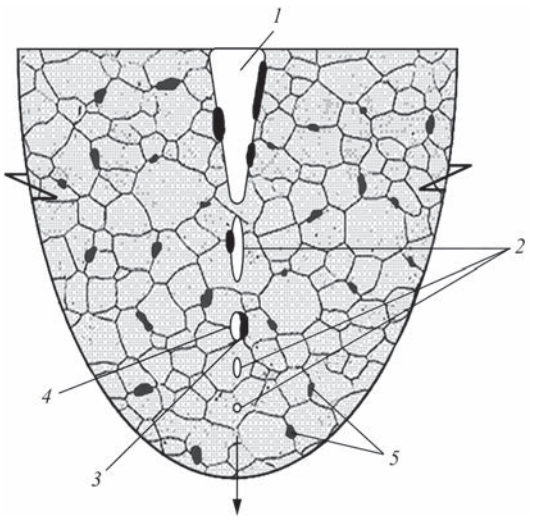

Figure 12. Scheme of fatigue crack formation: *1* — crack; *2* — fatigue micropores; *3* — carbide coagulating in length; *4* — creep micropore; *5* — carbides

In the places of contact of steps with precipitations of the second phases, at a long operation of welded joints in the conditions of creep, embryonic fatigue microcracks are formed. Micropores are originated the fusion of which provides the further formation of wedge-shaped microcracks (see Figures 2, 3). The study of the peculiarities of forming fatigue cracks, taking into account the structural condition, allowed providing the scheme of their formation (Figure 12).

It should be noted that the formation of fatigue microcracks is also contributed by the creep pores, located mainly on the grain boundaries of the α-phase in places where coagulating carbides $M_{23}C_6$ or M_7C_3 are located. The propagation of fatigue microcracks has an intercrystalline nature, and the mechanism of their propagation in the metal of welded joints (operating time is 270000–300000 h) is mostly brittle. The initiation and propagation of fatigue cracks is facilitated (to a large extent) by an increase in the cyclic nature of loads of welded joints of steam pipelines (over the last 5–8 years, a number of starts-stops of TPP power units has increased by about 30–50 %).

It is shown that in the slip bands, classified as fatigue ones, in the α-phase grains (operating time of welded joints is 270000–300000 h) the formation of microdiscontinuities is observed, which can be formally considered as embryonic micropores, the average diameter of which is approximately 100–400 Å. The shape of micropores may differ from spherical and ellipsoidal, which allows considering micropores as microcracks. The formation of embryonic fatigue micropores in the slip bands was for the first time discovered by V.S. Ivanova [10]. The initiation of fatigue microcracks mainly occurs by coalescence micropores and microdiscontinuities, which is possible at a directed diffusion of vacancies. As the operating time of welded joints increases (over 270000 h), the energy of activation of vacancies movement decreases, which is facilitated by the structural transformations occurring in their metal and the accelerated formation of microdiscontinuities.

An increase in the operating time of welded joints (over 300000 h) is characterized by a further change in the structural condition and features of forming fatigue cracks, which requires an additional study.

Conclusions

1. The structural condition of welded joints of steam pipelines made of steel 15Kh1M1F long time operating (270000–300000 h) in the conditions of creep and low-cycle fatigue, has a significant impact on their fatigue damageability.

2. The presence of structures in the metal of welded joints that can be attributed to the rejection ones, contributes to their accelerated degradation, which leads to approximately 15–20 % increase in the level of forming fatigue cracks in the metal of welded joints operating for a long time in the conditions of creep and low-cycle fatigue.

1. Dimić, I., Arsić, M., Medjo, B. et al. (2013) Effect of welded joint imperfection on the integrity of pipe elbows subjected to internal pressure. *Technical Gazette*, 20(**2**), 285–290.
2. Lazić, V., Aleksandrović, S., Arsić, D. et al. (2016) The influence of temperature on mechanical properties of the base material and welded joint made of steel S690QL. *Metalurgija*, 55(**2**), 213–216.
3. Katavić, B, Jegdić, B. (2007) Analysis of damages on water boiler shield pipes. *Welding and Welded Structures*, **4**, 123–130.
4. Khromchenko, F.A. (2002) *Residual life of welded joints of steam pipelines*. Moscow, Mashinostroenie [in Russian].
5. Trukhnij, A.D., Korzh, D.D., Kochetov, A.A., Rezinskikh, V.F. (1986) Investigation of low-cycle fatigue of steels 34KhM1A and EI415 after long-time operation in steam turbines. *Teploenergetika*, **3**, 32–35 [in Russian].
6. Dityashev, B.D., Popov, A.B. (2007) Complex approach to determination of residual life of steam pipelines of thermal power stations. *Ibid*., **2**, 21–25 [in Russian].
7. Dmitrik, V.V., Baumer, V.N. (2007) Carbide phases and damageability of welded joints at long-time operation. *Metallofizika. Novejshie Tekhnologii*, 2(**7**), 937–947 [in Russian].
8. Glushko, A.V., Dmitrik, V.V., Sirenko, T.A. (2018) Creep of welded joints of steam pipelines. *Ibid*., 40(**5**), 683–700 [in Russian].
9. Lazić, V., Arsić, D., Nikolić et al. (2016) Selection and analysis of material for boiler pipes in a steam plant. *Procedia Engineering*, **149**, 216–223. doi:10.1016/j.proeng.2016.06.659.
10. Ivanova, V.S. (1979) Fracture of metals. Moscow, Mashinostroenie [in Russian].
11. (2003) RD 10-577–03: *Model guidelines for inspection of metal and prolongation of the service life of main components of boilers, turbines, and piping systems of thermal power stations*. Moscow, NPO Prombezopasnost [in Russian].
12. (1987) MU 34-70-161–87: *Guidelines on metallographic analysis and examination of damage causes of steam pipeline welded joints from steels 12Kh1MF and 15Kh1M1F of thermal power stations*. Moscow, VTI [in Russian].
13. Dmitrik,V.V., Glushko, A.V., Tsaryuk, A.K. (2019) Recrystallization in the metal of welding joints of steam trucks. *Problems of Atomic Science and Technology*, 123(**5**), 49–52.
14. Dmitrik, V.V., Sirenko,T.A. (2012) To the mechanism of diffusion of chromium and molybdenum in the metal of welded joints of steam pipelines. *The Paton Welding J*., **10**, 20–24.

Received 11.03.2020

https://doi.org/10.37434/tpwj2020.06.04

INFLUENCE OF LOW-TEMPERATURE TEMPERING ON STRUCTURE AND PROPERTIES OF WELDED JOINTS OF HIGH-STRENGTH STEEL 30Kh2N2MF

O.A. Gaivoronskyi, V.D. Poznyakov, O.M. Berdnikova, T.O. Alekseenko and **O.S. Shyshkevych**
E.O. Paton Electric Welding Institute of the NAS of Ukraine
11 Kazymyr Malevych Str., 03150, Kyiv, Ukraine. E-mail: office@paton.kiev.ua

The results of investigations of influence of low-temperature tempering on structural changes, physical and mechanical properties of HAZ metal and crack resistance of welded joints of high-strength medium-carbon alloy steel 30Kh2N2MF are given. It is shown that the use of a low-temperature tempering is absolutely necessary during welding of products by low-alloy materials, which significantly increases the crack resistance of welded joints. During welding of joints by high-alloy materials in the hardened HAZ metal a relatively more ductile and less stressed structure is formed, in which the maximum level of stresses is lower than that which can be achieved after thermal tempering of a welded joint with a low-alloy weld. Therefore, the level of crack resistance of welded joints is sufficiently high in any case and in this situation there is no need to use low-temperature tempering. This is an unnecessary technological operation that does not significantly affect the reliability during operation of products, but only makes their cost higher. 13 Ref., 4 Tables, 6 Figures.

Keywords: high-strength steel, welded joints, low-temperature tempering, structure, properties, crack resistance

Thermal tempering of critical products of high-strength alloy steels, which are preliminary subjected to hardening, is a recognized technological operation. During tempering, in the metal diffusion processes of carbon redistribution in the structure and degassing of the hardened metal take place, which significantly increases its ability to microplastic deformation under the action of external load [1–3]. This contributes to a significant increase in crack resistance of critical products during operation, which is the main purpose of applying thermal tempering.

The similar positive changes during thermal tempering occur also in the structure of a hardened metal of HAZ and welded joints [4–6]. In addition, during degassing the level of hydrogen in the metal of welded joint, with which it is saturated during welding, is significantly reduced. Typically, in manufacture of metal structures from high-strength alloy steels, during welding of which low-alloy materials were used, low-temperature tempering is performed. After welding, not later than in 24 hours, they are subjected to tempering at a temperature of 200–250 °C for at least 3 h.

However, rationality of perfoming thermal tempering of joints, during welding of which high-alloy materials were used, remains a controversial issue today. First, as a result of carbon diffusion heat treatment of welded joints with a high-alloy weld can lead to the formation of brittle interlayers in the fusion zone [4–6]. Secondly, in a hardened HAZ metal of a welded joint with a high-alloy weld, as a result of the action of physical and metallurgical processes, already during welding proper a more ductile and less stressed structure is formed [7, 8]. And in the third, high-alloy metal has a high ability to dissolve hydrogen [9]. Therefore, during cooling of welded joint, its diffusion from a high-alloy deposited metal into the HAZ will proceed much more slowly as compared to a low-alloy one. This causes a significantly lower content of hydrogen in the HAZ metal of joints during welding by a high-alloy material and still there is no need in a further reduction of its content. In addition, it should also be taken in account that thermal tempering of welded metal structures is a high-cost technological operation, it requires the use of complex equipment and significant power consumption. Sometimes the material costs on thermal tempering amount up to 50 % of the cost of manufacturing a welded metal structure.

Taken the abovementioned into account, it can be assumed with a high degree of probability that it is most likely impractical to perform low-temperature tempering (LTT) of metal structures, in the welding of which high-alloy materials were used. But to prove this conclusion, it was necessary to conduct special comparative studies of changes in the parameters of the structure of a hardened HAZ metal and crack re-

O.A. Gaivoronskyi — https://orcid.org/0000-0002-5922-5541, V.D. Poznyakov — https://orcid.org/0000-0001-8581-3526,
O.M. Berdnikova — https://orcid.org/0000-0001-9754-9478, T.O. Alekseenko — https://orcid.org/0000-0001-8492-753X

sistance of welded welds of high-strength steel with low- and high-alloy joints before and after LTT. This was the purpose of the investigations, the results of which are given below.

Procedure of investigations. As the object of investigations, model specimens and welded joints of high-strength medium-carbon alloy steel of type 30Kh2N2MDF were used. On the model specimens, the influence of LTT on the change of physical and mechanical properties of a hardened HAZ metal was determined. At the same time steel of grade 30Kh2N2M0F of the following composition, wt.% was used: 0.36 C, 1.32 Si, 0.81 Mn, 1.65 Cr, 2.34 Ni, 0.50 Mo, 0.21 V. And during comparative investigations of changes in the structure of a hardened HAZ metal the welded joints were used, which after welding were not subjected to LTT. At the same time, steel of grade 30Kh2N2MDF was used having the composition similar to the abovementioned, but the carbon content in it was closer to the lower limit of alloying (0.31 % of C). In all cases, LTT, in case of its using, was performed during 3 h at a temperature of 230 °C within 15–20 h after simulation of thermodeformation cycle on the model specimens or after welding of joints.

The simulation of thermodeformation cycles of arc welding with the use of model specimens was performed in the installation MSR-75 [10]. At the same time, model specimens of two types were used – with a cross-section of 12×12 mm and 20×10 mm. The first specimens were used to determine strength ($\sigma_{0.2}$, σ_t), ductility (δ_5, ψ) and impact toughness (KCU_{+20}) and the second to determine critical stress intensity factor (K_{1C}) of a hardened HAZ metal. According to the accepted method of simulation, the maximum heating temperature of the model specimens was 1250 °C, the heating rate was 180–200 °C/s (heating time was 6–7 s). After heating, the specimens were immediately cooled at the rates from 4 to 20 °C/s ($w_{6/5}$), which are the most typical for the conditions of arc welding of multilayer joints. In the central part of the specimens, an area of metal of 40 mm width was formed homogeneous as to its structure. Then, from the model specimens, special specimens were made for testing on static tension and impact bending in accordance with GOST 1497 and GOST 9454, or static bending in accordance with GOST 25-506.

To determine the factor $K_{1C,}$ sequence of experiments was as follows. After simulating thermodeformation cycle of arc welding, a notch was prepared in the central part of the model specimens, from the top of which fatigue cracks of 3 mm depth were grown. After that, the specimens were tested under static bending load. During the tests, the value of critical load during propagation of the main crack was determined and the index of critical stress intensity factor K_{1C} was calculated according to the method of fracture mechanics [11].

The specimens of butt welded joints were prepared as follows. They were 10 or 20 mm thick and had a V-shaped groove, which was welded in a mechanized way in a mixture of shielding gases (82 % Ag + 18 % CO_2) by two materials. During welding of some specimens, the wire Sv-10GSMT was used, and other were welded using the wire Sv-08Kh20N9G7T. In both cases, the diameter of the wires was 1.2 mm. Welding modes were the same, namely: welding current was 160–180 A, arc voltage was 26–28 V, welding speed was 12–15 m/h (input energy was 8–10 kJ/cm). In case of welding using low-alloy wire, in order to avoid the probability of cold cracks formation in the HAZ metal of joints, preliminary heating of the metal to a temperature of 250 °C was used. When using high-alloy wire, the specimens were welded without a preheating. The temperature of the metal during multilayer welding of the specimens did not exceed 30–50 °C, to achieve which the specimens were cooled in air after applying each layer of the weld.

Crack resistance of welded joints was determined during their tests on resistance to the formation of fatigue cracks under cyclic bending loading in the installation UMP-02 in accordance with generally accepted methods [12]. The cycle stress under loading of welded joints was 60 MPa with a frequency of 14 Hz. As the evaluation criterion during tests, a critical number of load cycles was accepted, during which in the welded joint a fatigue crack with a length of 2–3 mm is formed.

To study structural changes in the metal of welded joints, standard methods of optical and electronic metallography were used. For optical metallography, the microscope Neophot-32 and the durometer M-400 were used. Parameters of a fine structure and dislocations density in a hardened HAZ metal were investigated in the transmission electron microscope (TEM) JEM-200CX of the JEOL Company. Subsequently, using experimentally detected structural parameters by the method of analytical evaluation, local inner stresses ($\tau_{l.in}$) were calculated [13].

Results of investigations and their analysis. At the first stage of investigations, the effect of LTT on the change of physical and mechanical properties of a hardened HAZ metal during testing of model specimens was determined. The determined indices of mechanical properties and fracture toughness of a hardened HAZ metal depending on its cooling rate are summarized in Table 1 and Table 2.

Comparing the obtained results of the tests given in Table 1, it is seen that after LTT the indices of temporary strength of HAZ metal are decreased to 10 %

Table 1. Effect of LTT on mechanical properties of HAZ metal of steel 30Kh2N2MF

Presence of LTT	$w_{6/5}$, °C/s	$\sigma_{0.2}$, MPa	σ_t, MPa	δ, %	ψ, %	KCU_{+20}, J/cm^2
No/Yes	Steel	1460	1780	11.1	48.6	80
	5	1262/1250	1490/1420	12.7/12.8	55.0/55.0	62.1/64.3
	15	1445/1430	1705/1580	11.2/12.1	48.3/50.3	54.6/58.0
	20	1502/1480	1805/1640	10.6/11.8	47.3/49.8	48.7/52.9

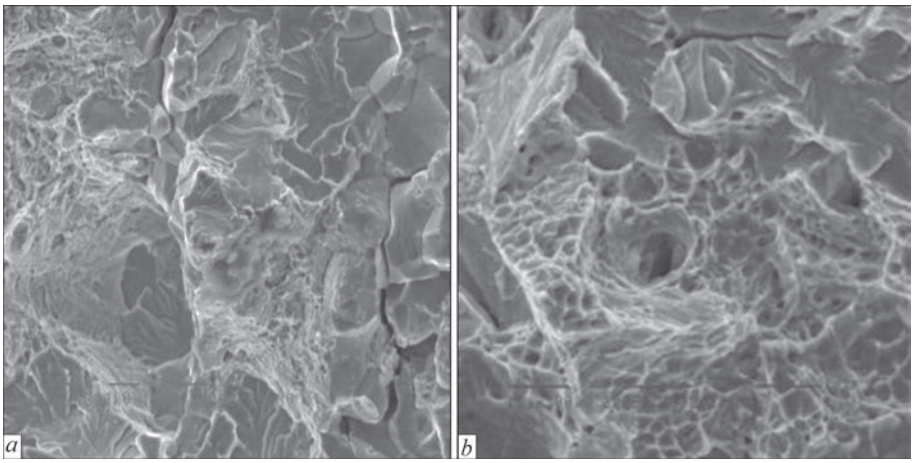

Figure 1. Typical surface of fracture of HAZ metal of steel 30Kh2N2MF ($w_{6/5}$ = 12.0 °C/s) in the area of main crack propagation without (*a*) and at the presence of LTT (*b*): *a* — ×1010; *b* — ×2020

(from 1490−1805 to 1420−1640 MPa), and the yield strength of the metal almost does not change and is at the level of 1250−1480 MPa. In this case, the values of ductility of a hardened metal at a static load δ_5 and ψ and the fracture impact toughness KCU_{+20} at an increased cooling rate is gradually increased by approximately 5.3 and 11.3 % and 8.6 %. The indices of critical factor of crack propagation K_{1C} are increased more significantly from 14 to 61 %, depending on the cooling rate (Table 2). After LTT, they are equalized in value regardless of the metal cooling rate during welding and are in the range from 96.8 to 100.9 MPa√m. In this case, the share of a viscous component on the surface of the specimens fractures increases significantly, more than 2 times, the fracture of which in both cases is characterized by a predominantly brittle intragranular type (Figure 1), and in case of absence of LTT — by the presence of intergranular brittleness with secondary cracks along the grain boundaries (Figure 1, *a*).

The carried out tests showed that during LTT of welded joints a hardened HAZ metal improves its ductile properties. This should be reflected also in an increased crack resistance of welded joints, which was determined in the second stage of investigations. For the tests under cyclic bending loading, the specimens of welded joints of steel 30Kh2N2MF were selected, during welding of which the wires Sv-10GSMT and Sv-08Kh20N9G7T were used. To testing butt welded joints with a thickness of 20 mm with a V-shaped groove were subjected, the welding of which was performed with a full penetration (welding of the weld root on the reverse side). The conditions of welding and testing of specimens are given above. The generalized results of test are presented in Figure 2.

Table 2. Effect of LTT on resistance of HAZ metal of steel 30Kh2N2MF to brittle fracture

Presence of LTT	Critical stress intensity factor K_{1C}, MPa√m		
	$w_{6/5}$ = 4.0 °C/s	12.0	20.0
No	87.8	69.7	60.0
Yes	100.9	100.1	96.8

As is seen, LTT facilitates the increase in crack resistance of welded joints of steel 30Kh2N2MF with both low-alloy as well as high-alloy weld. But the initial level of crack resistance and the degree of impact of LTT differs significantly depending on alloying of the deposited metal. During welding by a low-alloy

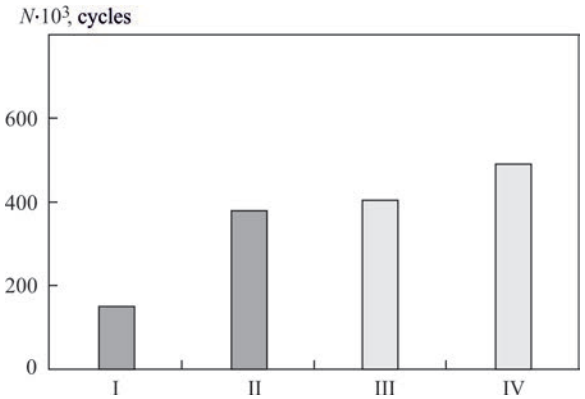

Figure 2. Resistance to the formation of fatigue cracks of butt joints of steel 30Kh2N2MF during welding by the wire Sv-10GSMT (I, II) and Sv-08Kh20N9G7T (III, IV) without (I, III) and at the presence of LTT (II, IV)

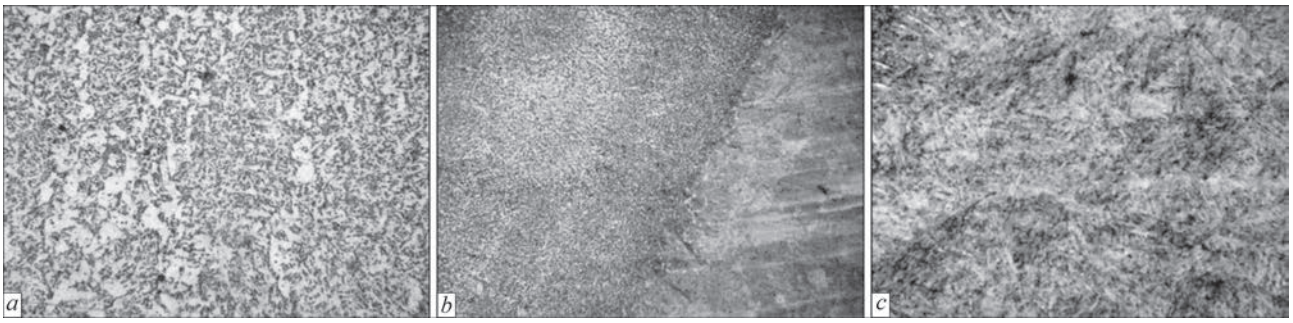

Figure 3. Microstructure of metal of joint of steel 30Kh2N2MF during welding by the wire Sv-10GSMT: *a* — central area of weld metal (×500); *b* — fusion zone (×200); *c* — near-weld area of HAZ at a distance of up to 700 μm from the fusion line (×500)

wire Sv-10GSMT, the resistance of welded joints to the formation of fatigue cracks without the use of LTT is almost 2.73 times lower than during welding with the wire Sv-08Kh20N9G7T. A comparative number of load cycles before the formation of fatigue cracks is 150 and 410 thousand cycles, respectively. It should be noted that welding of steel specimens with a low-alloy wire was performed using preheating to a temperature of 250 °C, and by a high-alloy wire without preheating. At the same time, the cooling rate in the HAZ metal was 3−5 and 20−25 °C/s, respectively. Therefore, in the HAZ metal of welded joint with a high-alloy wire, the conditions for the formation of a hardening structure were more rigid.

After LTT, the resistance of welded joints to fatigue cracking with a low-alloy weld is more than 2.5 times imcreased (from 150 to 380 thou cycles) and that of joints with a high-alloy weld is only 19.5 % (from 410 to 490 thou cycles). It should be noted that after LTT, the number of load cycles before the formation of a fatigue crack for a low-alloy weld does not exceed the level of high-alloy welds, even if they are welded without a preliminary heating and LTT. It is obvious that the established changes in the levels of crack resistance occurred as a result of positive changes in the metal structure of the welded material firstly, and secondly, directly while performing of LTT. Investigations in this direction was the goal of the third stage of research works.

The generalized results of investigations of influence of LTT on the change of a structural condition of the weld and near-weld area of HAZ of welded joints of steel 30Kh2N2MF are given in Table 3 and Table 4, and Figures 3−6 show the characteristic structures of the welded joints metal.

The examinations of the microstructure of the metal of welded joints with a low-alloy weld by the methods

Table 3. Structural parameters of metal of welded joints of steel 30Kh2N2MF during welding by the wire Sv-10GSMT

Area	Presence of LTT	Structural parameters					
		V_a, %	D_{gr} (for weld h_{cr}), μm	$HV_{0.1}$, MPa	h_l, μm	ρ, cm^{-2}	$\tau_{l.in}$, MPa
Weld	No	B_{gr}, 100	40−150	2450−2640	–	–	–
	Yes	B_{gr}, 100	60−160	2450−2640	–	–	–
HAZ	No	M, 100	20−50	5140−5720	0.4−0.8	$9\cdot10^{10}$–$1.6\cdot10^{11}$	1867−2988
	Yes	M, 100	20−50	4880−5420	0.4−0.8	$8\cdot10^{10}$–$1\cdot10^{11}$	1474−1867

Table 4. Structural parameters of metal of welded joints of steel 30Kh2N2MF during welding by the wire Sv-08Kh20N9G7T

Area	Presence of LTT	Structural parameters					
		V_a, %	D_{gr} (for weld h_{cr}), μm	$HV_{0.1}$, MPa	h_l, μm	ρ, cm^{-2}	$\tau_{l.in}$, MPa
Weld	No	A + F, 97 + 3	7−30	2210−2300	–	–	–
	Yes	A + F, 97 + 3	7−30	2210−2300	–	–	–
HAZ	No	B_l, 2−5	25−55	4210	0.4−0.6	$5–6\cdot10^{10}$	924−1109
		M, 95−98		4880−5090		$8–9\cdot10^{10}$	1474−1600
	Yes	B_l, 2−5	25−60	4210	0.4−0.6	$4–5\cdot10^{10}$	739−924
		M, 95−98		4420−4880		$7–8\cdot10^{10}$	1294−1474

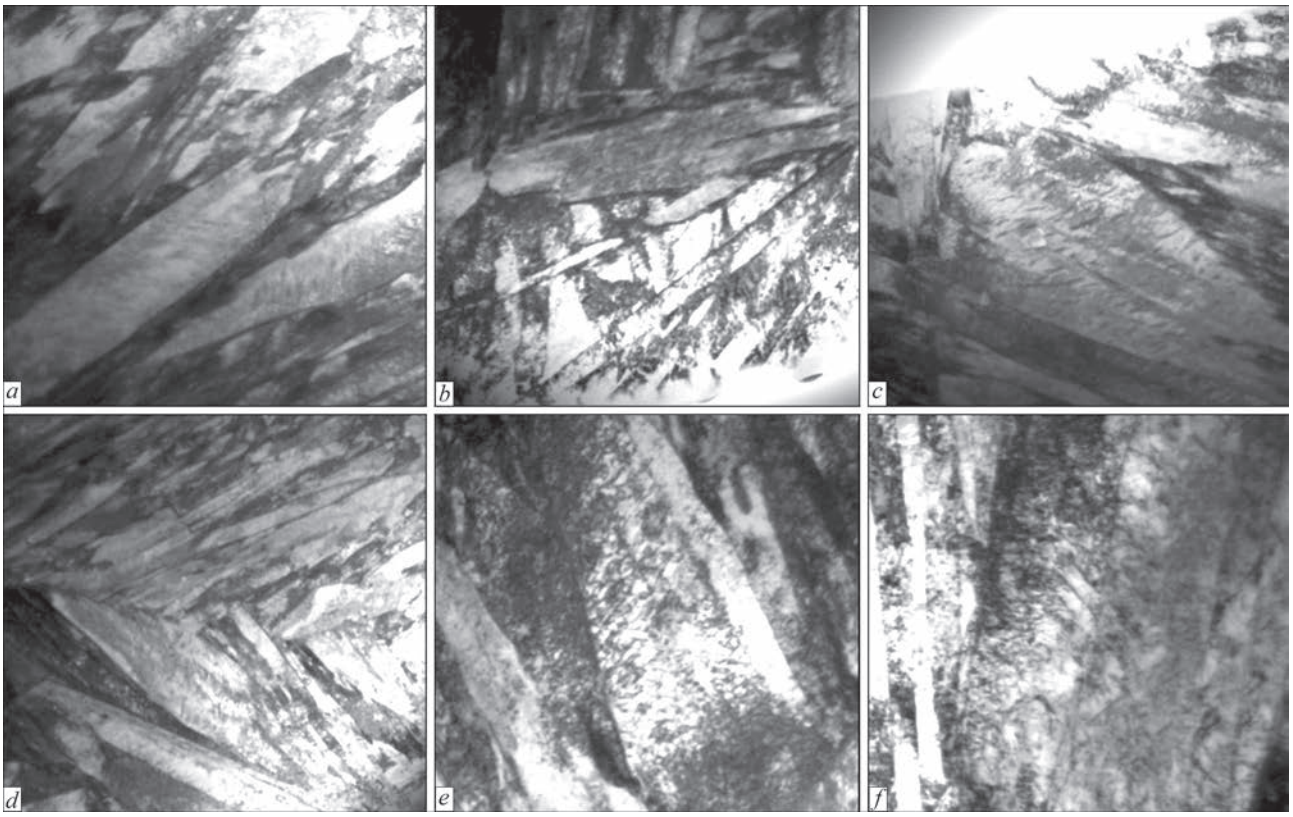

Figure 4. Fine structure of metal of near-weld area of HAZ of welded joints of steel 30Kh2N2MF (wire Sv-10GSMT) without (*a–c*) and at the presence of LTT (*d–f*): *a* — ×22000, *b* — ×25000, *c* — ×35000 — hardening martensite; *d* — ×22000, *e* ×52000, *f* — ×35000 — martensite tempering

of optical metallography showed that in the weld metal the structure of granular bainite (B_{gr}) with a crystallite size h_{cr} = 40−150 μm is formed and a microhardness of *HV*0.1 = 2450−2640 MPa (Figure 3, *a*). The structure of the metal around the near-weld area of the HAZ (coarse grain area) at a distance of 700 μm from the fusion line (FL) is represented exclusively by martensite with a grain size D_{gr} = 20−50 μm and a microhardness of 5140−5720 MPa (Figure 3, *c*). More detailed examinations applying the TEM method revealed that there is a hardening martensite (Figure 4, *a*, *b*) and partially a tempering martensite (Figure 4, *c*), with a size of laths h_l = 0.4−0.8 μm, dislocations density ρ in which is from $9 \cdot 10^{10}$ to $1.6 \cdot 10^{11}$ cm^{-2}.

After LTT, the phase composition, dimensions of crystallites in the weld metal and grains in the HAZ metal almost do not change. Microhardness of structural components in the weld metal also do not change. But, unlike the weld, in the near-weld area of the HAZ, the microhardness of martensite decreases by approximately 9 % — down to 4880−5420 MPa, and the density of dislocations in it decreases to $8 \cdot 10^{10}$–$1 \cdot 10^{11}$ cm^{-2} at a more uniform distribution (Figure 4, *d–f*). Moreover, the maximum level of local structural stresses ($\tau_{l.in}$), which is calculated as compared to the theoretical strength of the metal, is reduced to 40 % — from 2988 to 1867 MPa. Such reduction in the level of local stresses significantly contributes to the ability of hardened metal to microplastic deformation and its resistance to the formation and propagation of cracks under the action of external loads increases significantly. Therefore, during welding of joints of steel 30Kh2N2MF by a low-alloy wire Sv-10GSMT, the application of low-temperature tempering is absolutely necessary.

In the joints of steel 30Kh2N2MF, which were welded by a high-alloy wire Sv-08Kh20N9G7T, in the central part of the weld metal an austenitic-ferritic structure (A + F) is formed, in which the volume fraction of ferrite does not exceed 3 %. The size of the crystallites is 7−30 μm, microhardness of the structural components is in the range of 2210−2300 MPa (Figure 5, *a*). Near the fusion line, the size of the crystallites and microhardness are increased to 6−50 mm and 2450−2640 MPa, respectively (Figure 5, *b*).

The structure of the metal around the near-weld area of the HAZ, the depth of which is up to 300 μm, is mainly martensitic (95−98 %) with a small volume of bainite (2−5 %), the grain size is 25−55 μm (Figure 5, *c*). Without low tempering of welded joints, the microhardness of bainite is 4210 MPa and martensite is 4880−5090 MPa. Morphologically, this is a lower bainite (Figure 6, *a*) and a lath dislocation tempering martensite with a size of laths of 0.4−0.6 μm

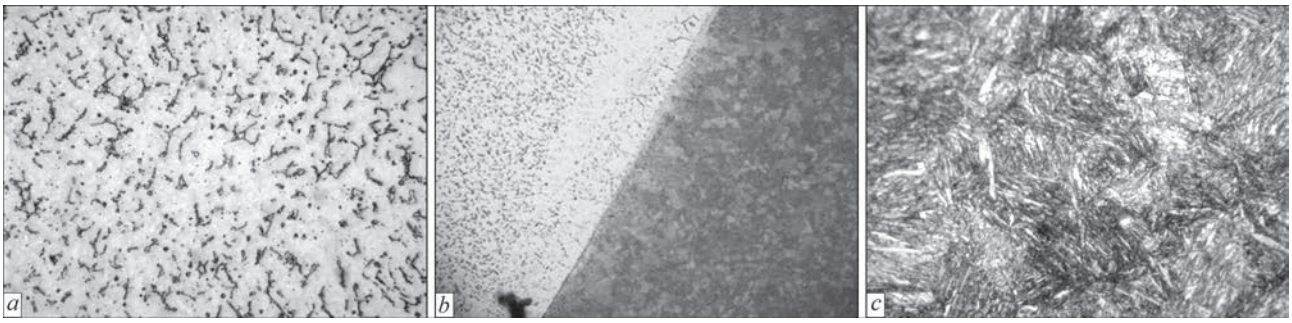

Figure 5. Microstructure of metal of joint of steel 30Kh2N2MF during welding by the wire Sv-08Kh20N9G7T: *a* — central area of weld metal (×500); *b* — fusion zone (×200); *c* — near-weld area of HAZ at a distance of up to 300 μm from the fusion line (×1000)

(Figure 6, *b*, *c*). The density of dislocations in the structural component of bainite, without the use of a low tempering, is $(5–6)\cdot10^{10}$cm^{-2}, and martensite is $(8–9)\cdot10^{11}$ cm^{-2}.

It should be noted that these values of dislocation density in the components of the structure of a near-weld area of the HAZ of welded joint with a high-alloy weld are much lower than during welding by the wire Sv-10GSMT. These values are lower even than those, which were obtained after LTT of welded joints with a low-alloy weld. This is associated with the peculiarities of the influence of thermodeformation processes in a high-alloy weld metal during cooling of joints on structural-phase transformations in the HAZ metal. In this case, the transformations are shifted to the area of higher temperatures with the formation of an intermediate structure of bainite, and during the formation of martensite the processes of its tempering occur [8].

After LLT the phase composition, sizes of crystallites and microhardness of strucutral components in a high-alloy weld metal and grain sizes in the HAZ metal, as well as in the welded joints with a low-alloy weld also almost do not change. But the changes in the following parameters of the metal structure of the near-weld area of the HAZ are observed. Thus, microhardness of the lower bainite does not change, and the density of dislocations in it decreases to $(4–5)\cdot10^{10}$ cm^{-2} (Figure 6, *d*). Microhardness of the martensite component decreases by 5 % to 4420–4880 MPa, the density of dislocations in it decreases to $(7–8)\cdot10^{11}$ cm^{-2} (Figure 6, *e*, *f*). At the same time, the maximum level of $\tau_{l.in}$ in bainite and martensite is reduced by 17 % (from 1109 to 924 MPa) and 8 % (from 1600 to 1474 MPa), respectively.

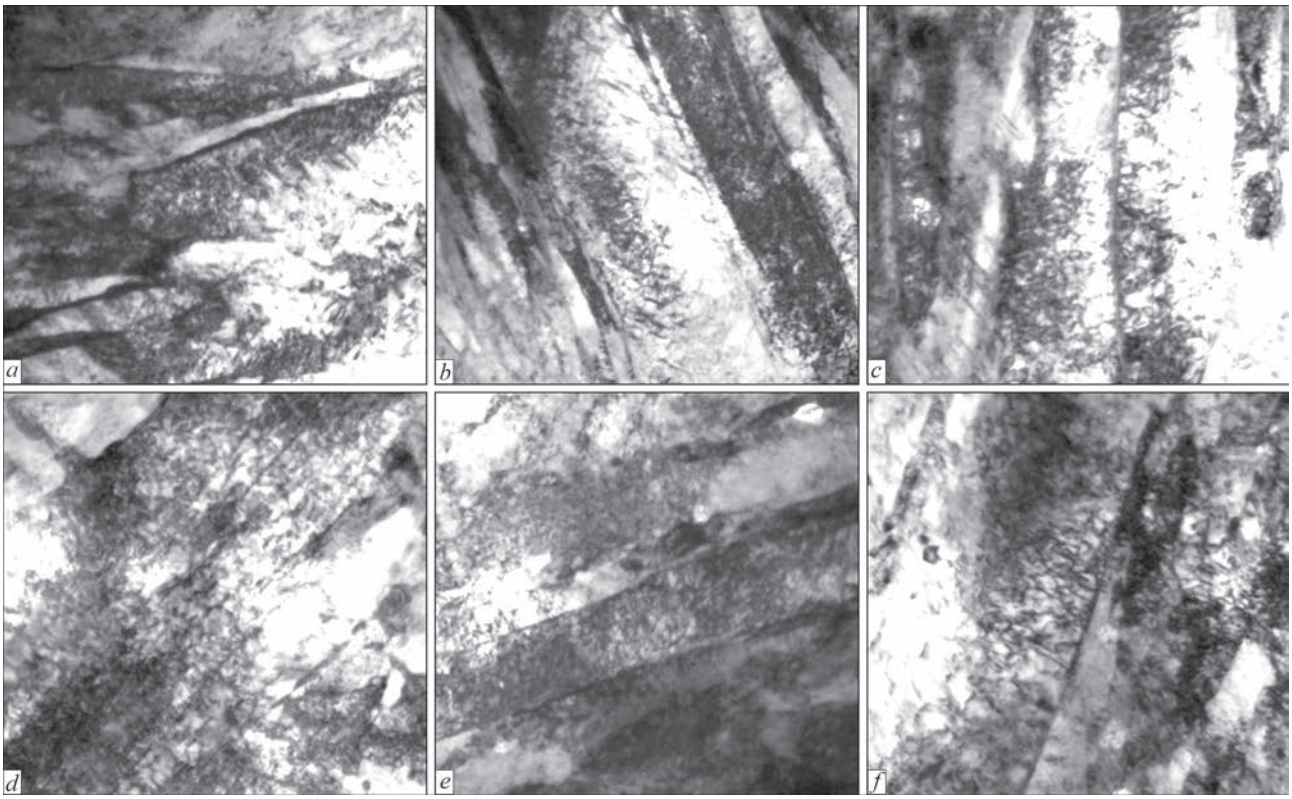

Figure 6. Fine structure of metal of near-weld area of HAZ of welded joints of steel 30Kh2N2MF (wire Sv-08Kh20N9G7T) without (*a*–c) and at the presence of LTT (*d*–*f*): *a* — ×52000, *d* — ×52000 — lower bainite; *b* — ×35000, *c* — ×52000, *d* — ×35000, *e* — ×52000 — tempering martensite

Comparing the obtained data, it is seen that the effect of LTT on the structure of joints welded by the wire Sv-08Kh20N9G7T is not as significant as for the joints with a low-alloy weld (Sv-10GSMT wire). If in the welded joints with a low-alloy weld after tempering the maximum level of structural stresses in the basic component of martensite is reduced to 40 %, then in the joints with a high-alloy weld to only 8 %. Moreover, in the initial state, without LTT, the difference in the levels of structural stresses amounts up to 1.9 times (respectively 2988 and 1600 MPa, see Tables 3 and 4).

The obtained data regarding the changes in the structure parameters correlate well with the results of tests of welded joints on fatigue failure. Therefore, during welding of joints of steel 30Kh2N2MF by high-alloy materials in a hardened HAZ metal, during the welding process proper a more ductile and less stressed structure is formed than that which can be produced after LTT of the welded joint with a low-alloy weld. Therefore, the crack resistance of welded joints of this steel during welding by high-alloy materials is at a high level even without additional heat treatment. LTT for such joints contributes to a slight additional increase in crack resistance, but it is not decisive. Therefore, the use of LTT for the products of a medium-carbon alloy steel 30Kh2N2MF under the conditions of their welding by high-alloy materials will not be significantly critical in terms of providing the reliability of welded joints during operation, and its use is irrational. This conclusion can be applied to all steels of this class. When using steels of other classes for critical products, additional investigations are required.

Conclusions

1. As a result of low-temperature tempering of welded joints of steel 30Kh2N2MF the changes in the parameters of a fine structure in a hardened HAZ metal occur. At the same time, in the HAZ metal of welded joints, the welding of which is performed by low-alloy materials, the processes of self-tempering of martensite run more actively, and the maximum level of local structural stresses is reduced to 40 %. Such a reduction of local stresses significantly contributes to the ability of a hardened metal to microplastic deformation under the action of external load. As a result, the resistance to fatigue formation of joints is more than 2.5 times increased. Therefore, during welding of joints of steel 30Kh2N2MF by a low-alloy wire Sv-10GSMT, the use of low-temperature tempering is absolutely necessary.

2. During welding of joints of steel 30Kh2N2MF by high-alloy materials in a hardened HAZ metal, a relatively more ductile and less stressed tempering martensite structure with a small amount of lower bainite is formed. The maximum stress level in this structure is 17 % lower than that, which can be obtained after LTT of a low-alloy weld. The crack resistance of welded joints during welding by high-alloy materials is at a sufficiently high level and does not require an additional increase. Therefore, there is no need to subject welded metal structures of products of steel 30Kh2N2MF to a low-temperature tempering under the conditions of their welding by high-alloy materials. This is an unnecessary technological operation, which does not significantly affect the reliability of the operation of products, but only makes their cost higher.

1. Bernshtejn, M.L. (1968) *Thermomechanical treatment of metals and alloys.* In: 2 Vol. Moscow, Metallurgiya [in Russian].
2. Lakhtin, Yu.M. (1983) *Metal science and heat treatment of metals.* Moscow, Metallurgiya [in Russian].
3. Fillipov, G.A., Sarrak, V.I. (1980) Local distribution of hydrogen and internal microstresses in structure of hardened steel. *Fizika Metallov i Materialovedenie*, **49**, 121–125 [in Russian].
4. Grabin, V.F., Denisenko, A.V. (1978) *Metal science of low- and medium-alloyed steels.* Kiev, Naukova Dumka [in Russian].
5. Efimenko, M.G., Radzivilova, N.O. (2003) *Metal science and heat treatment of welded joints*. Kharkiv, NTU KhPI [in Ukrainian].
6. Anokhov, A.E., Korolkov, P.M. (2006) *Welding and heat treatment in power engineering.* Kyiv, Ekotekhnologiya [in Russian].
7. Makarov, E.L. (1981) *Cold cracks in welding of alloyed steels.* Moscow, Mashinostroenie [in Russian].
8. Gordonny, V.G., Gajvoronsky, A.A., Sargevsky, V.A., Lebedev, Yu.M. (1992) Influence of type of weld metal on structure, properties and resistance of joints of high-strength hardening steels to cold cracking. *Avtomatich. Svarka,* **11–12**, 13–16 [in Russian].
9. Kozlov, R.A. (1969) *Hydrogen in welding of hull plate.* Leningrad, Sudostroenie [in Russian].
10. Poznyakov, V.A., Kostin, V.A., Gajvoronsky, A.A. et al. (2015) Effect of welding thermal cycle on structure-phase transformations and properties of HAZ metal of alloyed 30Kh2N2MF type medium-carbon steel. *The Paton Welding J.*, **2**, 7–13.
11. (1972) N*ew methods for evaluation of brittle fracture resistance of metals.* Ed. by Yu.N. Robotnov. Moscow, Mir [in Russian].
12. (1990) *Strength of welded joints under alternating loads.* Ed. by V.I. Trufyakov. Kiev, Naukova Dumka [in Russian].
13. Markashova, L.I., Grigorenko, G.M., Poznyakov, V.D. et al. (2009) Structural criterion for evaluation of strength, ductility, crack resistance of metals, alloys, composite materials and their welded joints. In: *Proc. of 4th Int. Conf. on Fracture Mechanics of Materials and Strength of Structures*, 447–451.

Received 12.05.2020

https://doi.org/10.37434/tpwj2020.06.05

EFFECT OF Co ADDITION ON INTERFACE REACTION BETWEEN Sn–Ag–Cu SOLDER AND Cu SUBSTRATE

Jianxin Wang, Yun Zhou and **Taikun Fan**
Jiangsu Provincial Key Laboratory of Advanced Welding Technology,
Jiangsu University of Science and Technology,
Zhenjiang, Jiangsu, China. E-mail: wangjx_just@126.com

Sn−Ag−Cu (SAC) alloys are considered as the most promising Pb-free solders in electronic industry. The solidification microstructure and interface reaction behaviors of SAC alloys are therefore of fundamental importance for the service reliability of electronic devices. This is particularly true for these SAC alloys with low silver contents, partially because the coarsened interfacial intermetallics (IMCs) of these low-Ag SAC alloys with higher surface tension than conventional near-eutectic SAC alloys. As a result, it is desirable to refine the grain size of interfacial IMCs between low-Ag alloys and common substrates such as Cu. In this work, the effects of addition of trace amount of Co on the interface reaction between both conventional SAC305 and low-Ag SAC107 alloys on Cu substrate have been studied by reflowing experiments at temperature close to 260 °C. In addition, effects of Co additions on the solid state growth of interfacial IMCs have been studied at 150 °C after ultra-long annealing treatment for 384h, 768, and 1536h. Both top-view and cross-section micro-graphs have been obtained using electron microscopes. It has been found that addition of trace amount of Co can significantly refine the interfacial Cu_6Sn_5 IMCs grains after reflow process and impede the growth of Cu_3Sn after annealing treatment. This attributed to the replacement of Cu atoms by Co atoms in Cu_6Sn_5 crystals, which in turn depresses the diffusion of Cu and impedes the transformation from Cu_6Sn_5 to Cu_3Sn during aging.

Keywords: lead-free solder, Sn−Ag−Cu, intermetallic compound, microstructure

Sn−Ag−Cu (SAC) alloys are considered as the most promising Pb-free solders in electronic industry. In order to further reduce the cost of SAC solder, new SAC alloys with lower Ag content have been widely studied [1], and alloying elements, such as Ni, Bi, Co, are selected as additions into these alloys [2−4]. In particular, the addition of trace amount of Co can effectively reduce the undercooling of Sn−Ag−Cu solder alloys, improve the mechanical properties, retard the formation of Cu3Sn IMCs, and suppress the void formation during interfacial reactions with Cu substrate [5−7].

In this work, the effects of addition of trace amount of Co on the interface reaction between both conventional SAC305 and low-Ag SAC107 alloys on Cu substrate have been studied by reflowing experiments at temperature close to 260 °C. In addition, effects of Co additions on the solid state growth of interfacial IMCs have been studied at 150 °C after ultra-long annealing treatment for 384h, 768, and 1536h. Both top-view and cross-section micro-graphs have been obtained using electron microscopes.

Experimental. Sn−3.0Ag−0.5Cu−*x*Co (*x* = 0, and 0.2 wt.%) and Sn−1.0Ag−0.7Cu−*x*Co (*x* = 0, and 0.07 wt.%) alloys were prepared, and then reflowed on Cu substrate using a RMA flux. The maximum soldering temperatures for Sn−3.0Ag−0.5Cu−*x*Co and Sn−1.0Ag−0.7Cu−*x*Co alloys were 260 °C and 265 °C, respectively, and the samples were cooled in the air after reflowing for 30 seconds. To reveal the effects of Co additions on the interface morphology of IMCs, microstructure observation was performed using an optical microscopy (VHX-900) and electron microscopy (JSM 6480).

Results and discussion. The cross-sections of IMC layers at solder/Cu interface in the as-sol-

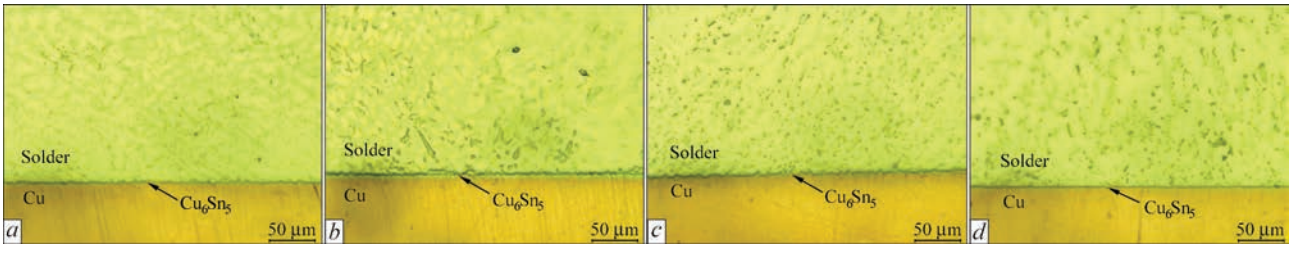

Figure 1. Cross-sections of IMC layer in as-soldered samples: *a* — Sn−3.0Ag−0.5Cu; *b* — Sn−3.0Ag−0.5Cu−0.2Co; *c* — Sn−1.0Ag−0.7Cu; *d* — Sn−1.0Ag−0.7Cu−0.07Co

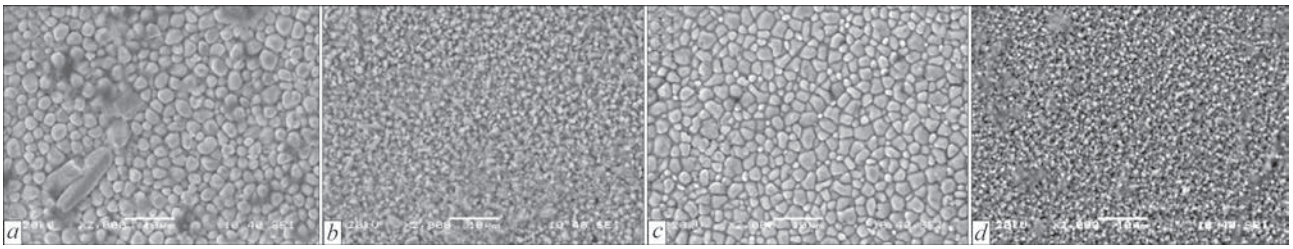

Figure 2. Top-views of IMC layer in as-soldered samples: *a* — Sn–3.0Ag–0.5Cu; *b* — Sn–3.0Ag–0.5Cu–0.2Co; *c* — Sn–1.0Ag–0.7Cu; *d* — Sn–1.0Ag–0.7Cu–0.07Co

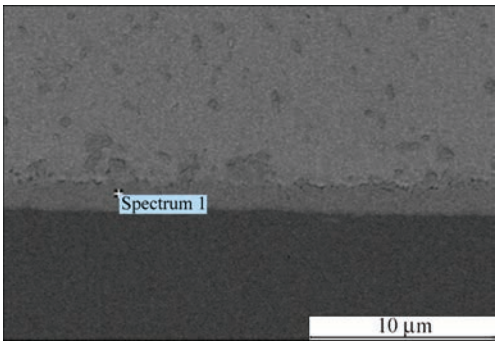

Figure 3. EDX test of IMC layer in as-soldered Sn–1.0Ag–0.7Cu–0.07Co sample

dered samples are shown in Figure 1. The morphologies of Cu_6Sn_5 are scallop-like in the as-soldered Sn–3.0Ag–0.5Cu and Sn–1.0Ag–0.7Cu samples (Figure 1, *a*, *c*), and thicker interfacial IMCs can be observed in the other two samples.

In the top-views as shown in Figure 2, it is found that the morphology of interfacial IMC is round shape in all the as-soldered samples after deep etching, while the sizes of interfacial IMCs grains with Co addition are much smaller than those of without Co addition. In other words, the addition of trace amount of Co can significantly refine the interfacial Cu_6Sn_5 IMCs grains after reflow process.

Table 1 shows the EDX results of interfacial IMC layers in as-soldered Sn–3.0Ag–0.5Cu–0.2Co and Sn–1.0Ag–0.7Cu–0.07Co samples in Figures 2, 3, in order to determine the composition of the interfacial IMC layer between the Sn–Ag–Cu–Co solder and Cu substrate. The intermetallic phase is likely to be expressed as $(Cu, Co)_6Sn_5$ phase, which is considered to be formed by substituting Cu atoms in binary compounds by Co atoms, consistent with previous result reported by Nishikawa et al. [7].

The morphologies of IMCs layer at the interface change obviously after isothermal aging, and severe coarsening and planarization of IMC grains can be found. The morphologies of Cu_6Sn_5 in Sn–3.0Ag–0.5Cu and Sn–1.0Ag–0.7Cu samples are planarized to be a thick layer after isothermal aging, while the interfacial IMC are much thicker with addition of trace amount of Co, as the cross-sections of the interface aged at 423 K for 384h in Figure 4. In the top-views of the IMC layers as shown in Figure 5, the morphologies of interfacial IMC are changed from roundshape into polyhedron-shape after isothermal aging. The grain sizes of interfacial IMC with Co addition are still smaller, and the grain refinement effect is obtained with 0.2 % Co addition.

After aged for 768h and 1536h, the Cu_3Sn layer can be obtained obviously at the cross-sections of the interface between SAC alloys and Cu substrates as shown in Figure 6, 8, which decreases the mechanical strength of solder joint due to its brittleness nature and

Table 1. EDX results of interfacial IMC layers in as-soldered samples

Region	Solder	Element, at.%		
		Sn	Cu	Co
Cross-section in Figure 3	SAC107–0.07Co	46.68	50.45	2.87
Top-view in Figure 2	SAC305–0.2Co	44.75	47.13	8.12
Top-view in Figure 2	SAC107–0.07Co	43.06	53.90	3.04

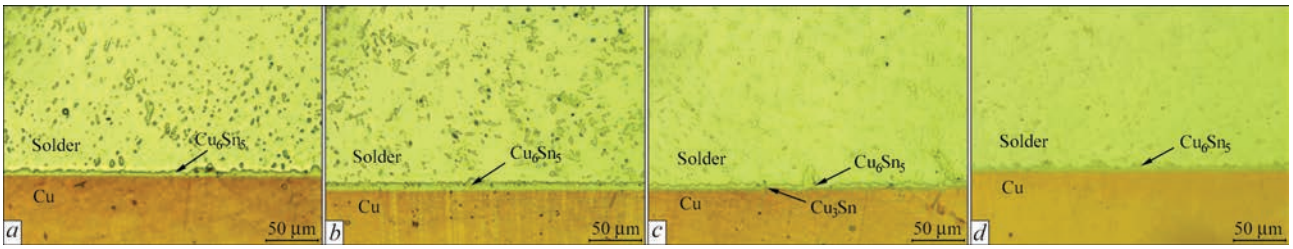

Figure 4. Cross-sections of IMC layer in 384h aged samples: *a* — Sn–3.0Ag–0.5Cu; *b* — Sn–3.0Ag–0.5Cu–0.2Co; *c* — Sn–1.0Ag–0.7Cu; *d* — Sn–1.0Ag–0.7Cu–0.07Co

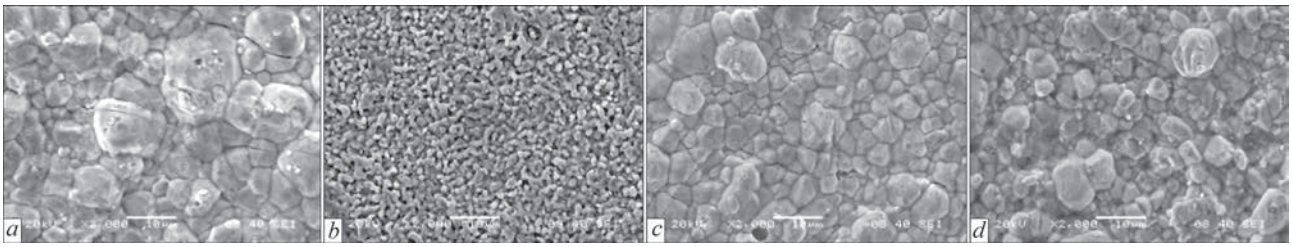

Figure 5. Top-views of IMC layer in 384h samples: *a* — Sn–3.0Ag–0.5Cu; *b* — Sn–3.0Ag–0.5Cu–0.2Co; *c* — Sn–1.0Ag–0.7Cu; *d* — Sn–1.0Ag–0.7Cu–0.07Co

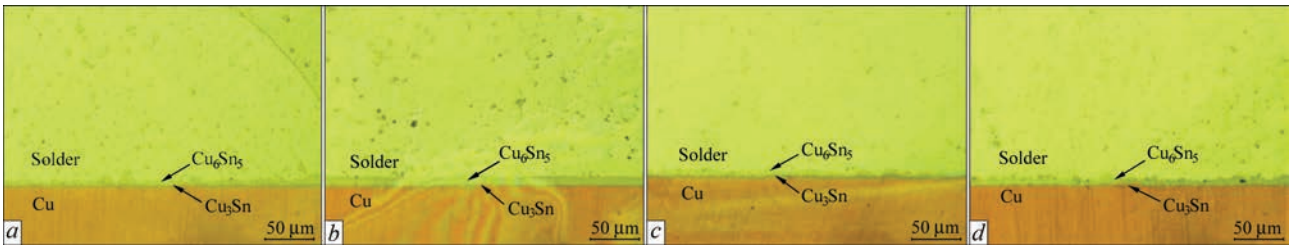

Figure 6. Cross-sections of IMC layer in 768h aged samples: *a* — Sn–3.0Ag–0.5Cu; *b* — Sn–3.0Ag–0.5Cu–0.2Co; *c* — Sn–1.0Ag–0.7Cu; *d* — Sn–1.0Ag–0.7Cu–0.07Co

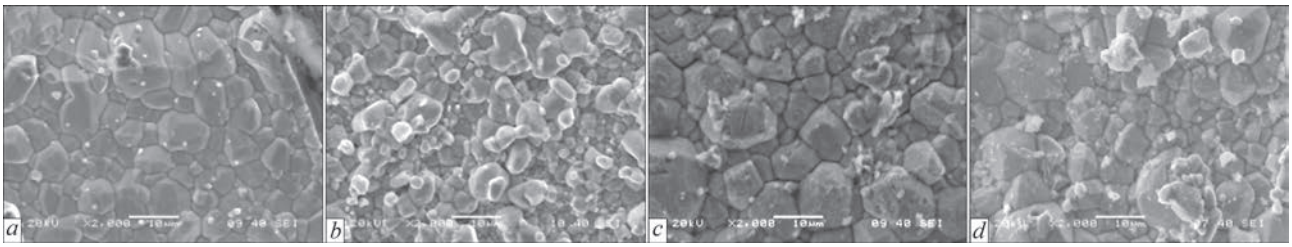

Figure 7. Top-views of IMC layer in 768h samples: *a* — Sn–3.0Ag–0.5Cu; *b* — Sn–3.0Ag–0.5Cu–0.2Co; *c* — Sn–1.0Ag–0.7Cu; *d* — Sn–1.0Ag–0.7Cu–0.07Co

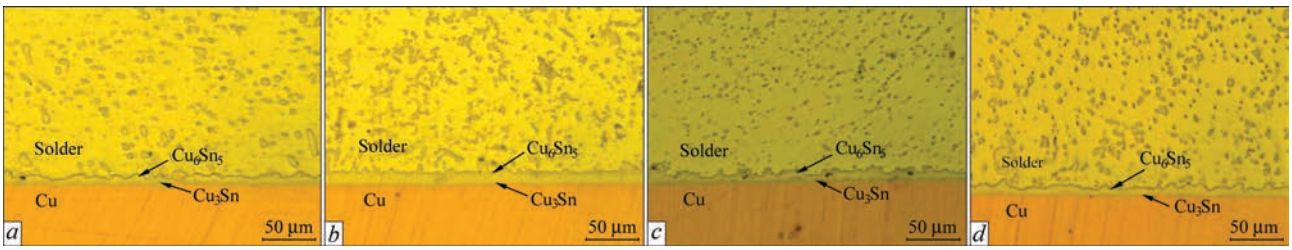

Figure 8. Cross-sections of IMC layer in 1536h aged samples: *a* — Sn–3.0Ag–0.5Cu; *b* — Sn–3.0Ag–0.5Cu–0.2Co; *c* — Sn–1.0Ag–0.7Cu; *d* — Sn–1.0Ag–0.7Cu–0.07Co

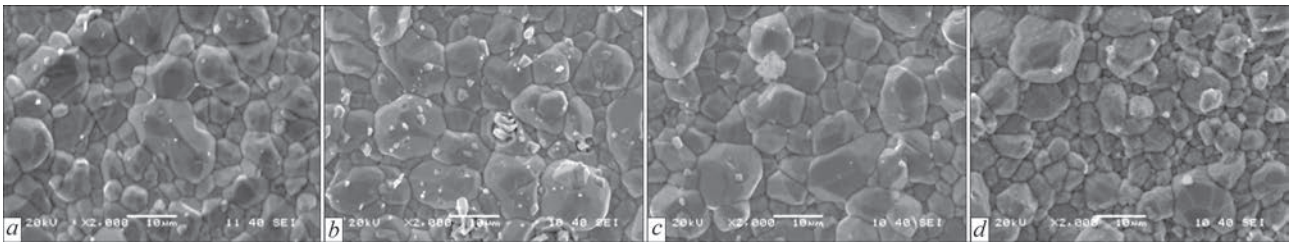

Figure 9. Top-views of IMC layer in 1536h samples: *a* — Sn–3.0Ag–0.5Cu; *b* — Sn–3.0Ag–0.5Cu–0.2Co; *c* — Sn–1.0Ag–0.7Cu; *d* — Sn–1.0Ag–0.7Cu–0.07Co

different CTE [8]. It is found that addition of trace amount of Co can impede the growth of Cu_3Sn after aging treatment, attributed to the replacement of Cu atoms by Co atoms in Cu_6Sn_5 crystals, which in turn depresses the diffusion of Cu and inhibits the transformation from Cu_6Sn_5 to Cu_3Sn during thermal aging. At the same time, the grain refinement effect of Co addition becomes weaker as the aging time increasing,

and the sizes of interfacial IMC grains in all samples become the same after 768h aging, according to the top-views in Figures 7, 9.

Conclusions

● Trace amount of Co can significantly refine the interfacial Cu_6Sn_5 IMCs grains after soldering.

● Co can inhibit the growth of Cu_3Sn after annealing treatment.

● Cu atoms are replaced by Co atoms in Cu_6Sn_5 crystals, depressesing the diffusion of Cu and impeding the transformation from Cu_6Sn_5 to Cu_3Sn during aging.

Acknowledgments. *The present work was carried out with the support of Natural Science Foundation of Jiangsu Province (BK20171308), Natural Science Foundation of the Jiangsu Higher Education Institutions of China (18KJA460002).*

1. Chen, X., Zhou, J., Xue, F. et al. (2015) Microstructures and mechanical properties of Sn−0.1 Ag−0.7 Cu− (Co, Ni, and Nd) lead-free solders. *J. Electron. Mater*., 44(**2**), 725−732.
2. Nishikawa, H., Komatsu, A., Takemoto, T. (2008) Effect of Ni or Co addition to Sn−Ag solder on microstructure and joint strength at interface. *Mater. Transact*., 49(**7**), 1518−1523.
3. Anderson, I.E. (2007) Development of Sn−Ag−Cu and Sn−Ag−Cu−X alloys for Pb-free electronic solder applications. *J. Mater. Sci.-Mater. El*., 18(**1**−**3**), 55−76.
4. Gao, F., Takemoto, T., Nishikawa, H. (2006) Effects of Co and Ni addition on reactive diffusion between Sn−3.5Ag solder and Cu during soldering and annealing. *Mater. Sci. Eng. A*., 420(**1**−**2**), 39−46.
5. Haseeb, A., Leng, T.S. (2011) Effects of Co nanoparticle addition to Sn−3.8Ag−0.7 Cu solder on interfacial structure after reflow and ageing. *Intermetallics*, 19(**5**), 707−712.
6. Kim, D.H., Cho, M.G., Seo, S.K., Lee, H.M. (2009) Effects of Co addition on bulk properties of Sn−3.5Ag solder and interfacial reactions with Ni-P UBM. *J. Electron. Mater*., 38(**1**), 39−45.
7. Nishikawa, H., Komatsu, A., Takemoto, T. (2007) Morphology and pull strength of Sn−Ag (−Co) solder joint with copper pad. *Ibid*., 36(**9**), 1137−1143.
8. Mu, D.K., McDonald, S.D., Read, J. et al. (2015) Critical properties of Cu_6Sn_5 in electronic devices: Recent progress and a review. *Curr. Opin. Solid. St. M*., 20(**2**), 55−76.

Received 26.05.2020

https://doi.org/10.37434/tpwj2020.06.06

GEOMETRICAL PARAMETERS OF THE BRAZED SEAM AND ITS STRUCTURE IN PLASMA BRAZING OF GALVANIZED STEEL

S.V. Maksymova, I.V. Zvolinskyy and **V.V. Yurkiv**
E.O. Paton Electric Welding Institute of the NAS of Ukraine
11 Kazymyr Malevych Str., 03150, Kyiv, Ukraine. E-mail: office@paton.kiev.ua

The paper presents the results of investigations of brazed joints of 08Yu galvanized sheet steel, produced by welding, arc and plasma brazing. It is confirmed that in the first case, spattering of the liquid pool metal, zinc evaporation and porosity formation take place. The influence of energy input on brazed seam parameters was studied in plasma brazing with application of BrKMts 3-1 brazing filler metal. It was found that increase of energy input leads to reduction of face reinforcement height, but promotes increase of back reinforcement height, that requires a greater amount of brazing filler metal. It was empirically determined that energy input value in the range of 520–590 J/cm ensures producing butt joints of galvanized 08Yu steel with optimum size of back reinforcement. X-ray microprobe analysis showed that high-quality dense welds form in this mode that have the structure of copper-based solid solution with dispersed inclusions of iron-based phase, enriched in silicon. 11 Ref., 1 Table, 9 Figures.

Keywords: plasma brazing. galvanized steel, brazing filler metal, energy input, seam parameters, structure

Corrosion protection of different structures is often realized through wide application of galvanized steel. In a number of cases, application of galvanized steel is related to producing permanent joints, which causes considerable difficulties. It is known that zinc starts melting at the temperature of 419.58 °C and at 907 °C it evaporates. In welding when the temperature of base material edges exceeds that of zinc boiling, the zinc coating burns out from both sides. To ensure reliable corrosion protection, the destroyed zinc layer has to be restored that leads to additional expenses. More over, zinc penetration into the liquid metal of the weld pool leads to formation of porosity, cracks, spatter, incomplete penetration and unstable arc burning [1–3].

Brazing is a promising method of producing joints of sheet steel with zinc coating. Unlike welding, brazing makes a much smaller thermal impact on the base material. The process of consumable electrode brazing (MIG-brazing) is used extensively to produce galvanized steel joints. The brazing filler metal is fed into the joint zone instead of the welding wire. The disadvantages of MIG-brazing are the dependence of current on wire feed rate; relatively high value of current for brazing sheets (high heat input leads to weld shrinkage and greater deformation) and brazing filler metal spattering that is related to zinc evaporation and defect formation [4–8].

The process of plasma brazing can be used as an alternative to MIG-brazing. In this case, the filler material (brazing filler metal) that is fed into the arc, is not live, that allows controlling the parameters of the brazed seam, irrespective of the filler material feed rate, by smooth adjustment of voltage and current. It reduces the heat input and the HAZ, and also ensures the stability of the process of producing permanent joints. Moreover, the higher pressure of the plasma arc promotes formation of a sound dense joint with preservation of zinc coating integrity.

The objective of the work is investigation of the structure, establishing the interrelation between the geometrical parameters of the weld, energy input and the size of the gap in galvanized steel joints that were produced by plasma brazing with application of BrKMts3-1 brazing filler metal.

Materials and investigation procedures. A special stand was prepared for conducting the experiments, (Figure 1), which includes argon-arc welding machine Master TIG MLS 2300 of Kemppi Company, pilot arc ignition block, wire feed device with smooth regulation range within 0–130 mm/s and a device for torch displacement at the speed of 0–25 mm/s.

Used as the brazing filler metal was copper alloy in the form of BrKMts 3-1 wire of 1 mm diameter with solidus temperature of 980 °C, and liquidus temperature of 1020 °C [9]. For comparative studies, welding was performed with application of wire of Sv08G2S grade as the filler material. Base metal was used in

S.V. Maksymova — https://orcid.org/0000-0003-0158-5760, I.V. Zvolinskyy — https://orcid.org/0000-0003-1442-7980,
V.V. Yurkiv —— https://orcid.org/0000-0001-8440-0391

Figure 1. Stand for arc (plasma) brazing

the form of plate samples of 08Yu galvanized steel of 150×60×0.8 mm size.

The composition of the used materials was as follows, wt.%:

BrKMts 3-1 . . . 2.75–3.5 Si; 1–1.5 Mn; 0.5 Zn; 0.3 Fe; 0.25 Sn; 0.2 Ni, Cu — base
08Yu steel . . . . . 0.35 Mn; up to 0.07 C; 0.02–0.07 Al; 0.03 Si; up to 0.025 S; up to 0.02 P; Fe — base
Sv08G2S . . . . 1.82.1 Mn; 0.7–0.95 Si; 0.25 Ni; 0.2 Cr; 0.2 Cu; 0.15 Mo; 0.05–0.11 C; 0.015 P; 0.018 N; Fe — base

Investigations were conducted on galvanized steel samples, produced by MIG-welding, MIG-brazing and plasma brazing in the horizontal position. Samples were cut out of permanent joints, and microsections for metallographic investigations were prepared by a standard procedure.

Microstructure and local elemental composition of the brazed joints were studied, using scanning electron microscope TescanMira 3 LMU, which is fitted with energy-dispersive spectrometer Oxford Instruments X-max 80 mm^2 and INCA software. Local distribution of chemical elements was determined in back-scattered electrons that allows studying the microsections without chemical etching.

Measurements of brazed seam parameters in joints of galvanized steel produced using plasma brazing, were performed in keeping with the scheme (Figure 2).

The energy input value was calculated by the following formula

$$Q = \frac{q}{V}, \text{ J / cm}, \qquad (1)$$

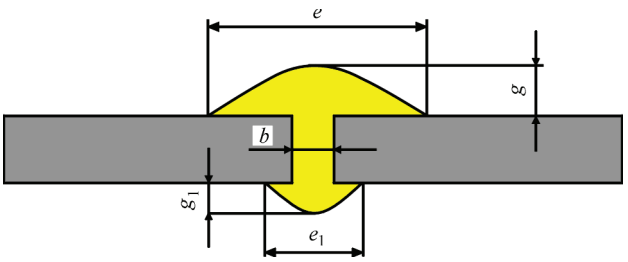

Figure 2. Scheme of brazed seam parameters: e — face reinforcement width; e_1 — back reinforcement width; g — face reinforcement height; g_1 — back reinforcement height; b — brazing gap size

where $q = \eta IU$ is the effective thermal power (J/s); η is the effective efficiency of the process of plasma heating of parts in an argon atmosphere (0.627; U is the arc voltage drop (V); I is the current (A); V is the welding-brazing speed (cm/s).

Experimental results and their analysis. Appearance of samples from galvanized steel, produced with application of MIG-welding (consumable electrode at reverse polarity) showed poor seam formation, and appearance of porosity (Figure 3, *a*, *b*) that is due to zinc evaporation from base metal surface.

MIG-brazing leads to spattering of filler material (through zinc evaporation), which is a disadvantage of this process (Figure 3, *c*).

In plasma brazing (Figure 4) of butt plate samples formation of dense brazed seams is observed without spattering of brazing filler metal (Figure 5, *a*), and without pores or defects (Figure 5, *b*).

Overlap joints are widely used in the car industry. As shown by experiments, producing overlap joints requires slight correction of the brazing process. So, the plasmatron is located at an angle to the vertical surface of base metal plates. As the vertical (at 90° angle) positioning of the plasmatron leads to the arc deflection towards the upper plate, in the optimized mode good formation of the overlap joint (Figure 6, *a*, *b*) is observed with appearance of a complete fillet section (Figure 6, *c*).

Results of investigation of the impact of energy input on the geometrical parameters of brazed seams showed that the back reinforcement height g_1 increases monotonically at a constant rate at increase of energy input (Figure 7, *a*). This leads to increase of the volume of metal from the weld back side, and has a

Figure 3. Appearance (*a*), and macrostructure (*b*) of the weld produced by MIG-welding and MIG-brazing (*c*) of galvanized steel

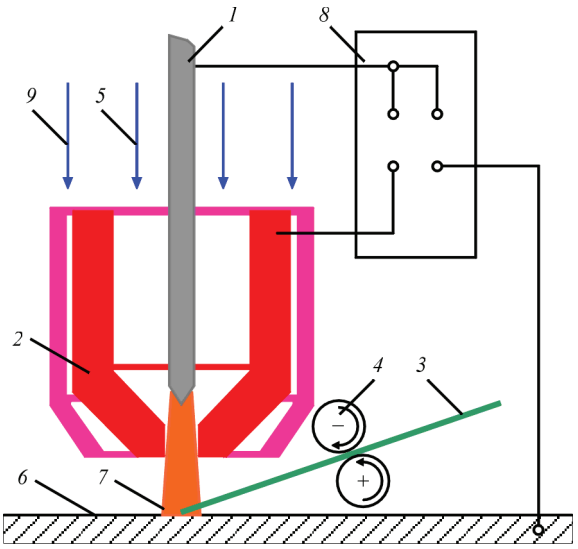

Figure 4. Scheme of plasma brazing process: *1* — tungsten electrode; *2* — plasma-forming nozzle; *3* — brazing filler metal; *4* — feed rollers; *5* — plasma gas; *6* — base metal; *7* — plasma arc; *8* — power source; *9* — shielding gas

negative impact on filler material consumption (Figure 7, *a*).

Another mode is observed when studying the height of face reinforcement *g*, which becomes smaller with increase of energy input. At the same time, the width of face reinforcement *e* first increases to 4.5 mm at energy input of 590–750 J/cm, then decreases, and starting from 916 J/cm it is stabilized.

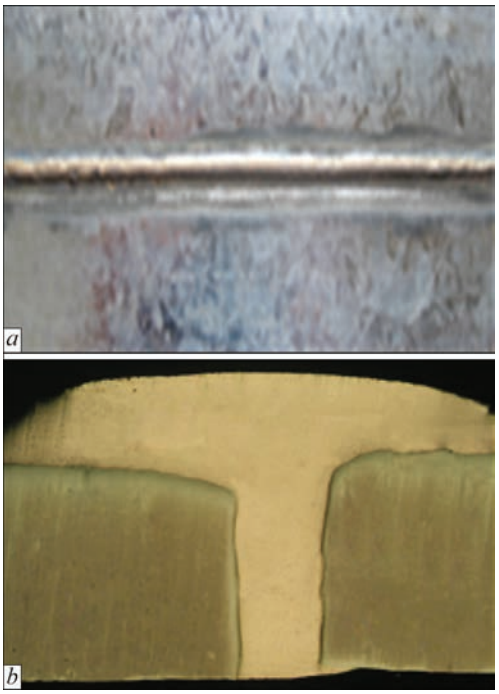

Figure 5. Appearance (*a*) and macrostructure (*b*) of brazed butt joint of galvanized steel (*b*), produced using plasma brazing

Conducted studies of the impact of energy input on formation of butt plate brazed joints show that sound dense brazed seams (without defects) with an optimum size of the face and back reinforcement form at the energy input value, which is in the range of 520–

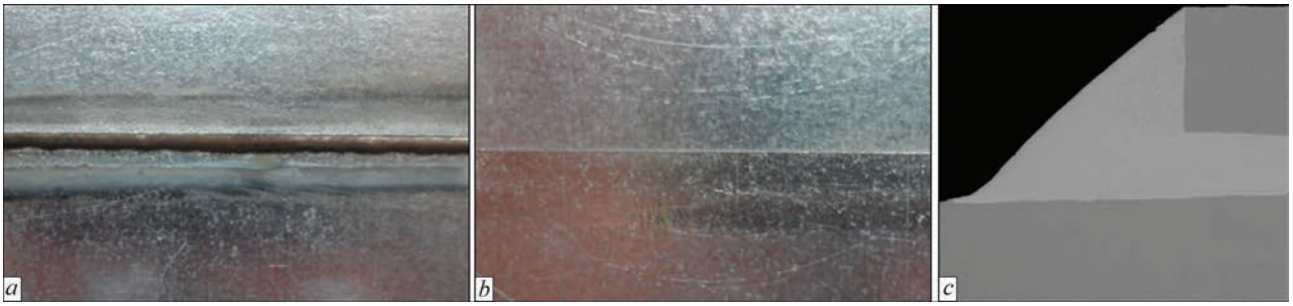

Figure 6. Face (*a*), back side (*b*) and macrostructure (*c*) of brazed overlap joint of galvanized steel

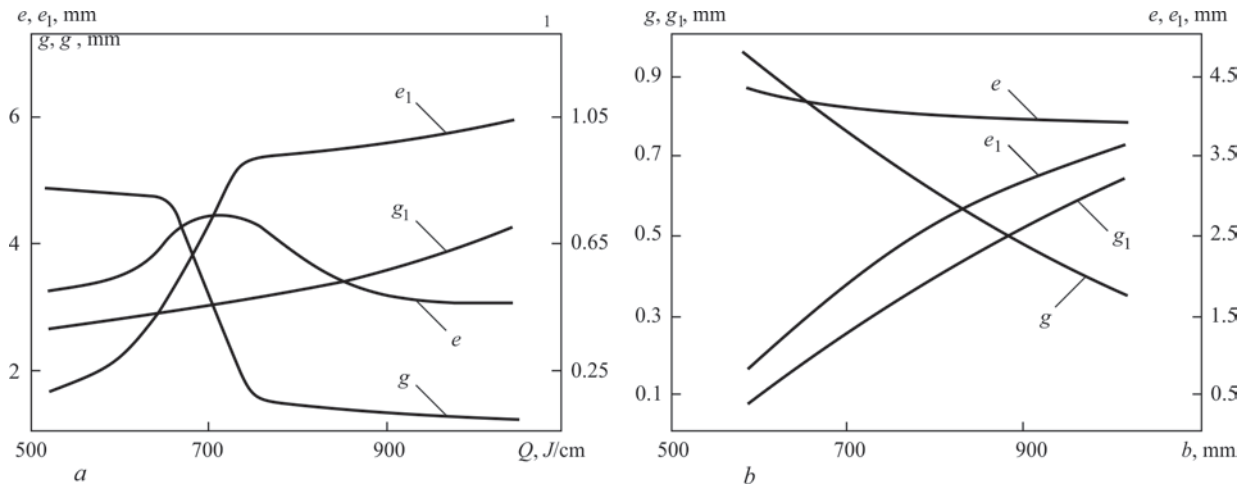

Figure 7. Dependence of brazed seam parameters on energy input value (*a*) and gap size (*b*): width e_1 and height g_1 of back reinforcement; width *e* and height *g* of face reinforcement

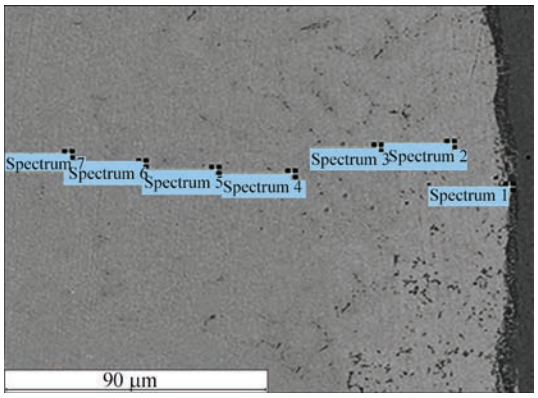

Figure 8. Electron image of the microstructure of brazed joint of galvanized steel produced with energy input of 567 J/cm and gap of 0.4 mm

590 J/cm. At brazing of overlap samples, the energy input value should be corrected, taking into account the features of the technological process of brazing and geometrical parameters of the joints.

In brazing without a gap (capillary brazing) there is the probability of partial filling of the capillary gap by the brazing filler metal. Conducted investigations of the influence of the gap size on formation of brazed butt joints revealed that it has a big role not only in seam formation, filler metal consumption, but also in energy heat transfer into the base metal. Experiments were conducted with a variable gap in the range of 0.2–0.6 mm. It follows from the derived results that at constant parameters of the mode (I, U, V and filler material feed rate) the width of face reinforcement (brazed seam) e decreases slightly, and that of back reinforcement e_1 increases rapidly with increase of the gap (Figure 7, *b*). This leads to reduction of the height of face reinforcement (brazed seam) g and increase of the height of back reinforcement g_1. It is obvious that brazing with small gaps is advantageous in terms of saving the brazing filler metal.

The derived results of local X-ray microprobe analysis and determination of chemical inhomogeneity of brazed joints of galvanized steel are indicative of the fact that the brazed seam microstructure is

Content of chemical elements in the seam, %

Spectrum number	Si	Mn	Fe	Cu	Zn
1	9.08	1.08	43.35	35.01	11.48
2	2.71	1.18	0.89	77.87	17.35
3	3.67	0.92	0.68	79.91	14.82
4	3.15	1.04	–	87.30	8.51
5	3.53	0.97	–	93.05	2.44
6	2.77	0.97	–	96.26	–
7	2.96	1.05	–	95.99	–

formed by the copper-based solid solution, along the grain boundaries of which dispersed inclusions of an iron-based phase (43.35 wt.%) precipitate. They are enriched in silicon and contain other components of brazing filler metal (Figure 8, Table).

A thin layer (1–2 μm) of iron-based phase, that contains 9.08 wt.% silicon, forms on the interphase boundary. In keeping with the binary state diagrams of metal alloys [10], in iron-silicon system the latter is characterized by low solubility and forms silicides, which in this case precipitate in the form of a thin interlayer. They also contain up to 11.48 % zinc.

The binary state diagram of copper-zinc metal system is also characterized by limited solubility [10], but the area of zinc dissolution in copper is much larger, compared to silicon solubility in iron. That is why in the grains of the solid solution zinc concentration rises up to 17.35 %. With greater distance from the interphase boundary with the base metal, zinc concentration gradually decreases and no zinc was found at 100 μm distance from the base metal. Such features of brazed seam formation are due to the structure of state diagrams, presence of a concentrational gradient between the elements of brazing filler metal and base metal and nonequilibrium conditions of solidification of the brazed seam metal that leads to running of interdiffusion processes on the interphase boundary. The brazed seam metal is saturated by iron during brazing that promotes formation of an iron-based phase that is enriched in silicon.

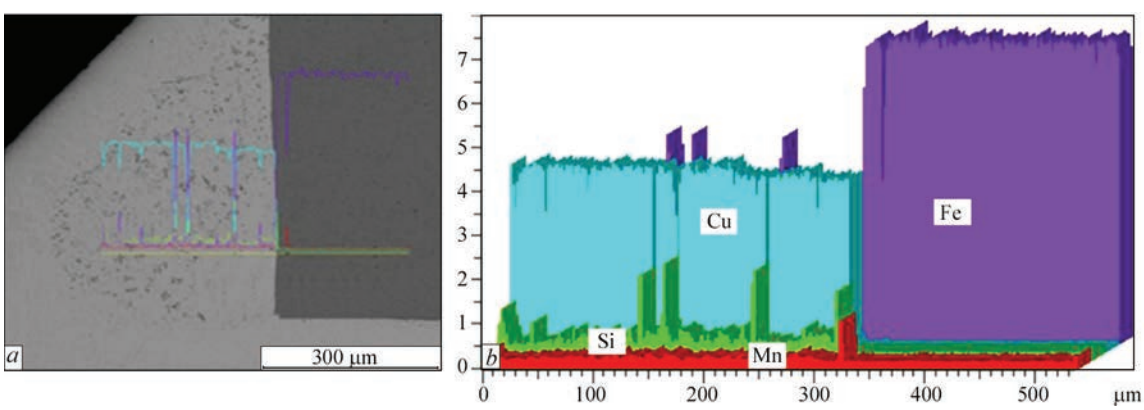

Figure 9. Microstructure (*a*) and characteristics spectra of elements (*b*) in the joint produced by plasma brazing

The characteristic spectra obtained with application of X-ray microprobe analysis by scanning of the overlap joint with an electron beam, correlate well with previous results and confirm formation of iron-based dispersed phases (Figure 9, *a*, *b*) that are enriched in silicon (silicides).

Copper concentration in this phase decreases. It should be noted that silicide inclusions, which are observed on the interphase boundary of brazing filler metal–galvanized steel, have an increased manganese content (Figure 9, *b*) that is indicative of partial substitution of iron by manganese and formation of a complex compound $(MnFe)_xSi_y$, the crystalline lattice of which is isomorphous to the lattices of Mn_xSi_y and Fe_xSi_y [11]. Formation of such phases in the brazed seam promotes increase of the temperature of unbrazing of the produced joint and increase of operating temperature.

Conclusions

Studying the geometrical parameters of welds, produced by plasma brazing of galvanized steel showed that the value of back reinforcement become larger with increase of the heat input. The width of face reinforcement first increases and then this parameter is stabilized after 900 J/cm.

It is determined that increase of the brazing gap width from 0.2 up to 0.6 mm promotes a reduction of face reinforcement height from 0.95 to 0.37 mm and increase of the height of back reinforcement from 0.1 up to 0.62 mm. Thus, increase of the heat input and value of the gap at plasma brazing leads to increase of the metal volume in the back reinforcement that has a negative impact on brazing filler metal consumption.

The value of energy input in the range of 520–590 J/cm was empirically established. This value ensures producing sound butt welded joins of 08Yu galvanized steel with optimum parameters of the brazed seam.

X-ray microprobe investigations showed that the microstructure of the brazed seam is formed by copper-based solid solution and dispersed inclusions of iron-based phase, that are enriched in silicon (silicides), which precipitate in the form of a thin interlayer (of 1–2 μm width) on the interphase boundary of base metal–brazing filler metal and along the grain boundaries of the copper-based solid solution.

1. Killing, R. (2005) Plasma brazing − Advantages and disadvantages compared with MIG brazing. *Welding and Cutting*, 4(**3**), 147−149.
2. Pavol, Sejc (2010) MAG zvaranie pozinkovanych plechov v ochrannom plyne CO_2 a Ar + 18 % CO_2. *Zvarac*, VII(**3**), 8−13 [in Slovak].
3. Pavol, Sejc (2002) Oblukove zvaranie MAG ocelovych plechov pokrytych protikoroznym naterrom na baze zinku. *Zvaranie-Svarovani*, 4(**3**), 71−73 [in Slovak].
4. Haller, H. (2002) Metal gas inverters from galvanized steel profiles. *Der Praktiker*, **10**, 377−380.
5. Wesling, V., A. Shram A. Ait-Mekideche (2003) Plasma soldering of surface-coated thin sheets. *Ibid*., **7**, 196−200.
6. Belkacem, Bouaifi (2003) Low — heat process enhances joining of coated sheet metals. *Welding J*., **1**, 26–30.
7. Chovet, C., Guiheux, S. (2006) Possibilities offered by MIG and TIG brazing of galvanized ultra-high strength steels for automotive applications. *La Metallurgia Italiana*, **7−8**, 47−54.
8. Walduck, B. (1999) Using plasma-brazing in car body fabrication. *Welding and Metal Fabrication*, 67(**8**), 11−14.
9. Smiryagin, A.P., Smiryagin, N.A., Belova, A.V. (1974) *Commercial nonferrous metals and alloys*: Refer. Book. 3rd Ed. Moscow, Metallurgiya [in Russian].
10. Massalski, T.B., Okamoto, H., Subramanian, P.R., Kacprzak, L .(1990) Binary alloy phase diagrams. The materials information society. *ASM International*, **1**.
11. Goldschmidt, X.D. (1971) *Implanted alloys*. Ed. by N.T. Chebotarev. Moscow, Mir, 56–68 [in Russian].

Received 27.05.2020

https://doi.org/10.37434/tpwj2020.06.07

SYSTEM OF CONTROL, REGISTRATION OF PARAMETERS AND MONITORING IN THE PROCESS OF PRESS WELDING OF PIPES USING MAGNETICALLY-IMPELLED ARC

M.P. Koval, S.I. Kuchuk-Yatsenko and **V.S. Kachynskyi**
E.O. Paton Electric Welding Institute of the NAS of Ukraine
11 Kazymyr Malevych Str., 03150, Kyiv, Ukraine. E-mail: office@paton.kiev.ua

The technical requirements to the basic elements of the control system are determined. The structural design of the control system is described. The influence of the process parameters of press welding using magnetically-impelled arc on the quality of the produced joints is investigated. The limits of fluctuations of values of the parameters and their influence on quality of the produced joint are determined. The software of the system for evaluation of quality of welded joints is developed. 7 Ref., 6 Figures.

Keywords: welding technology, press welding using magnetically-impelled arc, control system, registration of parameters, system for quality evaluation of produced joints, joints formation

Rapid development and widespread use of control systems in welding production [1] requires the developers of equipment to search new ways and hardware implementation to improve the efficiency of welding equipment in order to increase the efficiency of welding process and guaranteed quality of welded joints [2, 3]. The widespread use of press magnetically-impelled arc butt (PMIAB) welding in different industries and development of new welding machines to implement this method requires the improvement of existing systems for evaluating the quality of welded joints and control.

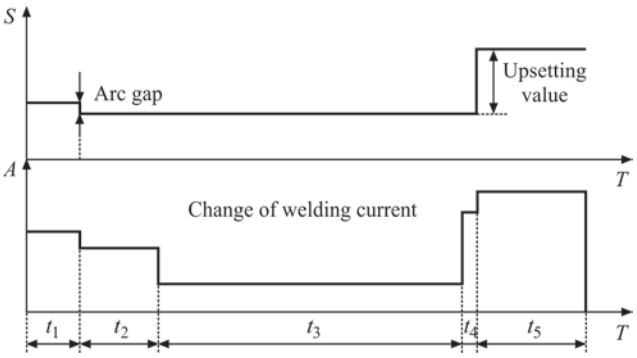

Figure 1. Changes in welding current and position of moving part of welding machine during welding: *S* — graphical representation of position of moving part of welding machine during welding process; *A* — sequence of changes of welding current during heating of parts; *T* — running time of heating and welding process; t_1 — time interval, during which the process is initialized (excitation of welding arc); t_2 — duration of stage of stabilization of process of moving welding arc along the edges of parts; t_3 — stage of heating welded parts; t_4 — endurance of time, during which a sharp increase in welding current occurs (stage of forcing heating process); t_5 — time of performing compression of heated parts to form a joint (upsetting) with the switched-on welding current

During resistance butt welding the use of parametric quality control of welding is known [4]. The use of this method of quality control is based on real-time registration of welding parameters and determination of probable deviations of parameters from the set program values. At the same time, the acceptability of these deviations and their impact on the quality of joints is determined and the quality of a produced joint is evaluated.

The appropriate programs for control of basic parameters are also used in PMIAB production, but the control of parameters has so far not been used in industrial conditions.

The differences in the technological process during resistance butt welding and PMIAB and namely, the presence of a controlling magnetic field, the nature of welding current (constant current), process duration, upsetting rate, etc., make the use of control methods [4] during resistance butt welding impossible.

The aim of the work is to develop the initial conditions, software and create a computerized control system for welding process and quality evaluation of welded joints produced by magnetically-impelled arc, analyzing the technological parameters.

Realization of the canonical scheme of PMIAB is implemented according to the program in which the change of a parameter (welding current) is performed over time and has the form shown in Figure 1.

M.P. Koval — https://orcid.org/0000-0001-9695-6434, S.I. Kuchuk-Yatsenko — https://orcid.org/0000-0002-1166-0253,
V.S. Kachynskyi — https://orcid.org/0000-0003-2066-3365

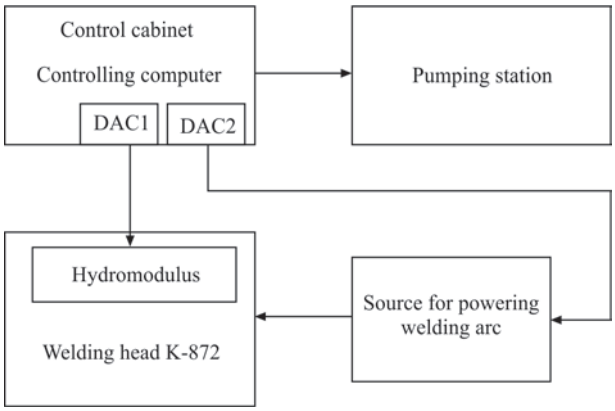

Figure 2. Block diagram of welding installation

When heating of pipes is performed, a step change of welding current occurs. Each of the current steps has a preliminary set duration. Programming a value of current over time has the following disadvantages:

- low repeatability of final temperature field formation during joining of parts;
- limited range of welded products;
- system of registration and quality evaluation that can be applied to such a system, will not have a high degree of reliability about the quality of a produced joint.

Taking into account the experience of operating of PMIAB equipment and taking into account the results of investigations [5, 6] and in order to eliminate the abovementioned drawbacks, the PMIAB method was tested, in which the process parameters are corrected without a rigid binding to the duration of welding program but taking into account the energy characteristics of welding arc in order to obtain the programmed temperature field required for the formation of a joint. This guarantees the repetition of heating process and formation of a joint.

The scheme of the system of control and evaluation of quality of welded joints was developed in the machine K-872 and in the composition of:

- control computation module (PC);
- devices for normalization of analogue input signals;
- analogue-to-digital converters;
- welding arc current sensor;
- arc voltage drop sensor;
- potentiometric sensor of moving part position;
- measuring sensor of absolute pressure in hydraulic system.

To provide implementation of the control and quality evaluation algorithm, the cabinet of control system was modernized (Figure 2). Registration of technological parameters of the PMIAB process in the modernized K-872 machine takes place according to the scheme shown in Figure 3.

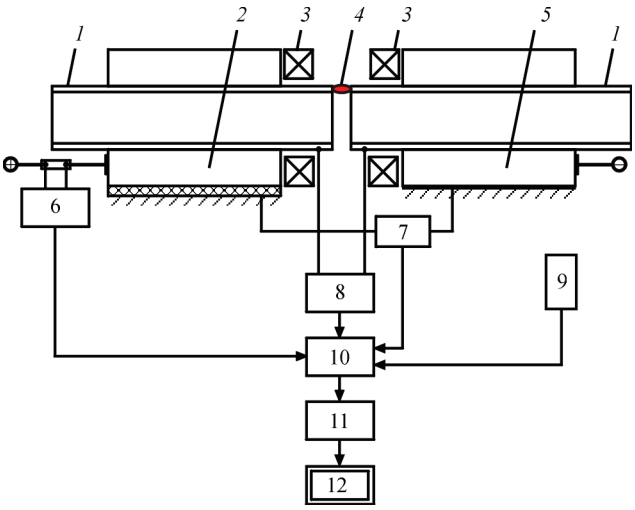

Figure 3. Block diagram of the model of quality evaluation of welded joints: *1* — welded pipes; *2* —movable clamping device; *3* — elements of magnetic system; *4* — electric arc column; *5* — fixed clamping device; *6* — current sensor; *7* — position sensor; *8* — voltage drop sensor on welding arc; *9* — sensor for measuring absolute pressure of hydraulic system; *10* — normalizing instrumental amplifier (with low-pass filter F_c = 100 Hz); *11* — receiving ADC; *12* — industrial computer

The compliance of the computer evaluation of quality control with the real situation is guaranteed by providing the system (Figure 3) with real output data, in case of PMIAB of pipes, such data are current, welding arc voltage, common arrangement of pipes in the clamping devices of the machine, pressure in hydraulic system during the performance of upsetting (as derivatives of this parameter, rate and value of upsetting).

For registration and analysis of the process parameters the multifunctional device USB-4711AE (Figure 4) was used, which has the following main characteristics:

Maximum sampling frequency of input signal, kHz	150
Operating range of input voltage, V	0–10
Maximum input voltage, V	30
Input resistance of analogue channel, MOhm	>1
Number of bits in ADC, bits	12
Sampling error, bits	+(m)1
Maximum number of reading channels	16

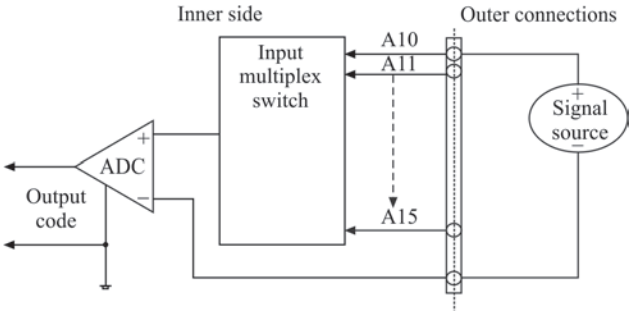

Figure 4. Diagram of connecting sensors of the system of recording PMIAB parameters and ADC structure

Current data from the sensors of the registration system during heating of the parts are obtained as follows (on the example of obtaining a voltage drop on welding arc). The input of the normalizing input amplifier 8 is connected directly to the terminals located on clamping devices of the welding machine (according to the electrical circuit, such a connection corresponds to the connection to the output terminals «+» and «–» of the welding arc power source). In the amplifier, the voltage drop of welding arc, which occurs at the beginning of the process and is in the range of 20−30 V of direct current (at the moment of constant arc movement along the edges of parts to be welded), is normalized to the output voltage of 2−3 V. The signal corresponding to the input voltage is filtered to a 100 Hz cut-off frequency of amplitude-frequency response. In this way, the derived voltage signal of welding arc is cleared from pulsations and interferences of harmonics of higher orders, but such a filtering frequency allows preserving the dynamics of tracking change in welding voltage drop and registering negligible deviations in welding voltage from a preliminary set one. For further processing and analysis, the derived signal of the welding voltage drop from the output of the amplifier 8 is sent to the input of the analogue-to-digital converter (ADC). During operation of the software (start of the quality evaluation program), the ADC is set so that interrogation frequency of the analogue inputs is 10 interrogation points per one reading of data from the ADC output. Therefore, a more accurate data transfer to the control program is achieved. This principle is shown in Figure 5.

The choice of such a type of device for reading data of running the technological process is predetermined by the versatility and mobility of the obtained system for registration of parameters. The complex of data collection devices, built on devices with a USB busbar for data transfer, is not tied to specific executive equipment and in case of need to solve new problems, the emergence of which is inevitable during any research work, allows a quick rearrangement of the system without a loss of data obtaining quality. Such a principle of building a data registering system allows using any main device, such as PC of «laptop» class and industrial computers.

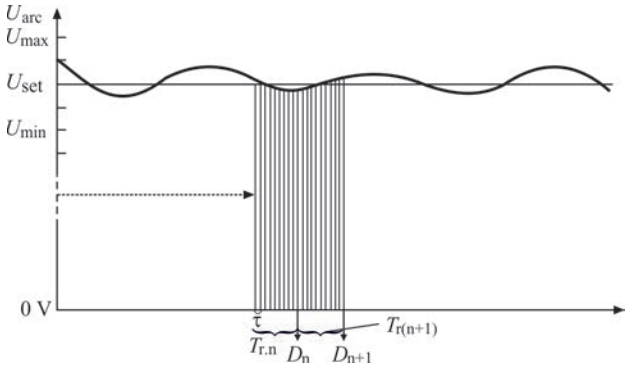

Figure 5. Cycles of interrogation one ADC input and reading data to the software of the model of quality control system

For setting the sampling frequency of analogue inputs the following parameters were determined;

U_{min} — minimum value of arc voltage drop, which occurs due to the influence of different factors during heating process;

U_{max} — maximum value under the same initial conditions;

U_{set} — technological parameter;

τ – delay between the reading cycles of one ADC input channel;

T_{rn} — total duration of one reading cycle of the ADC output (sampling duration for the formation of data package coming to the program of analysing parameters);

$T_{r(n+1)}$ — next package read from ADC;

D_n — data package read from ADC (consists of an array of interrogation points of four channels by n-times) (number of averaging points).

Averaging allows avoiding the phenomenon of the appearance of capacitive parasitics in building the circuit of the input ADC multiplex switch.

In the process of welding pipes, in the random access memory of the PC the accumulation and formation of an array of data from the four ADC channels is performed. This allows simplifying the procedure of processing and analysis of the data obtained after welding.

The customization of the software of the control complex was carried out by updating the parameters of the existing software modules. It allowed expanding the time and parametric limits of operating the actuating devices, performing more accurate adjustment of technological welding parameters and obtaining data on the process performance.

During welding process, the system sensors are scanned, the obtained data are processed and the formation of data files and a summarized file of a daily report is performed, in which the following parameters are fixed;

- welding time by stages of heating T_1, T_2, T_3, T_4, T_5, T_6;
- arc current by stages of heating I_2, I_3, I_4, I_5 (I_1 is the current of the initial stage of heating process during the analysis is not taken into account due to its small impact on welding process);
- voltage of welding arc at three stages of heating parts U_2, U_3, U_4 (U_1 is the voltage of excitation stage is not taken into account);
- total amount of energy spent on heating parts E_a;

● rate of upsetting V_{ups} (it was experimentally established that this is the average rate of the opposite movement on the first 1.5 mm of the arc gap before the contact of welded pipes);

● value of upsetting S_{ups} (value of total deformation L of parts during upsetting, for each of the parts is):

$$L = \frac{S_{ups}}{2} - l_{ag}, \quad (1)$$

where l_{ag} is the value of arc gap between the parts before the beginning of upsetting; upsetting pressure P_{ups}; temperature of oil of the hydraulic system and the environment.

According to the data of reports, a database of variations in the values of these parameters during welding over the entire period of operation of the equipment is formed, which will be used in the future to optimize the technological process.

Deviation of these parameters beyond the tolerances depends on many reasons. Therefore, the following algorithms were developed:

● control for the two-level system, which provides correction of welding mode in order to stabilize the process;

● weld butt quality evaluation;

● evaluation of technical condition of welding machine;

● formation of recommendations with correction of technological process parameters.

The existing quality control, at which the obtained data are compared with the reference ones, is the simplest logical function — the quality indices are in the tolerance at a simultaneous existence of all the controlled parameters in the tolerance. However, during such a control the following factors are not taken into account:

● significance of the impact of each of the parameters on the quality index;

● uncertainty of the limit of tolerances of process parameters;

● probable increase in the influence of a totality of certain combination of deviations on the quality of welding.

For the control of welding quality the following algorithm was developed and tested, based on the analysis of process parameters at three stages of its implementation:

1 — excitation of welding arc and heating of pipes. Period of temperature field formation at the ends of pipes;

2 — increase in welding current;

3 — upsetting and formation of joints.

The conclusion on the quality of a produced welded joint with a certain degree of probability (truth) is carried out on the basis of logical rules which are made according to the results of investigations of technological features of the process of welding pipes [7].

To control the welding process, the following parameters are used:

● time (duration) of welding by stages ($T_1 - T_6$);

● value of current at the stages of heating ($I_2 - I_5$);

● value of voltage at the stages of arc existence ($U_2 - U_4$);

● rates and values of upsetting (V_{ups} and L_{ups});

● pressure in the hydraulic system during upsetting P_{ups};

● energy spent on heating of parts E_a.

To perform the simplest method of control in the system for evaluation of quality of produced welded joints, the following rule can be entered:

IF some technological parameter X is determined in the tolerance field, THEN the produced joint meets the quality requirements according to this parameter.

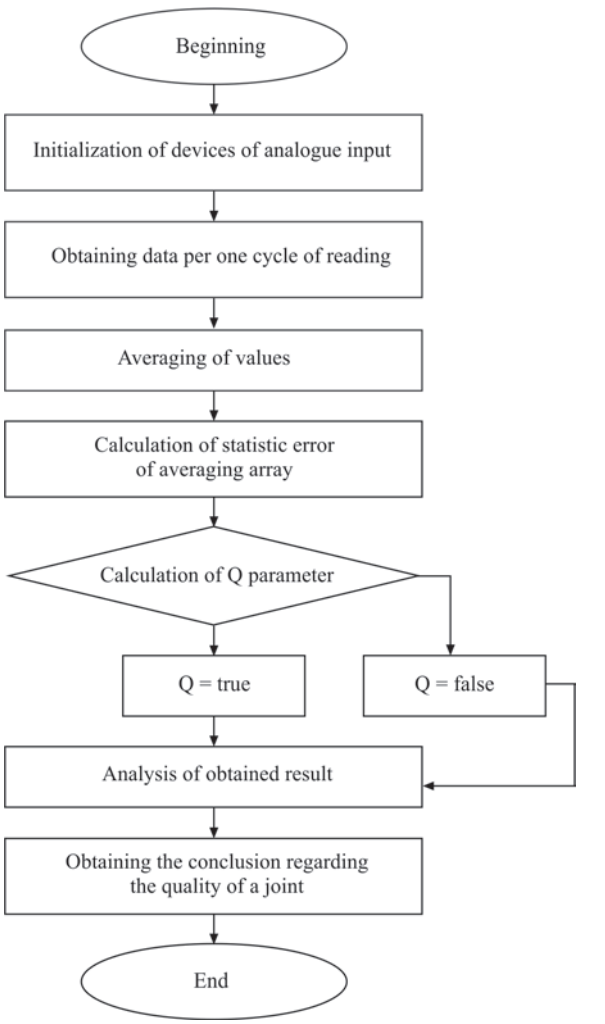

Figure 6. Algorithm for quality control of welded joints

According to the abovementioned, we obtain the following sequence to determine the quality of the produced joint:

IF in the tolerance the time intervals of the technological process $T_{1\text{-}6}$ are set AND the arc current $I_{1\text{-}4}$ is obtained AND the voltages $U_{2\text{-}4}$ are measured AND the upsetting rate V_{ups} in the tolerance AND the value of upsetting L_{ups} in the tolerance AND at the stage of upsetting slipping of pipes relatively to clamping devices is absent, THEN the welded butt is of high quality.

If a deviation of set time intervals of the technological process $T_{1\text{-}6}$ OR obtained arc current $I_{1\text{-}4}$ OR measured voltages $U_{2\text{-}4}$ are not within the established tolerances OR upsetting rate V_{ups} is lower than the lower limit of tolerance OR the value of upsetting L_{ups} is lower than that established in the tolerance OR at the stage of upsetting a longitudinal slipping of parts relative to the clamping devices takes place, THEN a welded joint is determined as low-quality.

In case of registering these process parameters using a computer control system, we have the following computational algorithm to determine the quality of welded joint.

$$\begin{cases} (T_{1\text{-}6}) \,\&\, (I_{2\text{-}5}) \,\&\, (U_{2\text{-}4}) \,\&\, (V_{ups}) \,\&\, (L_{ups}) \,\&\, (P_{ups}) \,\&\, !(S_{sl}) \\ !(T_{1\text{-}6}) \,\|\, !(I_{2\text{-}5}) \,\|\, !(U_{2\text{-}4}) \,\|\, !(V_{ups}) \,\|\, !(L_{ups}) \,\|\, !(P_{ups}) \,\|\, (S_{sl}) \end{cases}, \quad (2)$$

where Q is a logical correspondence, which can take the value «true» or «false» (respectively, «true» means that the quality of a produced joint meets the standards, «false» means that the quality of a produced joint does not meet the standards); $T_{1\text{-}6}$ are the values of duration of welding stages obtained during the technological process; $I_{1\text{-}4}$ are the measured values of welding current by stages of heating parts; $U_{2\text{-}4}$ is the welding arc voltage by heating stages; V_{ups} is the initial upsetting rate; L_{ups} is the value of upsetting; S_{sl} is a sign of existing longitudinal slipping of parts relative to the devices for holding welding machine; ! is a sign that corresponds to the value of the variable «does not meet the set tolerance»; & — meets the condition «YES»; || — meets the condition «OR».

The software realization of the abovementioned algorithm (2) is shown in Figure 6.

Conclusions

1. The initial requirements to the control system of basic technological parameters of PMIAB welding were determined.

2. The limits of changes of basic technological parameters in welding for producing sound joints were determined.

3. The software was developed to realize the algorithm of controlling the process of welding and quality control of joints.

4. The industrial technology of PMIAB welding of pipes was developed.

1. Rudenko, P.M., Gavrish, V.S. (2007) KSU KS 02 system for automatic control and monitoring of resistance spot welding process. *The Paton Welding J.*, **11**, 43–45.
2. Kuchuk-Yatsenko, S.I., Rudenko, P.M., Gavrish, V.S. et al. (2016) Statistical control of process of flash-butt welding of rails. Two-level control system. *Ibid*., **5–6**, 17–20.
3. Kuchuk-Yatsenko, S.I. (12018) Technologies and equipment for flash-butt welding of rails: 60 years of continuous innovations. *Ibid*., **11–12**, 29–46.
4. Rudenko, P.M., Gavrish, V.S., Kuchuk-Yatsenko, S.I. et al. (2017) Influence of flash-butt welding process parameters on strength characteristics of railway rail butts. *Ibid*., **5–6**, 75–78.
5. Kuchuk-Yatsenko, S.I., Kachynskyi, V.S., Koval, M.P. (2012) *Method of press welding*. Ukraine Pat. 100278 [in Ukrainian].
6. Kuchuk-Yatsenko, S.I., Kachynskyi, V.S., Galakhov, M.V., Klymenko, V.I., Koval, M.P. (2019) *Machine for press welding of pipes and pipe ends heated by magnetically impelled arc*. Ukraine Pat. on utility model, 136339 [in Ukrainian].
7. Kachynskyi, V.S., Kuchuk-Yatsenko, S.I., Koval, M.P. (2020) Press magnetically-impelled arc welding of high-strength steel tubular parts of hydraulic cylinders. *The Paton Welding J.*, **1**, 45–51.

Received 14.05.2020

https://doi.org/10.37434/tpwj2020.06.08

PECULIARITIES OF REPAIR OF WORN OPERATING ELEMENTS OF DRILL BITS

B.V. Stefaniv
E.O. Paton Electric Welding Institute of the NAS of Ukraine
11 Kazymyr Malevych Str., 03150, Kyiv, Ukraine. E-mail: office@paton.kiev.ua

The peculiarities of wear of operating elements of the bodies of steel, matrix drill bits and heads were considered and studied, and repairability criteria were determined. Performed analysis of worn areas of operating elements of used drill bit bodies showed that at drilling wear of cutters and sockets is the most common, and wear of flushing channel components of the drill bit bodies occurs less often. Metallographic examination showed that the deposited layer and the base metal are connected by a thin transition layer of diffusion origin, which shows that base metal melting and filler metal dissolution did not occur in it. It is established that the drill bit repair is cost-effective in those cases, when the cost of such repair does not exceed one third of the cost of the bit proper. Multiple repeated reconditioning of operating elements of worn areas reduces the cost of manufacturing new drill bits several times. Conducted production trials of reconditioned drill bits showed that repair of worn areas of the operating elements allows considerable extension of the service life and saving 30−50 % of the initial cost of a specific drill bit type. 12 Ref., 2 Tables, 8 Figures.

K e y w o r d s : wear, surfacing, tungsten carbides, area, bridge, diamond-carbide cutter, polycrystalline diamond cutter, carbide coating, microstructure, wear resistance

Development of the technological processes of drill tools repair does not stand still, and now the enterprises and firms in Ukraine and abroad propose different methods of repair of worn areas of drill bit bodies. Drill tools that are used in the gas and oil industry wear during service that leads to shortening of operating life and often requires replacement or repair.

The main characteristics of wear of the operating elements of drill bits (both own and foreign production bits) in the fields of Ukraine are as follows: cutter wear — 17 %, cutter breaking — 30 %; cutter chipping — 31 %; loss of cutters — 3 %; wear of protective coating — 5 % and 19 % — absence of wear. For instance, abroad the headway of drill bits of PDC type (Polycrystalline Diamond Cutter) that are used for oil and gas drilling (by the data of Smith Inc.), is equal to 1067.5 m on average [1]. In Ukraine, the headway of domestic drill bits (usually, produced by Bakul ISM) is equal to 300–400 m on average.

At present, the new methods of repair and reconditioning of the worn areas by wear-resistant coating allow effectively resisting a number of problems of wear of the blades and bodies of drill bits under the conditions of alternating and shock loads, hydroabrasive wear, corrosion, etc., due to high adhesive strength of the protective surface layer, reduction of friction coefficient, improvement of corrosion resistance in an aggressive environment at increased value of hydrogen index (pH = 7 – 12).

B.V. Stefaniv — https://orcid.org/0000-0002-7159-8762

Leading developer-companies Baker Hughes INTEQ, Bit-Tech, Dowdco, Halliburton Security DBS, Hughes Christensen, Ulterra Drilling, Reed Hycalog, Smith Tool, Varel, Tri-Max (all US), TIX (Japan), United Diamond (Canada), Kingdrelm (China) and oth. have used coatings of different functional purposes for a long time, at manufacture and repair of operating elements of drill bits. Development of technological processes of manufacture and repair of drill bits is continuously improved due to application of new composite materials and technologies of protective coating deposition.

There exist the main surfacing methods, depending on the kind of the used energy: oxyacetylene surfacing, arc surfacing (open arc, gas-shielded, vibroarc, plasma), electroslag, induction, laser, and electron beam. When selecting the surfacing method, first the possibilities of its application in a specific case are assessed, then the possibility is determined of ensuring the technical requirements that are made to deposition of the base materials and, finally, the cost-effectiveness of surfacing is assessed. At assessment of cost-effectiveness of the surfacing process, the total cost of manual arc surfacing is taken to be 100 %, that of oxyacetylene surfacing — 74 % and of vibroarc surfacing — 82 %.

At deposition of the composite material on the worn areas of operating elements of the drill bits the advantage was given to arc surfacing. The essence of the surfacing process consists in the use of the heat for filler material melting and its joining with the base metal of the drill bit body. Using the possibili-

ties of arc surfacing, a deposited layer of the required thickness and chemical composition with the required properties can be obtained in the part surface.

In view of the above-said, the objective of the work consisted in investigation and development of the technology of repair of the worn areas of operating elements of drill bit bodies.

Materials and methods. The object of study are the worn areas of operating elements of the bodies of used steel and matrix drill bits. Microstructural investigations were conducted by a standard procedure in electron microscope Tescan Mira 3 LMU and optical microscope Neophot 32. PRS-3M welding unit, Casto Fuse gas torch, and TeroCote 7888T composite material were used.

Investigation results. In order to protect the operating elements of drill tools from different kinds of wear, composite materials based on Ni, Fe, NiCr, NiCrBSi, copper alloys, etc., strengthened by tungsten carbides, are widely used [2–5]. This is, first of all, related to unique properties of the reinforcing phase of such alloys — tungsten carbides. Tungsten carbide is one of the hardest and most shock-resistant carbides, and deposition of hard alloy coating (HC) is a fast and simple method of application of tungsten-carbide coating on the worn areas of the operating elements, that are exposed to the impact of intensive abrasive loads, and it preserves its mechanical properties in a wide range of temperatures, is resistant to friction corrosion and is capable of forming a strong bond with metals [6, 7].

Proceeding from the results of the performed work [8, 9] on reconditioning of the operating elements of drill bit bodies, TeroCote 7888 T composite material was selected. It readily wets the base metal of both the steel, and matrix drill bits, and has no defects at deposition of the coating layer on the worn areas of the sockets of the openings of diamond-carbide cutters (DCC) and this bridges between the sockets that, in its turn, promotes machining of the openings of the sockets after surfacing and preserves the geometry for DCC fastening.

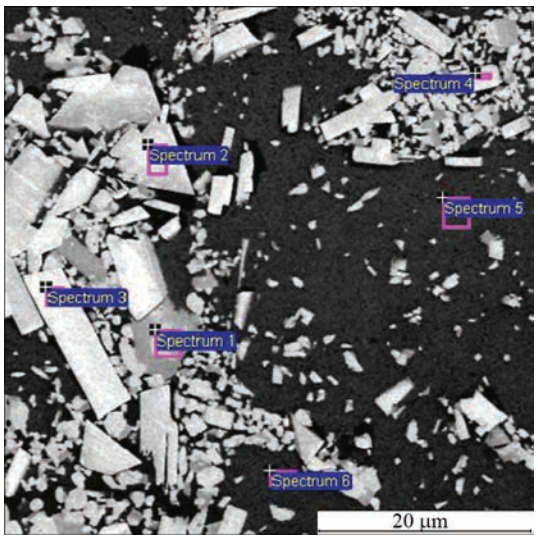

Figure 1. Microstructure of TeroCote 7888 T alloy

Conducted investigations of the composite material wear resistance under the conditions of hydroabrasive wear [10] showed that the wear resistance of protective coating from TeroCote 7888T, based on nickel with crushed particles of tungsten carbide is higher than that of «LZ-11-7» relite (spherical granules of tungsten carbide) and Diamax M (ground particles of tungsten carbide) based on iron by 1.7 and 2.9 times, respectively. Proceeding from the results of wear resistance studies, the TeroCote 7888T alloy was selected, on the base of which corrosion resistance studies of this material were conducted. Results of the performed corrosion resistance studies showed [11] that application of the protective coating deposited using TeroCote 7888T flexible cord, allows lowering the corrosion rate of operating elements of drill tools from 30Kh steel almost 53 times that will promote extension of its service life. Proceeding from the results of investigations of hydroabrasive and corrosive wear of composite materials, the main attention was given to this alloy, which belongs to the category of corrosion-resistant protective materials.

TeroCote 7888T composite material was used to restore the worn coating areas of drill bit body. This material of 5 mm diameter has a core from nickel wire of 1.2 mm diameter and a sheath from nickel-based matrix alloy (Ni–Cr–B–Si system), reinforced by tungsten-carbide particles of irregular shape. Tungsten carbides are characterized by different dimensions from 0.7 to several microns, and their quantity in the volume is < 65 %. The working temperature of melting is equal to 1170 °C (± 50 °C). The main structural phase of the alloy is γ-oversaturated solid solution based on nickel, reinforced by tungsten carbides, with the following depressant content in wt.%: silicon up to 1.36 and boron up to 0.6 (Figure 1, Table 1).

Figure 2 gives the distribution of elements in TeroCote 7888 T composite material, which provides convincing proof of the fact that the base of matrix alloy is the nickel-based solid solution (74.31 wt.%), coated by an alloy of Ni–Cr–Fe–Si–B system. This is confirmed by quantitative microanalysis in the studied areas (see Table 1).

Deposition of the coating layer on the worn areas of operating elements of the matrix and steel drill bits was performed by nonconsumable tungsten electrode TIG-process in the shielding gas – commercial argon (Table 2). Surfacing of worn areas of operating elements was performed in the horizontal position of

Table 1. Composition of the studied areas, wt.%

Spectrum number	B	C	Si	Cr	Fe	Ni	W	Total
1	0.56	4.84	1.08	8.77	0.00	18.83	65.91	100.00
2	0.63	8.19	0.00	0.25	0.71	1.70	88.52	100.00
3	0.65	8.19	0.00	0.00	0.00	2.42	88.73	100.00
4	0.62	9.10	0.00	0.30	0.00	0.00	89.98	100.00
5	0.52	3.60	1.36	6.08	2.50	74.04	11.89	100.00
6	0.00	3.32	1.25	6.27	2.54	74.31	12.32	100.00
Average	0.50	6.21	0.62	3.61	0.96	28.55	59.56	100.00
Deviation	0.25	2.58	0.68	3.88	1.24	35.99	37.84	–
Max	0.65	9.10	1.36	8.77	2.54	74.31	89.98	–
Min	0.00	3.32	0.00	0.00	0.00	0.00	11.89	–

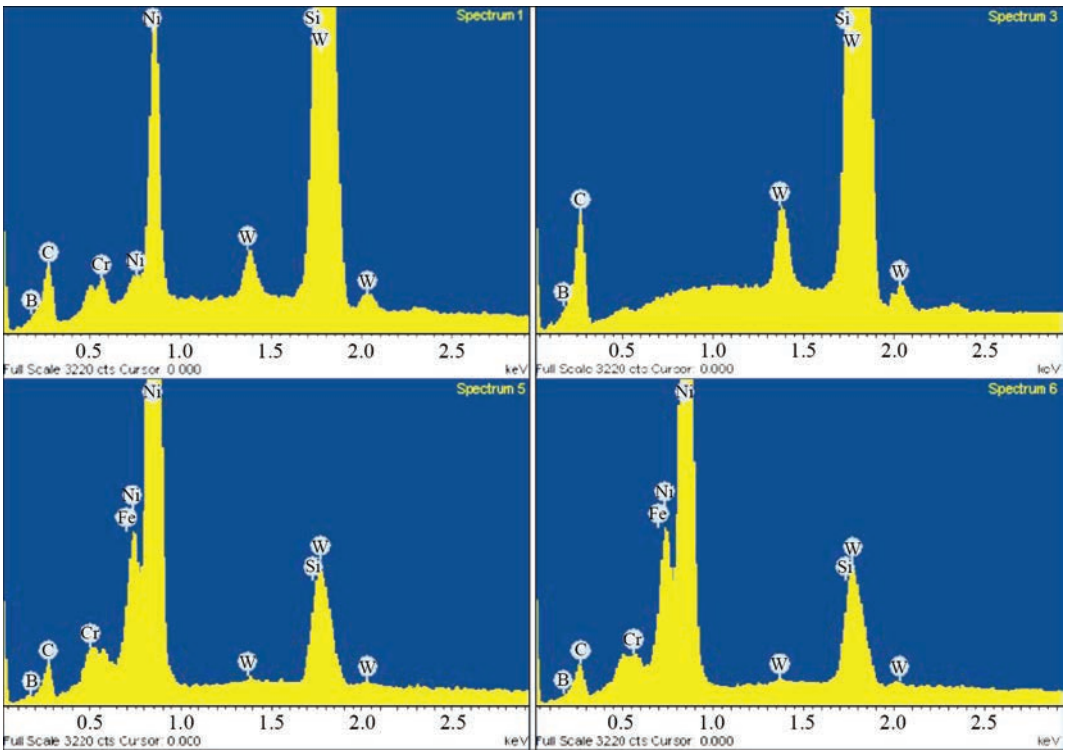

Figure 2. Qualitative distribution of elements in TeroCote 7888 T matrix alloy

the drill bit body. Average thickness of the deposited layer was equal to 2–4 mm, depending on worn area thickness.

The main method of repair of the worn areas of operating elements of matrix (Figure 3, *a*) and steel drill bits (Figure 3, *b*) consists in step-by-step performance of the technological operations: diagnostics of the worn areas, dismantling the worn diamond-carbide cutters and carbide inserts, machining of the worn areas of the body blades; machining of the sockets of blade operating elements; close fitting of graphite plugs into these sockets; flame or induction heating of the body operating elements up to the temperature of 400–500 °C; surfacing the areas between the plugs from the upstream and downstream sides of the mounting sockets of the operating elements by a wear-resistant alloy; body cooling to room temperature; removal of graphite plugs; machining the openings after surfacing; mounting the diamond-carbide cutters and carbide inserts into the socket openings; preheating the sockets up to the temperature in the range of 450–500 °C; brazing the diamond-carbide cutters and carbide inserts up to the temperature of 650–680 °C, as higher temperature starts affecting the strength properties of polycrystalline diamonds; and cooling the drill bit body to room temperature.

In order to determine the microstructure of the protective coating, microsections were cut out of the steel

Table 2. Arc surfacing mode

Voltage, V	Kind of current	Current, A	Argon flow rate, dm^3/min	Deposition rate, m/h	Power source
10–12	Direct, straight polarity	80–100	2.5–3.0	2–4	PRS-3M

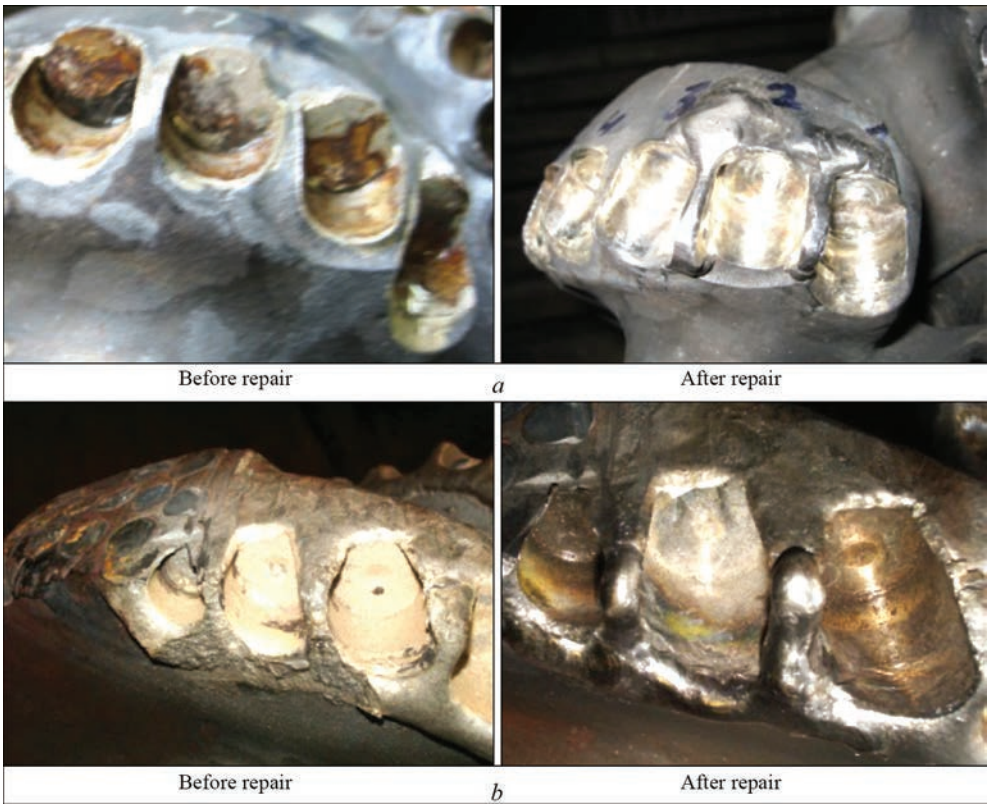

Figure 3. Appearance of worn areas of operating elements: *a* — matrix drill bit; *b* — steel drill bit

(Figure 4) and matrix drill bits (Figure 5) with the deposited layer. Metallographic investigations showed that the deposited layer and base metal are connected by a thin transition layer of diffusion origin, which indicates than no surface melting of the base metal or dissolution of filler metal in it occurred.

The microstructure of the deposited layer of the steel drill bit contains solid solution, based on nickel-chromium strengthened by tungsten carbides, and a certain amount of silicon and boron depressants. Presence of boron and silicon in the composition of filler wires gives them self-fluxing properties at deposition on steel. Tungsten carbides of an irregular shape (of different dimensions) are distributed over the entire microsection field. It is known from publications that sound wear-resistant coating should have a uniform distribution of the hard phases with the distance between these phases smaller than the size of the abrasive particles [12]. Work was also performed on deposition of a protective coating on the worn areas of the matrix drill bit. The microstructure of the deposited layer of the matrix drill bit (Figure 5) is similar to that of the steel drill bit deposited layer (Figure 4).

The obtained structure of the deposited coating of steel and matrix drill bits allows effectively protecting the surface of operating elements from erosion and

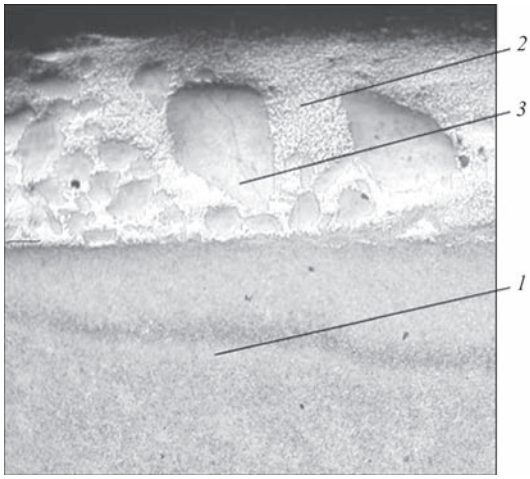

Figure 4. Microstructure (×50) of steel drill bit coating: *1* — 30Kh steel; *2* — matrix based on NiCrBSi alloy; *3* — tungsten carbides

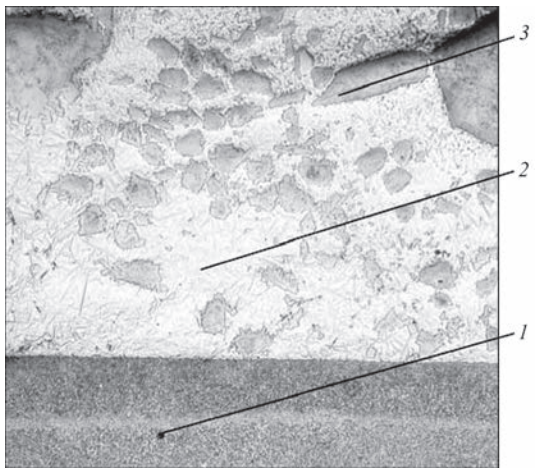

Figure 5. Microstructure (×50) of matrix drill bit coating: *1* — tungsten carbide matrix; *2* — matrix based on NiCrBSi alloy; *3* — tungsten carbides

Figure 6. Matrix drill bit of 215.9 mm diameter: *a* — before repair; *b* — after repair

Figure 7. Integral steel drill bit of 295.3 mm diameter of «Volgaburmash» (Russia): before (*a*) and after repair (*b*)

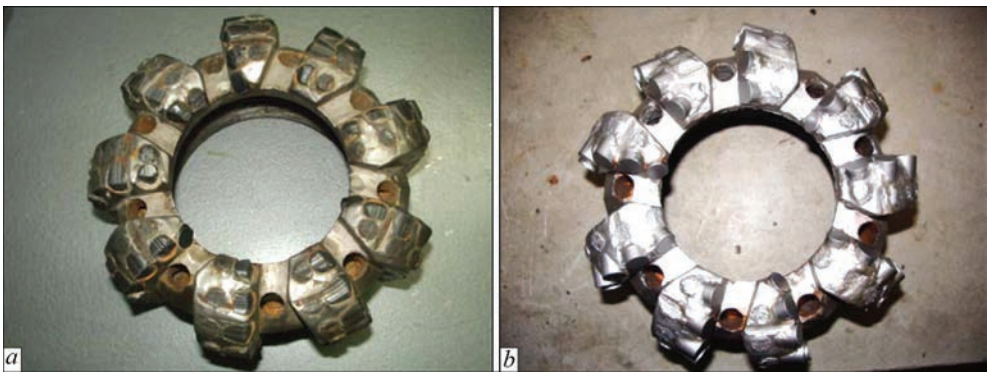

Figure 8. Integral drill head of 212.7 mm diameter of «Burinteks» (Russia): before (*a*) and after repair (*b*)

abrasive wear, caused by impact of such materials as sand, gravel, soil, minerals, etc. The viscous matrix of the alloy absorbs the shock loads and improves the corrosion resistance, whereas the special form of tungsten carbides makes it impossible to pull them out of the matrix.

The features of restoration of the worn areas of operating elements are demonstrated in the case of repair of drill bits of various sizes: restoration of operating elements of the blades of matrix body of 215.9 mm diameter drill bit of Smith Bits Company (USA), restoration of the worn area of the coating of operating elements of blades of the steel body of 295.3 mm diameter drill bit, manufactured by «Volgaburmash», Russia (Figure 7) and restoration of worn operating elements of blades of a drilling head of 212.7 mm diameter, manufactured by «Burinteks», Russia (Figure 8).

The steel and matrix drill bits, restored by PWI, have been successfully tested in the oil-gas-condensate fields of the Poltava region. Based on the testing results, Acts of industrial application of these drill bits have been obtained.

In keeping with the results of investigations and the conducted work, a compulsory repair procedures for the worn areas of the operating elements were drawn up for all the standard sizes of matrix and steel drill bits.

Conclusions

1. The current method of repair of the worn areas allows a significant (2 to 3 times) extension of the service life of the operating elements of bodies of

drill bits, operating under harsh conditions of corrosion-abrasive wear.

2. Proceeding from the results of industrial tests of the restored steel and matrix drill bits, it was established that application of this repair technology when drilling gas and oil wells allows extension of the service life and saving approximately up to 100% of the initial cost of this drill bit.

1. Draganchuk, O.T., Prygorovska, T.O. (2008) Analysis of drill bit working out of PDC type in deposits of Ukraine and world. *Nafrogazova Energetyka*, 4(**9**), 11−15 [in Ukrainian].
2. Wear-resistant materials. Rods for gas and TIG welding. https://docplayer.ru/32381351-Iznosostoykie-materialy-it-vyordye-splavy-na-osnove-kobalta.html
3. Laansoo, A., Kübarsepp, J., Vainolab, V., Viljus, M. (2012) Induction brazing of cermets to steel. *Estonian J. of Engineering*, 18(**3**), 232–242.
4. *Materials for brazing and surfacing TeroCote*. http://www.castolin.com.ua/
5. *Materials of Postalloy Company for surfacing of protective coatings*. http://www.postle.com
6. Samsonov, G.V., Vitryanyuk, V.N., Chaplygin, F.I. (1974) *Tungsten carbides*. Kiev, Naukova Dumka [in Russian].
7. Pierson, H.O. (1996) *Handbook of refractory carbides and nitrides*. New Jersey, Noyes Publications.
8. Stefaniv, B.V., Khorunov, V.F., Sabadash, O.M. et al. (2014) Features of reconditioning steel drill bit watercourse. *The Paton Welding J.*, **11**, 50−54.
9. Stefaniv, B.V., Khorunov, V.F., Sabadash, O.M. et al. (2015) Peculiarities of restoration of working parts of drilling bit matrix bodies. *Ibid*., **8**, 47−50.
10. Stefaniv, B.V. (2016) Investigation of wear resistance of protective coatings under conditions of hydroabrasive wear. *Ibid*., **9**, 26–29.
11. Stefaniv, B.V., Nyrkova, L.I., Larionov, A.V., Osadchuk, S.O. (2020) Corrosion resistance of composite material deposited by TIG method using flexible cord TeroCote 7888T. *Ibid*., **9**, 26−29.
12. *Wear-resistant materials*. http://www.svarka52.ru/upload/osnovnoi_katalog_po_paike_i_Terocote_BRAZING_1.pdf

Received 02.06.2020